การศึกษาและสร้างแบบจำลองคณิตศาสตร์สองมิติของปฏิกิริยาการคู่ควบมีเทนโดยใช้ออกซิเจนในเครื่องปฏิกรณ์แบบเบดนิ่งและแบบเยื่อแผ่น

นางสาวสะลามะฮ์ มนูญดาหวี

วิทยานิพนธ์นี้เป็นส่วนหนึ่งของการศึกษาตามหลักสูตรปริญญาวิศวกรรมศาสตรมหาบัณฑิต
สาขาวิชาวิศวกรรมเคมี ภาควิชาวิศวกรรมเคมี
คณะวิศวกรรมศาสตร์ จุฬาลงกรณ์มหาวิทยาลัย
ปีการศึกษา 2554

MODELING STUDY IN TWO-DIMENSIONAL MATHEMATICAL MODEL OF OXIDATIVE COUPKING OF METHANE IN FIXED BED AND MEMBRANE REACTOR

Miss Salamah Manundawee

A Thesis Submitted in Partial Fulfillment of the Requirements

for the Degree of Master of Engineering Program in Chemical Engineering

Department of Chemical Engineering

Faculty of Engineering

Chulalongkorn University

Academic Year 2011

Thesis Title	MODELING STUDY IN TWO-DIMENSIONAL MATHEMATICAL MODEL OF OXIDATIVE COUPLING OF METHANE IN FIXED BED AND MEMBRANE REACTORS
By	Miss Salamah Manundawee
Field of Study	Chemical Engineering
Thesis Advisor	Professor Suttichai Assabumrungrat, Ph.D.
Thesis Co-advisor	Wisitsree Wiyaratn, Ph.D.

Accepted by the Faculty of Engineering, Chulalongkorn University in Partial Fulfillment of the Requirements for the Master's Degree

……Dean of the Faculty of Engineering
(Associate Professor Boonsom Lerdhirunwong, Dr.Ing.)

THESIS COMMITTEE

…….. Chairman
(Association Professor Muenduen Phisalaphong, Ph.D.)

……. Thesis Advisor
(Professor Suttichai Assabumrungrat, Ph.D.)

…….. Thesis Co-advisor
(Wisitsree Wiyaratn, Ph.D.)

…….. Examiner
(Assistant Professor Amornchai Arpornwichanop, D.Eng.)

…….. External Examiner
(Association Professor Navadol Laosiripojana, Ph.D.)

สะลามะฮ์ มนูญดาหวี : การศึกษาและสร้างแบบจำลองคณิตศาสตร์สองมิติของปฏิกิริยาการคู่ควบมีเทนโดยใช้ออกซิเจนในเครื่องปฏิกรณ์แบบเบดนิ่งและแบบเยื่อแผ่น (MODELING STUDY IN TWO-DIMENSIONAL MATHEMATICAL MODEL OF OXIDATIVE COUPLING OF METHANE IN FIXED BED AND MEMBRANE REACTOR) อ. ที่ปรึกษาวิทยานิพนธ์หลัก: ศ. สุทธิชัย อัสสะบำรุงรัตน์ อ. ที่ปรึกษาวิทยานิพนธ์ร่วม: ดร.วิศิษฐ์ศรี วิยะรัตน์, 131 หน้า.

ปฏิกิริยาการคู่ควบมีเทนในเครื่องปฏิกรณ์แบบเบดนิ่งและแบบเยื่อแผ่นได้รับการศึกษาด้วยแบบจำลองเชิงตัวเลขสองมิติ ในเครื่องปฏิกรณ์แบบเบดนิ่ง, ตัวเร่งปฏิกิริยาที่เหมาะสมถูกเลือกโดยการพิจารณาเปรียบเทียบระหว่างตัวเร่งปฏิกิริยาชนิด Li/MgO, La_2O_3/CaO และ Na-W-Mn/SiO_2 โดยจากผลการจำลองแสดงให้เห็นว่าตัวเร่งปฏิกิริยา Na-W-Mn/SiO_2 เสนอผลการดำเนินงานที่ดีที่สุด จากนั้นศึกษาตัวแปรในการดำเนินการซึ่งคือ อุณหภูมิ, อัตราส่วนระหว่างมีเทนและออกซิเจนและค่า GHSVโดยพบว่าเมื่อเพิ่มอุณหภูมิ, มีการเพิ่มค่าการเปลี่ยนของมีเทนแต่ค่าการเลือกเกิดของสารผลิตภัณฑ์ C_2 ลดลง อย่างไรก็ตามผลของอัตราส่วนระหว่างมีเทนและออกซิเจนและค่า GHSV แสดงผลในทางตรงกันข้ามกัน ในเครื่องปฏิกรณ์แบบเยื่อแผ่น, เยื่อแผ่นที่เหมาะสมถูกเลือกโดยการเปรียบเทียบระหว่างเยื่อแผ่น Membranox, BSCFO และ LSGFO จากผลแสดงให้เห็นว่าเยื่อแผ่นชนิด BSCFO เสนอผลที่ดีที่สุด และพบว่าตัวแปรในการดำเนินการซึ่งคือ อุณหภูมิ, อัตราการไหลของมีเทน และอัตราการไหลของออกซิเจน นั้นมีอิทธิพลต่อประสิทธิภาพของการดำเนินปฏิกิริยานี้ โดยพบว่าเมื่อเพิ่มอุณหภูมิเป็นผลให้ ค่าการเปลี่ยนของมีเทนเพิ่มขึ้นแต่ค่าการเลือกเกิดของสารผลิตภัณฑ์ C_2 ลดลง ซึ่งลักษณะเช่นนี้ให้ผลไปในทิศเดียวกันกับผลของอัตราการไหลของออกซิเจนแต่ตรงกันข้ามกับผลของอัตราการไหลของมีเทน เมื่อทำการเปรียบเทียบประสิทธิภาพการทำงานระหว่างเครื่องปฏิกรณ์แบบเบดนิ่งและแบบเยื่อแผ่น พบว่าเครื่องปฏิกรณ์แบบเยื่อแผ่นให้ค่าผลได้ของผลิตภัณฑ์ C_2 สูงกว่าในเครื่องปฏิกรณ์แบบเบดนิ่งและเมื่อสังเกตโปรไฟล์อุณหภูมิของทั้งสองเครื่องพบลักษณะสำคัญคือการเกิดจุดร้อนในเครื่องปฏิกรณ์แบบเบดนิ่งซึ่งไม่พบในเครื่องปฏิกรณ์แบบเยื่อแผ่น ขนาดของเครื่องปฏิกรณ์แบบเยื่อแผ่นที่ดีที่สุดที่เส้นผ่านศูนย์กลาง0.018 เมตร และ ยาว 0.2 เมตร ประสิทธิภาพที่ดีที่สุดพที่ GHSV เท่ากับ 38,904.54 1/h และอุณหภูมิที่ 1073 K, โดยได้ค่าการเปลี่ยนของมีเทน 43.713%, ค่าการเลือกเกิดของสารผลิตภัณฑ์ C_2 61.352% และผลได้ของผลิตภัณฑ์ C_2 26.82 %

ภาควิชา วิศวกรรมเคมี ลายมือชื่อนิสิต.....

สาขาวิชา วิศวกรรมเคมี ลายมือชื่อ อ.ที่ปรึกษาวิทยานิพนธ์หลัก.....

ปีการศึกษา 2554 ลายมือชื่อ อ.ที่ปรึกษาวิทยานิพนธ์ร่วม .....

5270529821: MAJOR CHEMICAL ENGINEERING

KEYWORDS: OXIDATIVE COUPLING OF METHANE / FIXED BED REACTOR / MEMBRANE REACTOR / TWO-DIMENSIONAL MODEL

SALAMAH MANUNDAWEE: MODELING STUDY IN TWO-DIMENSIONAL MATHEMATICAL MODEL OF OXIDATIVE COUPLING OF METHANE IN FIXED BED AND MEMBRANE REACTOR. ADVISOR: PROF. SUTTICHAI ASSABUMRUNGRAT, Ph.D., CO ADVISOR: WISITSREE WIYARATN, Ph.D., 131 pp.

The oxidative coupling of methane (OCM) in a fixed bed reactor (FBR) and a membrane reactor (MR) were studied by two-dimensional numerical simulations. In FBR, a suitable catalyst was selected by comparing between Li/MgO, La_2O_3/CaO and Na-W-Mn/SiO_2 catalysts. The simulation results indicated that Na-W-Mn/SiO_2 catalyst offers the best performances. Different operating conditions, such as temperature, CH_4/O_2 ratio and GHSV were studied. Increasing operating temperature resulted in increasing of CH_4 conversion but decreasing C_2 selectivity. However, the effects of CH_4/O_2 ratio and GHSV showed the contrary results. In MR, the suitable membranes were selected by comparing between porous Membranox, a dense BSCFO and LSGFO membrane. Simulation results indicated that BSCFO membrane offers the best performances. Various operating conditions, such as methane flow rate, air flow rate and temperature have influences on performance of OCM reaction. Increasing operating temperature resulted in increasing of CH_4 conversion and decreasing of C_2 selectivity. Moreover, increasing of methane feed flow rate resulted in lower CH_4 conversion but increased C_2 selectivity. The effect of air flow rate showed the contrary results. When comparing the performance between FBR and MR, it was found that the yield of MR was higher than FBR. The temperature profiles of FBR and MR revealed that significant hot spot temperature was observed for the FBR unlike that of the MR. Optimum dimension of MR was 0.018 m diameter and 0.2 m length. The best performance was found at GHSV of 38904.54 h^{-1} and temperature of 1073 K, offering CH_4 conversion of 43.713 %, C_2 selectivity of 61.352 % and C_2 yield of 26.82 %

Department : Chemical Engineering Student's Signature .....

Field of Study : Chemical Engineering Advisor's Signature .....

Academic Year : 2011 Co-advisor's Signature .....

ACKNOWLEDGEMENTS

First of all, the author would like to express my sincere and deepest appreciation to my advisor and co-advisor, Professor Suttichai Assabumrungrat and Dr. Wisitsree Wiyaratn for their invaluable suggestions, support, encouragement, and help during the course of my graduate study. In additional, the author would also be grateful to Association Professor Muenduen Phisalaphong, as the chairman, Assistant Professor Amornchai Arpornwichanop, and Association Professor Navadol Laosiripojana as the members of the thesis committee.

Most of all, the author would like to express her highest gratitude to her parents who always pay attention to her all the times for their suggestions and have provided support and encouragements. The most success of graduation is devoted to her parents. Moreover, I would like to thanks Mr. Watcharapong Khaodee for the knowledge support.

Finally, the author wishes to thank the members and friends of the Center of Excellence on Catalysis and Catalytic Reaction Engineering, Department of Chemical Engineering, Faculty of Engineering, Chulalongkorn University and the member of Chemical Engineering Laboratory for their friendship and assistance. To the many others, not specifically named, who have provided his with support and encouragement, please be assured that he thinks of you.

CONTENTS

Page

Page

LIST OF TABLES

LIST OF FIGURES

FIGURE Page

FIGURE Page

NOMENCLATURES

C_i	=	Concentration of species i
C_p	=	Heat capacity (J/kg K)
$D_{i,k}$	=	Diffusion coefficient (m^2/s)
$E_{a,j}$	=	Activation energy in the reaction step j (k_j/mol)
F_i	=	Mass flow rate of species i (mol/s)
$\Delta H_{ad,j,C}$	=	Adsorption enthalpy for carbon (k_j/mol)
$\Delta H_{ad,j,O2}$	=	Adsorption enthalpy for oxygen (k_j/mol)
ΔH_{rxn}	=	Heat of reaction (j/mol)
J_{O2}	=	Oxygen flux (mol/m^2 s)
$K_{0,j}$	=	Pre-experiment factor in reaction step (mol/g s $Pa^{(m+n)}$)
k	=	Permeability (m^2)
La_2O_3/CaO	=	Lanthanum supported on Calcium oxide catalyst
Li/MgO	=	Lithium supported on Magnesium oxide catalyst
m_j	=	Reaction order
n	=	the normal vector to the boundary (in Appendix A)
n_j	=	Reaction order
Na-W-Mn/SiO_2	=	Sodium-Tungsten- Manganese supported on silica oxide catalyst
P_1	=	the oxygen partial pressure in the shell side (atm)
P_2	=	the oxygen partial pressure in the tube side (atm)
Q	=	Heat source (W/m^3)
r	=	Reaction rate (mol/m^3 s)
T	=	Temperature (K)
U	=	Overall heat transfer coefficient (W/m^3 K)
u	=	Axial velocity (m/s)

SUBSCRIPT

$CH_3^{\cdot}$	=	Methyl radical
C_2H_5	=	Ethyl radical
CH_4	=	Methane
C_2H_4	=	Ethylene
C_2H_6	=	Ethane
CO	=	Carbon monoxide
CO_2	=	Carbon dioxide
ex	=	external
H_2	=	Hydrogen
H_2O	=	Steam
i	=	Species i
j	=	Reaction step j
O_2	=	Oxygen

GREEK LETTERS

ρ_B	=	Density of bed catalyst (kg/m^3)
ρ_f	=	Density of fluid (kg/m^3)
λ	=	Thermal conductivity (W/m K))
η	=	Viscosity (Pa s)
τ	=	Tortuosity
ε	=	Porosity

ACRONYM

BSCFO	=	$Ba_{0.5}Sr_{0.5}Co_{0.8}Fe_{0.2}O_{3-\delta}$, membrane
FBR	=	Fixed bed reactor
GHSV	=	Gas hour space velocity (1/h)
LSGFO	=	$La_{0.4}Sr_{0.6}Ga_{0.4}Fe_{0.6}O_{3-\delta}$ membrane
MR	=	Membrane reactor

Chapter 1

INTRODUCTION

Introduction

Natural gas consists mainly of methane and a raw material for a number of synthetic products (Lunsford (2000)). The conversion of methane has important in industrial because upgrade natural gas to high value product. The oxidative coupling of methane (OCM) is, promising process because of the one of many processes for direction conversion of natural gas (methane) to C_2 hydrocarbons, especially ethane and ethylene. OCM has been reported since 1982 by the pioneering work of Keller and Bhasin (Keller and Bhasin (1982)). However, many researchers have been still interested on OCM because improvement to obtain higher conversion of methane and ethylene, and high C_2 hydrocarbons selectivity in the production process is still a great challenge.

In OCM process, several reactions occur simultaneously including homogeneous gas phase reactions and heterogeneous catalytic reactions, parallel and consecutive reaction with very complex reaction kinetics. Numerous kinetic reaction models have been presented to describe the performance of the OCM process over a large number of catalysts such as Li/MgO (Wang and Lin (1995)), La_2O_3 (Lacombe *et al.* (1995)), $CaTiO_3$ (Sohrabi *et al.* (1996)), La_2O_3/CaO (Stansch *et al.* (1997)), La_2O_3/MgO (Traykova *et al.* (1998)) and Na-W-Mn/SiO_2 (Shahri *et al.* (2009)). However, Li/MgO, La_2O_3/CaO and Na-W-Mn/SiO_2 are three of the most popular catalysts in literatures for studied OCM process because of high performance. For example, Li/MgO is one of the most commonly studied OCM catalyst system, particularly to show that higher yields are attained in the membrane reactor (Langille *et al.* (2006)) and it showed high catalytic activity in the low temperature range (Amin *et al.(*2006)). In additional, La_2O_3/CaO demonstrated a promising result with 42% methane conversion and yield up to 20 % (S. Jaso *et al.* (2010)). Their kinetic reaction for OCM has been a strong interest in Na-W-Mn/SiO_2 and is thus extensively studied by several researchers (Pak *et al.* (1998), Li *et al.* (2003), Thien *et al.* (2007), Liu *et al.* (2008), Daneshpayeh *et al*. (2009), Shari *et al.*

*(*2009)). Their experimental results suggested this catalyst had appealing prospects in commercial application (Shahri *et al.* (2009)). Despite many studies related to the mechanism of OCM over various catalysts, however, uncertainties concerning important features of the reaction have been existed. It is very important to obtain the applicable rate equations of the reaction for reactor design. Many researchers suggested this catalyst has appealing prospects in commercial application.

Various types of reactors such as fixed bed reactor, fluidized-bed reactor, catalytic jet-stirred reactor, moving bed chromatographic reactor, and membrane reactor have been reported. Fixed bed reactor was studied on OCM process which was the easiest to design, scale up, and could be analyzed using mathematical model. Membrane reactor seems to be the most suitable reactor type compared with other reactors. Applications of membrane reactor combining the separation and reaction in one unit to control oxygen concentration along the reactor were promising for enhancing CH_4 conversion, yield and C_2 selectivity for OCM process than fixed bed reactor. Recently, Wang *et al.* (2005) showed the remarkable study that the improvement of C_2 selectivity was observed when catalyst was packed in the membrane tube. Bhatia *et al.* (2009) compared the performances of different reactors for OCM and reported that the catalytic membrane reactor performed the best. Furthermore, two classes of inorganic membranes were reported in the literature including porous and dense membranes, which have different characteristics in selectivity and permeability. Oliver *et al*. (2009) compared both a two classes of membranes that the porous membranes exhibit high permeability but relatively low selectivity. On the other hand, dense membranes showed much better selectivity but lower permeability. Within the category of dense membranes, ionic oxygen conducting membranes (IOCM) offered the unique advantage to provide activated oxygen at its surface while preventing hydrocarbon losses to the trans-membrane side.

In addition, OCM is extremely exothermic reaction which temperature would rise inside the reactor. Increasing in temperature as a result of the hot spots always take place in catalyst and caused the explosion. Heat removal is therefore essential for real operation to limit the hot spots and run away condition. The important considerations in the operation of the reactors are likely to be operated under non-isothermal condition.

The two-dimensional model is more realistic and provides better prediction accuracy than the one-dimensional one. The need of the two-dimensional model becomes essential when a reactor with a large diameter is operated as the effect of radial dispersion becomes more pronounced. In the reactor design it is important to determine a location where the hot spot is severe so that the operation problem such as catalyst sintering can be avoided and suitable operating condition can be selected.

Therefore in this study, two-dimensional mathematical modeling of oxidative coupling of methane (OCM) to C_2 hydrocarbons (C_2H_4 and C_2H_6) in a fixed bed reactor and membrane reactors operated under isothermal and non-isothermal conditions was investigated using COMSOL® Multiphysics Program. The fixed bed reactor and membrane reactors are developed using available information on reaction kinetics of three different catalysts and permeation rate expressions through different membranes such as dense and porous membrane. The simulations are aimed to find suitable catalyst and membrane, which provide the best performance of the membrane reactor.

1.1 Objective

To develop two-dimensional mathematical models of OCM in non-isothermal fixed bed and membrane reactors, to compare performance between the two reactors, and to determine suitable catalyst and membrane for the membrane reactor operation.

1.2 Scope of work

1.2.1 Simulate OCM process in a fixed bed reactor using COMSOL® multiphysics program to select a suitable catalysts.

1.2.2 Simulate and compare performance of a fixed bed reactor and a membrane reactor for OCM process using COMSOL® multiphysics program.

1.2.3 Study effect of operating mode i.e. isothermal, non-isothermal condition on performance of OCM process.

1.2.4 Study affect of other operating variables i.e. feed temperature, CH_4/O_2 ratio and GHSV and feed flow rate on the reactor performance.

1.2.5 Study and compare effect of membrane type on performances of membrane reactor.

1.2.6 Find optimal operating condition and dimension of reactor

CHAPTER II

THEORY

2.1 Oxidative coupling of methane (OCM) process

2.1.1 Definition

Oxidative coupling of methane is a reaction which directly converts methane to C_2 hydrocarbons (ethane and ethylene), which are raw materials in the production of petrochemical compounds, polymers and liquid fuels. Ethylene is formed by coupling two methyl radicals after the abstraction of a hydrogen atom from each methane molecule; respectively however, the selectivity of ethylene is always reduced due to the formation of carbon oxides (CO and CO_2) from the combustion of methane and C_2 products with oxygen.

2.1.2 Mechanism of OCM reaction

OCM is a complex reaction. It occurs in gas phase and surface of catalyst, parallel and consecutive reaction step. Various reaction schemes were analyzed for description of reaction. However, general scheme of the reaction can be expressed as Figure 2.1 (Sun *et al.* (2008))

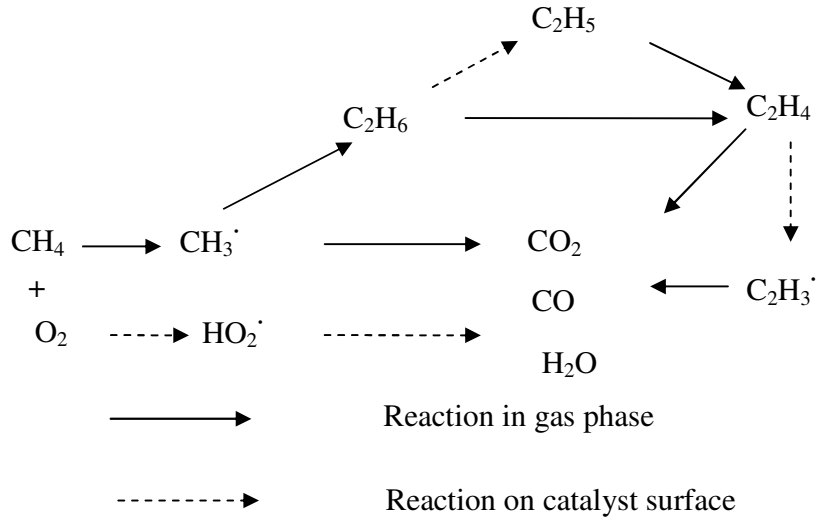

Figure 2.1 A general scheme of the reaction in oxidative coupling of methane

The mechanism of was proposed as follow. Methane is activated to methyl radical by the presence of oxygen a co-feed reactant. Then methyl radicals couple to form ethane, which can be oxidative or thermal dehydrogenated to ethylene (Lane & Wolf (1988)) via formation of ethyl radical (Morales and Lunsford (1989)) or may enter into chain branching reactions that ultimately result in the formation of CO_x (Lunsford (1995)) and (Lane and Wolf (1988)). The reported products are C_2H_6, C_2H_4, C_3H_8, C_3H_6, CO and CO_2.

2.2 Catalyst for OCM reaction

Several catalysts were found to be effective in this complex heterogeneous-homogeneous process. Parameters of metal oxides, such as basicity, band gap, and electrical oxidative coupling of methane conductivity were some of the important parameters in affecting the catalyst performance.

The more effective catalysts were divided into three groups;

a) Highly basic pure oxides, of which the early members of the lanthanide oxide series excluding CeO_2 are the best

b) Group IA or IIA ions supported on basic oxides for example, Li/MgO, Ba/MgO and Sr/La_2O_3

c) A few transition metal oxides that contain Group IA ions or transition metal-based catalyst for example $MnO/Na_2WO_4/SiO_2$, $LiOH/NiTiO_3$ and $Na_2CO_3/NiTiO_3$

In the early 1980s, catalyst Li/MgO has been widely studied (Lunsford (1995)) due to its impressive catalytic activity in OCM. Improvement in the methane conversion, C_{2+} products yield and selectivity can be achieved by doping other components such as Ce, La, Sn, Ti and B (Nagaoka *et al.* (1999)), which were believed, to improve the catalyst activity and stability.

Nowadays, a wide variety of metal oxides, mainly alkali, alkaline-earth and rare earth oxides and to a minor extent transition metal oxide based catalysts, have been studied (Keller *et al.* (1982), Hutchings *et al.* (1989), Carreiro *et al.* (1989), Lunsford *et al.* (1995))

$Sr(Ca)/La_2O_3$, Li/MgO and $Na\text{-}W\text{-}Mn/SiO_2$ have emerged as most promising catalysts for OCM reactions, exhibiting both relatively high activity and selectivity to coupling products (C_{2+})

The study on performance of catalyst, its morphology, stability, active sites, catalytic activity/selectivity, reproducibility, preparation method and properties in OCM have been extensively reported by Lunsford *et al.* (1995), Takenaka *et al.* (2001), Chou *et al.* (2002), Rane *et al.* (2006). The catalysts were characterized with SEM, XRD, TPD, UV, FT-IR and Raman spectroscopy and other techniques.

2.3 Reactor for OCM process

Different type of reactor have been proposed in literature for OCM process such as fixed bed reactor, membrane reactor, fluidized bed reactor, counter-current moving bed reactor etc. Reactors considered in this work are fixed bed reactor and membrane reactor.

2.3.1 Fixed bed reactor

Fixed bed reactor (FBR) consists of one tube filled with bed of catalyst. Configuration of FBR is presented in Figure 2.2. Methane and oxygen were fed to the reactor together. FBR design and scale up is easiest among all other reactors (Ching *et al.* (2004)) and therefore it is investigated in the most studied of OCM process.

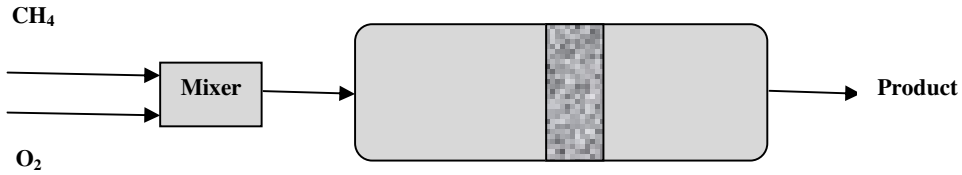

Figure 2.2 Configuration of FBR

2.3.2 Membrane reactor

2.3.2.1 Principle

Membrane reactor consists of shell and tube, like a shell and tube of heat exchanger configuration to perform multiple functions. A membrane can act as an extractor to remove reaction products and thus increase the conversion by shifting the reaction equilibrium, as a distributor to control reactants addition along the reactor wall and thus limit side reactions, or as an active contactor to control diffusion of reactants to the catalyst, can lead to an engineered catalytic reaction zone that all to enhance the overall of process. Figure 2.3 show configuration of membrane reactor.

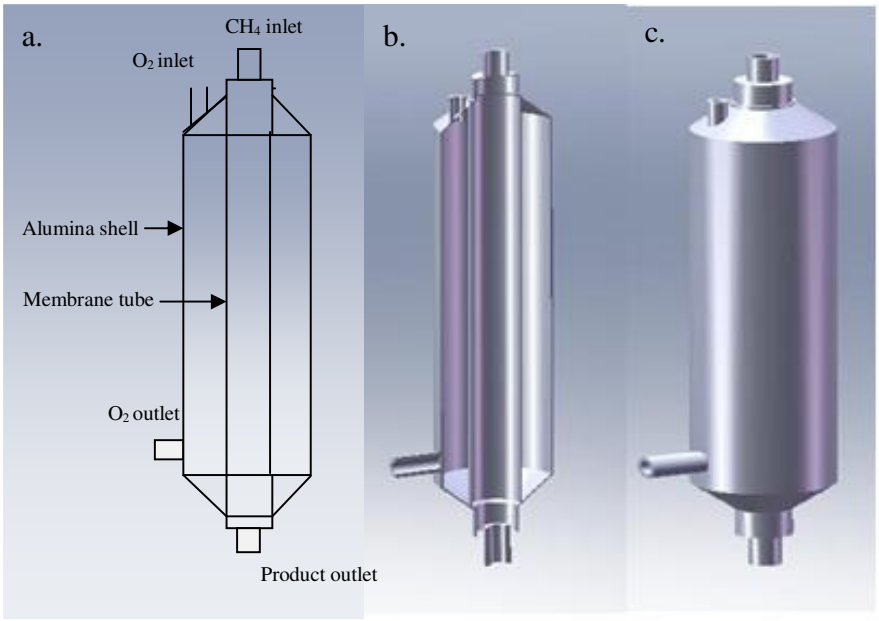

Figure 2.3 a. Detail of OCM in membrane reactor, b. Cross section of membrane reactor, c. Membrane reactor

2.3.2.2 Types of membrane reactor

Summarizes classification of membrane reactors shown in Table 2.1

Table 2.1 Classification of membrane reactors (Marciano, (2002))

Acronym	Description	Features
PBMR	Packed-bed membrane reactor	- Catalyst packed either in the interior or exterior the membrane volume. - Membrane acts as reactant distributor

Acronym	Description	Features
PBCMR	Packed-bed catalytic membrane reactor	- Catalyst packed either in the interior or the exterior of the membrane volume. - Membrane prepared by catalytic material and functions to separate certain substances
CMR	Catalytic membrane reactor	- A membrane with intrinsically catalytic layer or a membrane prepared by catalytic material. - Both separation and reaction occur at the membrane surface.
CNMR	Catalytic non-perms elective membrane reactor	- A membrane providing catalyst site but could not separate certain substances as CMR, mostly acts as reactant distributor than separator.
FBMR	Fluidized-bed membrane reactor	- Similar as PBMR but catalyst was not packed. - Has better temperature control than PBMR especially for exothermic process
FBCMR	Fluidized-bed catalytic membrane reactor	- Similar as FBMR but membrane with catalytic properties.

2.3.2.3 Type and characterization of membrane

Both dense and porous ceramic membranes have been intensively studied and used in OCM reactor. Permeability is considered to be directly related to the membrane structure which can be dense or porous and which defines the transport mechanisms through the membrane.

In porous membrane, the typical gas transport mechanisms in porous membranes are: molecular diffusion and viscous flow (macropores and mesopores), capillary condensation (mesopores), Knudsen diffusion (mesopores), surface diffusion (mesopores and micropores) and micropore activated diffusion. The contribution of the different mechanisms is dependent on the properties of the membranes and the gases as well on the operating conditions of temperature and pressure. At high temperature, when adsorption is no more effective, capillary condensation and surface diffusion are no more involved. In these conditions, the permselectivity increases when pore sizes decrease and pressure can be used to control the transport through membranes with macropores or big mesopores. (Julbe *et al.* (2001))

Dense membranes are for example, mixed ionic–electronic conducting membrane mainly based on perovskites ($ABO_{3-\delta}$ and $A_2BO_{4-\delta}$) and fluorites ($A_1B_{1-\delta}O_{2-\delta}$ and $A_{2(1-\delta)}B_2O_{3-\delta}$), or dual-phases. Oxygen transport through a dense material shown in Figure 2.3 involves three progressive steps: (i) the surface-exchange reaction on interface I; (ii) the simultaneous bulk diffusion of charged species and electron/electron holes in the bulk phase and (iii) the surface-exchange reaction on interface II (J. Sunarsoa, *et al.* 2009) Figure 2.4 shows the mechanism for oxygen permeation through a mixed-conducting membrane in OCM reaction

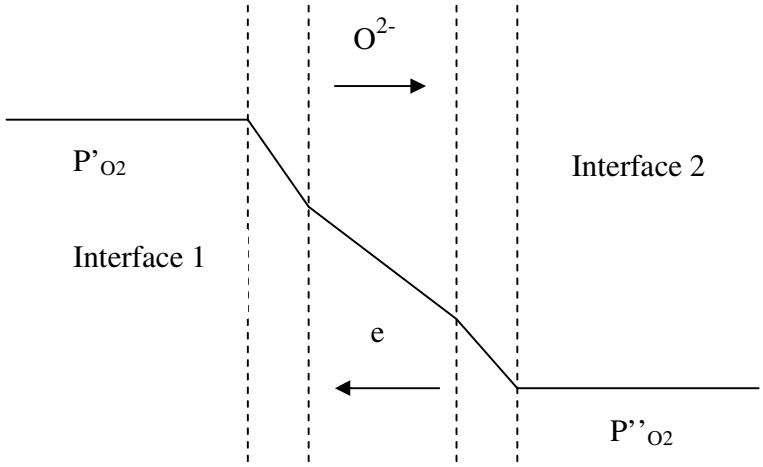

Figure 2.4 Different sections involved in oxygen transport during oxygen permeation.

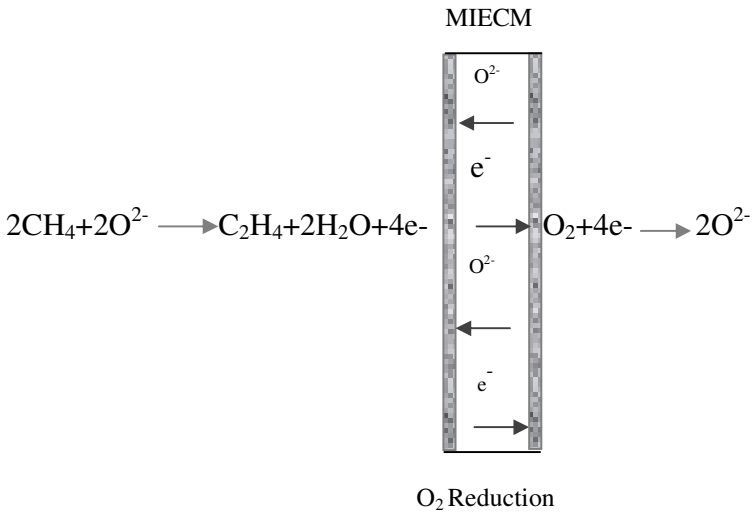

Figure 2.5 Mechanisms for oxygen permeation through a mixed conducting membrane in OCM reaction

2.3.2.4 Application of membrane reactor in OCM

Membrane reactor shows a further application by control of the oxygen supply through the membrane. The reaction site is extended along the membrane inner wall, thus reaction is faster with higher selectivity and yield, at the same time reducing the hot spot existing in catalyst packed bed reactor. The application of membrane reactor is favored in OCM process due to the fast reaction rate, and the utmost point is, to avoid the direct contact of gas phase oxygen and methane by feeding them in different chambers, shell side and tube side, respectively, in order to inhibit the complete oxidation of C2+ product to carbon oxide. Catalytic membrane reactor has the potential to advance the process industry by enhancing selectivity and yield, reducing energy consumption, improving operation safety, and miniaturizing the reactor system. The prospects of catalytic membrane reactor with mixed ionic and electronic conducting membrane for oxidative coupling of methane seem good as to render the technology economically competitive.

CHAPTER III

LITERATURE REVIEWS

The researches on oxidative coupling of methane (OCM) have been carried out extensively. This chapter is divided into four main parts. The first part is a review on mechanism of OCM reaction and kinetic models to be used in this work. The second part is about the research OCM in membrane reactor. The third part is experimental study of OCM process in various types of reactor and the last part is modeling and simulation of OCM process

3.1 Oxidative coupling of methane (OCM) process

3.1.1 Mechanism and kinetic rate expression

In this section, reaction rate expressions of different catalysts are summarized including Li/MgO (Wang and Lin (1995)), La_2O_3 (Lacombe *et al.* (1995)), $CaTiO_3$ (Sohrabi *et al.* (1996)), La_2O_3/CaO (Stansch *et al.* (1997)), La_2O_3/MgO (Traykova *et al.* (1998)) and Na-W-Mn/SiO_2 (Shahri *et al.* (2009) and Daneshpayeh *et al.* (2009)). The reaction steps of models are presented in Table 3.1 and described as follows. (Demonstrates rate expression of Wang and Lin (1995), Stansch *et al.* (1997), Daneshpayeh *et al.* (2009) which are used in this study)

Table 3.1 Represented stoichiometric equation of reaction model

Step (j)	**Step of reaction**	Model 1	Model 2	Model 3	Model 4	Model 5	Model 6
1	$2CH_4+0.5O_2 \rightarrow C_2H_6+H_2O$	✓	✓	✓	✓	✓	✓
2	$CH_4+O_2 \rightarrow CO+H_2O+H_2$				✓		
3	$CH_4+1.5O_2 \rightarrow CO+2H_2O$			✓		✓	✓
4	$CH_4+2O_2 \rightarrow CO_2+2H_2O$	✓	✓	✓	✓		✓
5	$2CH_4+O_2 \rightarrow C_2H_4+2H_2O$			✓			
6	$CO+0.5O_2 \rightarrow CO_2$		✓		✓		
7	$C_2H_6+0.5O_2 \rightarrow C_2H_4+H_2O$		✓		✓	✓	✓
8	$C_2H_6+O_2 \rightarrow 2CO+3H_2$		✓				
9	$C_2H_6+2.5O_2 \rightarrow 2CO+3H_2O$						
10	$C_2H_6+3.5O_2 \rightarrow 2CO_2+3H_2O$	✓	✓				
11	$C_2H_6 \rightarrow C_2H_4+H_2$				✓	✓	
12	$C_2H_4+O_2 \rightarrow 2CO+2H_2$		✓				
13	$C_2H_4+2O_2 \rightarrow 2CO+2H_2O$				✓		✓
14	$C_2H_4+3O_2 \rightarrow 2CO_2+2H_2O$						
15	$C_2H_4+2H_2O \rightarrow 2CO+4H_2$				✓		
16	$CO_2+H_2 \rightarrow CO+H_2O$				✓	✓	✓
17	$CO+H_2O \rightarrow CO_2+H_2$				✓	✓	✓

Wang and Lin (model 1), Lacombe et al. (model 2), Sohrabi et al(model 3),
Stansch et al. (model 4), Traykova et al. (model 5), and (Shahri et al. (model 6),

Wang and Lin *et al.* (1995) analyzed OCM over Li/MgO using a model based on equations that describe OCM kinetics in plug flow reactor and membrane reactor. Kinetic rate equation of C_2 production and carbon oxide are:

$$r_{cCO_x} = \frac{K_3 P_{O_2}^{1.251}}{4}\left[\left(1+\frac{8K_2(\frac{C_p}{C_T})P_{CH_4}}{K_3 P_{O_2}^{1.251}}\right)^{0.5}-1\right]+16S_0K_2\frac{C_p}{C_T}P_{C2} \quad (3.1)$$

$$r_{cC_2} = \frac{K_3 P_{O_2}^{1.251}}{16}\left[\left(1+\frac{8K_2(\frac{C_p}{C_T})P_{CH_4}}{K_3 P_{O_2}^{1.251}}\right)^{0.5}-1\right]^2-8S_0K_2\frac{C_p}{C_T}P_{C2} \quad (3.2)$$

Where Cp and C_T the concentration of electron-hole and total concentration of all defects in the catalyst determined by the partial pressure of reactant and product as

$$\frac{C_P}{C_T} = \frac{K_1 P_{O_2}^{0.5}}{K_1 P_{O_2}^{0.5}+K_1K_2K_4+K_2\left(P_{CH_4}+8S_0P_{O_2}\right)} \quad (3.3)$$

and S_0 is the fraction of ethyl radicals that undergo deep oxidation reaction at zero conversion condition

$$S_0 = \frac{2}{\left(1+8Z\left(\frac{8PK_2P_{CH_4}}{K_3P_{O_2}^{1.251}}\right)\right)+1} \quad (3.4)$$

$$Z = \frac{K_1 P_{O_2}^{0.5}}{K_1 P_{O_2}^{0.5}+K_1K_2K_4+K_2\left(P_{CH_4}+8S_0P_{O_2}\right)} \quad (3.5)$$

Kinetic parameters:

$$K_1 = 2.472\times10^7 e^{-49.649/RT} \quad (3.6)$$

$$K_2 = 10.10e^{-23.15/RT} \quad (3.7)$$

$$K_3 = 0.103\times10^{-3} e^{-4.548/RT} \quad (3.8)$$

$$K_4 = 0.093\times10^{-4} e^{27.94/RT} \quad (3.9)$$

The kinetic equations considering the involvement of lattice oxygen in the catalytic reactions are derived and extended, with the same parameters, to describe OCM kinetics on the oxide layer operated in the membrane mode. Calculation results show a possibility of achieving much higher C_2 yields (> 70%) for OCM in the dense oxide membrane reactors than in conventional packed-bed reactors. Using an impervious but

17

highly oxygen permeable ceramic membrane with an OCM catalytically active surface is essential to achieve the high C_2 yields for OCM in a membrane reactor.

Lacombe *et al.* (1995) reported reaction network based on mechanism conclusions obtained elsewhere of OCM over La_2O_3 catalyst. This model consists of seven heterogeneous reaction steps. Though the result of this work was not to perform a complete kinetic study of the OCM reaction on La_2O_3 catalyst (only one temperature was tested, the number of experiments was limited), it demonstrated the advantage of testing different mechanistic conclusions obtained elsewhere by subjecting them to kinetic considered. Thus, a simplified kinetic scheme has been proposed, accounting for the most suitable mechanistic features of the reaction.

Sohrabi *et al.* (1996) presented OCM perovskite titanate ($CaTiO_3$) at 760, 770 and780 ^oC. This model consists of four heterogeneous reaction steps. Methane is converted in four parallel reactions, At low oxygen partial pressure, formation of methyl radicals proceeds by the Mars-Van Krevelen type mechanism, whereas at higher partial pressures of oxygen, they are formed according to the Langmuir-Hinshelwood dual site mechanism.

Stansch *et al.* (1997) reported kinetic model of the oxidative coupling of methane to C_2+ hydrocarbons over a La_2O_3/CaO catalyst in a catalytic fixed-bed reactor and taking into reference research of Ching Thian Tye *et al.* (2002, 2004), Daneshpayeh *et al.*(2009), Nakisa *et al.*(2009) . Reaction scheme contained 10 reaction steps, the kinetics of oxidative reactions of hydrocarbons were described by Hougen-Watson type rate equation and other reactions were described by applying power-law rate equations and. Kinetics model was evaluated by experimental data comparing with calculation. Power law equations were applied; kinetic rate equations and parameters are:

$$r_j = \frac{k_{0j} e^{-\frac{E_{0,j}}{RT}} P_C^{m_j} P_{O_2}^{n_j}}{(1+K_{jCO_2} e^{-\Delta H_{od,O_2}/RT} P_{CO_2})^2} \quad j = 2,4,6,7,13 \qquad (3.10)$$

$$r_1 = \frac{k_{02} e^{\frac{-E_2}{RT}} (K_{0O_2} e^{-\Delta H_{od,O_2}/RT} P_{O_2})^{n_1} P_{CH_4}}{[1+(K_{0O_2} e^{-\Delta H_{od,O_2}/RT} P_{O_2})^{n_1} + K_{0O_2} e^{-\Delta H_{od,O_2}/RT} P_{O_2}]^2} \quad (3.11)$$

$$r_{11} = k_{07} e^{-\frac{E}{RT}} P_{C_2H_6}^{m_7} \quad (3.12)$$

$$r_{15} = k_8 e^{-\frac{E}{RT}} P_{C_2H_6}^{m_8} P_{H_2O}^{n_8} \quad (3.13)$$

$$r_{16} = k_{09} e^{-\frac{E}{RT}} P_{CO_2}^{m_9} P_{H_2}^{n_9}, \quad (3.14)$$

$$r_{17} = k_{10} e^{-E/RT} P_{CO}^{m_{10}} P_{H_2O}^{n_{10}} \quad (3.15)$$

The kinetic parameters are summarized in Table 3.2:

Table 3.2 Kinetic parameters of La_2O_3/CaO catalyst (Stensch *et al.* (1997))

step ($in\ Table.\ 3.1$)	step	$k_{0,j}$ ($mol \cdot g^{-1}s^{-1}Pa^{-(m+n)}$)	$E_{a,j}$ (kj/mol)	$K_{j,C}$ (Pa^{-1})	K_{j,O_2} (Pa^{-1})	$\Delta H_{ad,j,C}$ (kj/mol)	$\Delta H_{ad,j,O_2}$ (kj/mol)	m_j	n_j
4	1	0.20×10^{-5}	48	0.25×10^{-12}		-175		0.24	0.76
1	2	23.2	182	0.83×10^{-13}	-124	-186	0.23×10^{-11}	1.0	0.40
2	3	0.52×10^{-6}	68	0.36×10^{-13}		-187		0.57	0.85
6	4	0.11×10^{-3}	104	0.40×10^{-12}		-168		1.0	0.55
7	5	0.17	157	0.45×10^{-12}		-166		0.95	0.37
13	6	0.06	166	0.16×10^{-12}		-211		1.0	0.96
11	7	1.2×10^{-7}	226						
15	8	9.3×10^{3}	300					0.97	0
16	9	0.19×10^{-3}	173					1.0	1.0
17	10	0.26×10^{-1}	220					1.0	1.0

Traykova *et al.* (1998) reported OCM reaction over La_2O_3/MgO catalyst. This reaction network consists of five heterogeneous and one homogeneous reaction steps, including partial oxidation of ethane to ethylene and water gas shift.

Shahri *et al.* (2009) presented kinetic equations over Mn-Na-W/SiO_2. It consists of 5 steps Langmuir - Hinshelwood type rate and 2 steps of water-gas shift. All kinetic parameters were estimated from experimental data carried out in a micro-catalytic fixed bed reactor.

Daneshpayeh *et al.* (2009) provided comprehensive kinetic model for oxidative coupling of methane (OCM) on Na-W-Mn/SiO_2 catalyst developed based on a microcatalytic reactor data. Five kinetic models were analyzed to identify the best kinetic model for Na-W-Mn/SiO_2 catalyst. To measure the accuracy of each model, R-square (R^2) average absolute relative deviation (AARD) from analysis confirms that the reaction network of Stanch *et al.* (1997) has the best accuracy compared to other models and kinetic rate equations and parameters are:

$$r_1 = \frac{k_{01} e^{-E_1/RT} (K_{0O_2} e^{-\Delta H_{od,O_2}/RT} P_{O_2})^{n_1} P_{CH_4}^{m_2}}{[1+(K_{0O_2} e^{-\Delta H_{od,O_2}/RT} P_{O_2})^{n_1}]^2} \quad (3.16)$$

$$r_j = k_{0j} e^{-E/RT} P_C^{m_j} P_{O_2}^{n_j} \quad j = 2, 4, 6, 7, 13 \quad (3.17)$$

$$r_{15} = k_{07} e^{-\frac{E}{RT}} P_{C_2H_4}^{m_7} P_{H_2O}^{n_j}, \quad (3.18)$$

$$r_{11} = k_{08} e^{-E/RT} P_{C_2H_6}^{m_8} \quad (3.19)$$

$$r_{16} = k_{09} e^{-\frac{E}{RT}} P_{CO_2}^{m_9} P_{H_2}^{n_9}, \quad (3.20)$$

$$r_{17} = k_{10} e^{-E/RT} P_{CO}^{m_{10}} P_{H_2O}^{n_{10}} \quad (3.21)$$

The kinetic parameters are summarized in Table 3.3:

Table 3.3 Kinetic parameters of Na-W-Mn/SiO_2 catalyst **(**Daneshpayeh *et al.* (2009))

step ($in\ Table.\ 3.1$)	step	$k_{0,j}$ ($kmol \cdot kg^{-1}s^{-1}Pa^{-(m+n)}$)	$E_{a,j}$ (kj/mol)	K_{j,O_2} (Pa^{-1})	$\Delta H_{ad,j,O_2}$ (kj/mol)	m_j	n_j
1	1	2.94×10^{1}	212.6	4.39×10^{-11}	-121.9	1.00	0.75
4	2	3.07×10^{-7}	98.54			0.85	0.50
2	3	6.65×10^{-8}	146.8			0.50	1.57
6	4	5.26×10^{-4}	114.6			0.50	0.50
7	5	2.70×10^{-3}	153.5			0.91	0.50
13	6	1.81×10^{-1}	174.4			0.72	0.40
15	7	4.61×10^{2}	394.2			1.62	0.71
11	8	1.08×10^{7}	291.9			0.88	0
16	9	5.77×10^{-3}	158			1.00	1.00
17	10	5.24×10^{-6}	131.3			1.00	1.00

3.2 OCM in membrane reactor

3.2.1 Type of membrane reactor

Inorganic membrane for OCM process can be divided in 2 classes of porous and dense membranes were summarized membrane type in Table 3.4 and Table 3.5, respectively. Porous membranes exhibit high permeability but relatively low selectivity. On the other hand, dense membranes show much better selectivity but lower permeability. Within the category of dense membranes, ionic oxygen conducting membranes (IOCM) offer the unique advantage to provide activated oxygen at its surface while preventing hydrocarbon losses to the trans-membrane side (Oliver *et al*. (2009)).

From Table 3.4, it can be seen that $Ba_{0.5}Sr_{0.5}Co_{0.8}Fe_{0.2}O_{3-\delta}$ membrane exhibits higher performance than $La_{0.6}Sr_{0.4}Co_{0.8}Fe_{0.2}O_{3-\delta}$ and La-Ba-Co-Fe-O due to substitution of La_{3+} by the lower valence state of Ba_{2+} and $Ba(Co,Fe)O_{3-}$ exhibit stable oxygen fluxes at high (Wang *et. al.* (2005) and Shao *et al.* (2000,2001)) studied the influence of the barium content in $Ba_{0.5}Sr_{0.5}Co_{0.8}Fe_{0.2}O_{3-\delta}$ and showed that the addition of barium results in higher oxygen permeability and lower activation energy for oxygen transportation

Flux expression across membranes is given as:

Tan *et al.* (2002) reported flux equation of oxygen across $La_{0.6}Sr_{0.4}Co_{0.8}Fe_{0.2}O_{3-\delta}$ (LSCF) membrane.

$$J_{O_2} = \frac{\left(\frac{k_r}{k_f}\right)\left(\frac{1}{P''^{0.5}_{O_2}} - \frac{1}{P'^{0.5}_{O_2}}\right)}{\left(\frac{1}{k_f P'^{0.5}_{O_2}}\right) + \left(\frac{2L}{D_v}\right) + \left(\frac{1}{k_f P'^{0.5}_{O_2}}\right)} \qquad 3.22$$

This equation is derived specifically for disk-shaped membrane and has been shown to fit the oxygen flux of LSCF using a wide range of experimental data at T = 1023-1223 K, t = 1.68-3.99mm, $p'^{0.5}_{O_2}$ = 0.21-1 atm and $p''^{0.5}_{O_2}$ = 4.64×10^{-4} to 2.3×10^{-2} atm

Table 3.4 Typical dense membrane reported for OCM in literature:

No.	Type	Report by	Year	Catalyst	Temperature (K)	C_2 selectivity (%)	C_2 yield (%)
1	$La_{0.6}Sr_{0.4}Co_{0.8}Fe_{0.2}O_{3-\delta}$ (LSCF)	Elshof *et al.*	1995	$LaCoO_3$		70	-
2	La-Ba-Co-Fe-O (LBCF)	Xu *et al.*	1997	-		50	-
3	$SrFeCo_{0.5}O_{3-\delta}$ coat with $BaCe_{0.6}Sm_{0.4}O_{3-\delta}$	Lu *et al.*	2000	La/MgO		48.4	7
4	$BaCe_{0.8}Gd_{0.2}O_{3-\delta}$	Lu *et al.*	2000	La/MgO		62.5	16
5	$Bi_{1.5}Y_{0.3}Sm_{0.2}O_{3-\delta}$ fluorite structure (BYS)	Akin *et al.*	2002	BYS	1173	54	35
	$Bi_{1.5}Y_{0.3}Sm_{0.2}O_{3-\delta}$ (BY25)	Akin *et al.*	2000	BY25	1223	40	16
6	$Ba_{0.5}Sr_{0.5}Co_{0.8}Fe_{0.2}O_{3-\delta}$ (BSCF)	Wang *et al.*	2002, 2003, 2005	LaSr/CaO	1173	54-88	15
		Shao *et al.*	2000, 2001	LiLaNiO/g-Al_2O_3 with 10% Ni	1123	59.48	2
7	$La_{0.4}Sr_{0.6}Ga_{0.4}Fe_{0.6}O_{3-\delta}$ (LSGF)	Kiatkittipong *et al.*	2005	Li/MgO	1123	88	45
8	$Ba_{0.5}Sr_{0.5}Co_{0.8}Fe_{0.2}O_{3-\delta}$ (BSCF)	Haag *et al.*	2007	Pt/MgO	1223	59.5	2.02
9	$Ba_{0.5}Sr_{0.5}Mn_{0.8}Fe_{0.2}O_{3-\delta}$ (BSMF)	Haag *et al.*	2007	Pt/MgO		46	3
10	$BaBi_{0.4}Fe_{0.62}O_3$(BBFO)	Haag *et al.*	2007	Pt/MgO		Not stable at high temp.	
11	$Ba_{0.5}Sr_{0.5}Co_{0.8}Fe_{0.2}O_{3-\delta}$ (BSCF)	Oliver *et al.*	2009	LaSr/CaO	1173	70	18.4
12	$Ba_{0.5}Ce_{0.4}Gd_{0.1}Co_{0.8}Fe_{0.2}O_{3-\delta}$ (BCGCF)	Bhatia *et al.*	2009	Na-W-Mn/SiO	1123	67.4	34

Table 3.5 Typical porous membrane reported for OCM in literature:

No.	Type	Report by	Year	Catalyst	Temperature (K)	C_2 selectivity (%)	C_2 yield (%)
1	Porous Vycor	Ramachandra *et. al.*	1996	Sm_20_3	1023	33	11
2	commercial (α-alumina support, γ-alumina)	Kao *et al.*, Curonas *et al.*	2003	Li/MgO	1023	53	30
3	comercial porous alumina tube (produced by MKS Co.)	Lafarga *et al.*	2001	La/MgO	1173	13	7.41
4	α-alumina coated with amorphous Sit 2	Tonkovich *et al.*	1996	Sm_20_3 doped with MgO	973	23	3
5	Membralox (α-alumina support, γ-alumina)	Kiatkittipong *et al.*	2005	Li/MgO	1173	85	80

Shaula *et al.* (2003) reported flux equation of $La_{0.4}Sr_{0.6}Ga_{0.4}Fe_{0.6}O_{3-\delta}$ (LSGF) membrane

$$J_{O_2} = \frac{Per_{O_2}}{d} ln \frac{P_1}{P_2} \quad (3.23)$$

Where

$$Per_{O_2} = 0.0645 \exp\left(\frac{-108400}{RT}\right) \quad (3.24)$$

Where d is thickness of membrane (m) and the value of Per_{O2} of $La_{0.4}Sr_{0.6}Ga_{0.4}Fe_{0.6}O_{3-\delta}$ membrane was determined from Figure 3.1 in (Shaula *et al.* (2003))

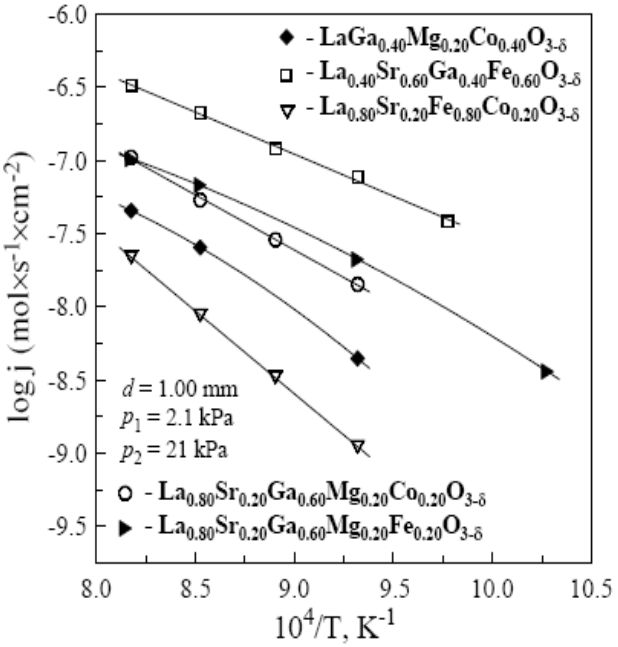

Figure 3.1 Using determine $PerO_2$ value of $La_{0.4}Sr_{0.6}Ga_{0.4}Fe_{0.6}O_{3-\delta}$ membrane

Z. Shao *et al.* (2000) reported flux equation of $Ba_{0.5}Sr_{0.5}Co_{0.8}Fe_{0.2}O_{3-\delta}$ (BSCF) membrane

$$J_{O_2} = \frac{RT}{4^2F^2L}\bar{\sigma} ln \frac{P'_{O_2}}{p''O_2} \quad (3.25)$$

This equation is fulfilled only in very rare cases such as the oxygen permeation in tubular BSCF at $p'^{0.5}_{O_2}$ = 0.0911925×10^5 to 1.01325×10^5 Pa (0.09-1 atm) and $p''^{0.5}_{O_2}$ = 942.3225 to 11621.9775 Pa (9.3×10-3 to 0.1147 atm) for T=973-1173 K

Wang *et al.* (2002) reported flux equation of $Ba_{0.5}Sr_{0.5}Co_{0.8}Fe_{0.2}O_{3-\delta}$ (BSCF) membrane can be expressed as

$$J_{O_2} = \frac{\pi LC_iD_a}{2Sln(\frac{r_1}{r_2})} \ln (\frac{P_1}{P_2}) \quad (3.26)$$

Where L is the effective length of the tube (cm), Ci is the density of oxygen ions (mol/cm^3), Da (cm^2/s) is the ambipolar oxygen ion–electron hole diffusion coefficient, S the effective area of the membrane tube (cm^2), r_1 and r_2 are the outer and inner radius of the membrane tube (cm).

Kao *et al*. (2003) reported flux equation of mesoporous membrane (e.g. 4 nm US-Filter Membranox alumina membrane) The membrane parameters were ϵ = 0.5, τ = 2.95, r = 2 × 10^{-9} m and membrane top-layer thickness δ = 5 × 10^{-5} cm for ceramic alumina membrane properties obtained from Jeffrey *al.* (1992). The diffusion flux of each species is calculated according to following equation:

$$J_i = \frac{D_{i,k}}{RT} \frac{(P^1y_i^1 - P^2y_i^2)}{\delta} \quad (3.27)$$

The Knudsen coefficient is calculated by the following formula :

$$D_{i,k} = \frac{2}{3}\frac{\varepsilon}{\tau} r (\frac{8RT}{\pi M_i})^{0.5} \quad (3.28)$$

Kiatkittipong *et al.* (2005) reported flux equation of Membralox (α-alumina support, γ-alumina separate layer) (produced by MKS Co. and Membralox) pore size of $1*10^{-8}$ m and a thickness of $5*10^{-6}$ m.

$$J_i = \frac{a}{\sqrt{M_i T}}\left(P_{s,i} - P_{t,i}\right) + \frac{b}{2\mu T}\left(P_{s,i}^2 - P_{t,i}^2\right) \quad (3.29)$$

Where

$a = 2.298 \times 10^{-4}\ molK^{1/2}Pa^{-1}m^{-2}s^{-1}$

$a = 4.779 \times 10^{-14}\ molK^{1/2}Pa^{-1}m^{-2}s^{-1}$

The gas viscosity can be estimated by Wilke's correlation.

3.3 Experimental study of OCM process in various type of reactor

Al-Zahrani *et al.* (1999) studied OCM reaction in turbulent fluidized-bed (TFB) reactor based on simulation works employing a two-phase model and the hydrodynamic structure of the TFB was characterized for the MgO catalyst particles. The overall gas phase distribution in bubbles and emulsion phases was estimated by using the probability distribution function of local voidage fluctuations in the bed. The two-phase model developed predicted satisfactorily the experimental data and can be used to quantify the influence of homogeneous and catalytic reaction in the TFB for the oxidative coupling of methane.

Akin *et al.* (2001) studied comparative oxidative coupling of methane and oxygen permeation in disk shaped and tubular $Bi_{1.5}Y_{0.3}Sm_{0.2}O_{3-\delta}$ fluorite structure (BYS) ceramic membrane reactor. In operating condition, temperature in rang 1073-1173 K, P_{O2} = 0.2-0.5 atm, P_{CH4} = 0.1 atm. The resulted show that membrane geometry and flow conditions have a significant effect on reaction results and oxygen permeation flux during the OCM reactions. Highest C_2 selectivity, C_2 yields and oxygen permeation flux in the tubular membranes were 78%, 22%, 2.6×10^{-7} mol/s.cm^2, and disk-shaped BYS was 44%, 10.4%, 1.7×10^{-6} mol/s.cm^2, respectively. The presence of more molecular oxygen showed lowers the selectivity for OCM in the disk-shaped membrane reactor. Hence,

tubular geometry showed more favorable result than disk-shaped geometry.

Wang *et al.* (2005) researched on oxidative coupling of methane in $Ba_{0.5}Sr_{0.5}Co_{0.8}Fe_{0.2}O_{3-\delta}$ (BSCF) tubular membrane reactor, which BSCF membrane tube was packed with an active OCM catalyst (La-Sr/CaO) and comparative with membrane reactor without catalyst and packed-bed reactor. They found in membrane reactor with La-Sr/CaO catalyst that both C_2 selectivity and CH_4 conversion were improved. Although the C_2 yield in the membrane reactor with the La-Sr/CaO catalyst was similar in a packed-bed reactor under the same conditions, the C_2H_4/ C_2H_6 ratio was much higher than that in the packed-bed reactor. They also studied effect of temperature and revealed that when the temperature increases, C_2 selectivity and C_2 yields increase. However, for T > 1098 K, the C2selectivity decreased with increasing temperature. These indicate that combustion rate increases faster than the OCM reaction rate. Regarding the effect of concentration of methane, the C_2 selectivity increased as the CH_4 concentration was increased. C_2 selectivity becomes lower at a higher oxygen concentration due to combustion of the C_2 products.

Bhatia *et al.* (2009) investigated oxidative coupling of methane in catalytic membrane reactor (CMR) and compared its performance with catalyst packed bed membrane reactor (PBMR) and packed bed reactor (PBR). CMR consisted of $Ba_{0.5}Ce_{0.4}Gd_{0.1}Co_{0.8}Fe_{0.2}O_{3-\delta}$ (BCGCF) membrane and coat inner membrane with Na-W-Mn/SiO_2 catalyst layer. They compared performances of three reactors at optimum condition (T=1123 K, CH_4/O_2=3, air flow rate=150 cm^3/min and He flow rate=100 cm^3/min) and found that CMR performed best among three reactors with CH_4 conversion of 51.6%, C_{2+} yield of 34.7%, PBR gave highest C_{2+} selectivity of 70.6% and PBMR did not perform well. Considering the effect of CH_4/O_2 ratio, performance of OCM reaction increase with increases CH_4/O_2 ratio and highest oxygen permeation flux was lowest performance due to recombination of lattice oxygen to gaseous oxygen occurred on membrane surface affect to OCM reaction. Considering effect of sweep gas flow rate, these had effect over the selectivity than the methane conversion. It was due to more sweeps off the C_2 product from the reaction site and shortening the contact time between

the intermediate products with the oxygen, limiting the formation of carbon oxides thus higher C_2 selectivity value.

Simon *et al.* (2007) proposed an original approach derived from Benson's techniques to estimate the kinetic parameters of surface reactions. Experimental investigations were performed and compared to simulated values derived from a kinetic model, taking into account heterogeneous and gas phase reactions. The experimental setup included a catalytic jet stirred reactor using La_2O_3 catalyst specifically developed for the investigation of hetero-homogeneous reactions. This study suggests that the surface mechanism of OCM over La_2O_3 essentially accounts for the initiation of the reaction, the production of CO_2, and the decomposition of C_2H_6. The OCM mechanism includes two reaction pathways. The first one leads to the formation of oxygenated species, and the second one leads to the formation of hydrocarbons.

Karimi *et al.* (2007) investigated the catalytic performance of OCM in a fixed-bed reactor and studied the effect of operating conditions, such as GHSV, temperature and CH_4/O_2 ratio at pressure 3 bar, 50 g of catalyst. Heat control in OCM was very important. With attention to this fact series of experiment were designed to investigate the influence of above-mentioned parameters on C_{2+} selectivity, CH_4 conversion and the yield of C_{2+}. The C_{2+} selectivity of 57.3% was obtained at a CH_4 conversion of 20.3% at 1113 K, 1620 hr^{-1} GHSV and CH_4/O_2 ratio 4 to 1 and pressure of 3 barg. The OCM reaction was strongly dependent on the operating condition particularly GHSV and the CH_4/O_2 ratio. The comparison of these results and micro-reactor in literatures showed that the scale up of fixed bed reactor in OCM reaction without too much change in yield and selectivity of C_{2+}, CH_4 conversion and COx selectivity, with an appropriate GHSV, CH_4/O_2 ratio is technically feasible and economic.

Prodip *et al.* (2009) reported OCM in the simulated countercurrent moving bed chromatographic reactor (SCMCR) which could offer significant improvement on the methane conversion and C_2 yield. This was particularly important for understanding the operation of this SCMCR system. In order to obtain the various process parameters, a

realistic and rigorous kinetics was adopted in reactors for OCM. They found that conversion reached as high as 93.0% and selectivity and yield reached 99.9% and 58.5% respectively, Finally, effects of operating parameters, such as switching time, methane/oxygen feed ratio, raffinate flow rate, eluent flow rate, etc., on the behavior of the SCMCR were studied systematically

The maximum performance value of each reactor in OCM process presented in Table 3.6

Table 3.6 Maximum performance on different reactor:

Type of reactor	efficiency value			Condition	Note	Report by
	CH_4 conversion,%	**C_2selectivity, %**	**C_2 yield, %**			
Catalytic membrane reactor	51.6	67.4	34.7	T= 1123 K., GHSV = 23947 cm^3/g h, CH_4/O_2 = 3, He flow rate = 100 cm^3/min	experimental	Bhatia *et al.*
Fixed bed reactor	43.1	70.6	30.4	T= 1123 K., GHSV = 23947 cm^3/g h, CH_4/O_2 = 7	experimental	Bhatia *et al.*
SOFC	23.7	91.7	21.7	T=1273 K	simulation	Quddus *et al.*
Fluidized bed reactor	43	55	23.7	CH_4/O_2 =7, T=1063 K,	experimental	Daneshpayeh *et al.*
Countercurrent moving bed chromatographic reactor	93	99.9	58.5	CH_4/O_2 =2.47 T=1023 K	simulation	Prodip *et al.*
Catalytic jet-stirred reactor	16.5	62	10.23	P= 1.05 bar, T=1173 K, CH_4:O=13.9:2.8	experimental	Simon *et al.*
Riser simulator reactor		58		T= 973 K	abstract only	Pekediz *et al.*
Electrocatalytic or catalytic reactor separator	97	88	85		abstract only	Yentekakis *et al.*

3.4 Modeling and simulation of oxidative coupling of methane (OCM) process

Kao *et al.* (1997) studied OCM reaction on a conventional fixed-bed reactor (FBR) and a mixed-conducting ceramic dense membrane reactor (DMR) packed with Li/MgO catalyst using plug-flow reactor models as reported by Wang and Lin (1995). For DMR, the membrane tube was used to separate the methane and oxygen feed .The oxygen permeation flux through the perovskite-type membrane were correlated with oxygen partial pressures with temperature (Itoh *et al.* (1994)). A perovskite membrane was made of $La_{1-x}Sr_xCoO_3$. The kinetic model was verified by comparing the simulation results with the experimental data for OCM in the fixed-bed reactor packed with Li/MgO reported by Ito *et al.* (1985). The validity of OCM kinetic equations employed in the modeling was confirmed according to excellent agreement between the simulation and experimental data for OCM. In DMR, that can be controlled by adjusting the feed pressure of oxygen at the shell side it had a significant advantage over the FBR. Higher Methane/oxygen ratio favors the OCM reaction and optimal feed ratio did not change with temperature. The highest C_2 yield was 21% and C_2 selectivity of 87.1% with operating temperature of 1023 K, feed mixture consisting of 70% methane and 30% oxygen and The C_2 yield and selectivity increase slightly at a higher operating temperature. Significant increasing of C_2 selectivity and yield were observed for the DMR as compared to the FBR.

Kao *et al.* (2003) reported optimum operation of OCM on Li/MgO packed porous membrane reactor (PMR) by kinetic model reported by Wang and Lin (1995). Comparative with membrane made of dense ionic or mixed-conducting oxide ceramics during OCM, the membrane was subjected to an extremely large oxygen partial gradient (membrane sides exposed, respectively, to oxygen and methane streams). The membrane was inherently unstable due to the chemical expansion induced stress, ion migration and phase segregation. Thus, porous ceramic (such as alumina or zirconia) membrane reactor was more attractive for OCM. Theoretical analysis showed that PMR can achieve, by operating with both side pressures at 1 bar at 1023 K, a maximal C_2 yield 30% at C_2 selectivity 53%. Parametric study showed that lowering the membrane permeability also

improved the performance. Higher oxygen feed pressure will reduce the yield as well as the selectivity. Homogeneous reactions at high shell-side pressure can have adverse effect on the performance due to the fact that homogeneous reaction rates were strongly pressure dependent. The shell (oxygen feed) side volume must be minimized to reduce the homogeneous reactions At a fixed methane feed rate there was an optimal oxygen feed pressure that will achieve the highest yield and the results of PMR model calculation fit well the published experimental result

Langille *et al.* (2006) performed preliminary simulations to make qualitative comparisons between the membrane and conventional reactors over Na-W-Mn/S_iO_2 catalyst. Discussions on the mechanism of the Li/MgO catalyst were provided by Wang and Lin (1995), Tung and Lobban (1992) and Li (2003). The qualitative observations revealed that the kinetics for the Li/MgO catalyst applied equally well to the Na-W-Mn/SiO_2 catalyst system.

Kiatkittipong *et al.* (2005) performed comparative study of OCM modeling process in various types of reactor including fixed bed reactor and membrane reactor (porous membrane reactor (PMR), mixed ionic and electronic conducting membrane reactor (MIEMR), solid fuel cell reactor (SOFCR) in order to improve performance of OCM process. The kinetic of the reactions on the Li/MgO catalyst were obtained from Kao *et al.* (1997). Operating condition is WHSV= 1.8×10^{-3} /mol Kg CH_4/O_2 ratio = 2, temperature= 1073 K (in SOFCR =1277 K) FBR gave C_2 selectivity lower than membrane reactor and not recommended for OCM. PMR is also not recommended for in the case of air feed or oxygen feed with impurities and the methane loss through the non-selective porous membrane PMR and MIEMR were suitable at temperatures lower than 877 $^{\circ}$C and higher than 1150 K. Operation at high pressure was beneficial to SOFCR. SOFCR was the requirement of higher operating temperature of approximately 200 K compared to the others However, the electricity simultaneously generated as a by-product might make SOFCR still attractive.

Amin *et al.* (2005), Istadi *et al.* (2006) and Thien *et al.* (2007) determined the optimal process parameters and effect of variables (such as temperature, inlet oxygen concentration, and F/W on ethylene production) via using Central composite experimental design (CCD) and response surface methodology (RSM) method. The results of the analysis revealed that the equation models fitted well with the experimental results for methane conversion and ethylene yield.

Yaghobi *et al.* (2008) reported the oxidative coupling of methane to ethylene over a perovskite titanate $SnBaTiO_3$ catalyst in a fixed bed reactor was studied experimentally and numerically. The two-dimensional steady state model accounted for separate energy equations for two phases coupled with an experimental kinetic model. The model was used to analyze the influence of temperature and feed gas composition on the conversion and selectivity of the reactor performance. Experimentally measured rate confirmed the derived kinetic model. The results from the model agreed well with experiment data. The analytical results indicate that the C_2 selectivity increases, whereas, conversion decreases by increasing gas hourly space velocity (GHSV) and the methane conversion also decreases by increasing the CH_4/O_2 ratio. The temperature was found to be a sensitive parameter in the OCM reaction.

Yaghobi *et al.* (2009) modeled the oxidative coupling of methane over titanate perovskite: Heterogeneous chemistry coupled with 3D flow field coupled with heat transfer. The reaction was assumed to take place both in the gas phase and on the catalytic surface using a kinetic model reported by Stansch *et al*. (1997). The simulation results agreed quite well with the data of OCM experiments, which were used to investigate the effect of temperature on the selectivity and conversion obtained in the methane oxidative coupling process. The conversion of methane linearly increased with temperature and the selectivity of C_2 was practically constant in the temperature range of 1046-1146 K. The study showed that Computational Fluid Dynamics (CFD) tools made it was possible to implement the heterogeneous kinetic model even for high exothermic reaction such as OCM.

CHAPTER IV

SIMULATIONS

The simulations in this study can be divided into four parts; the first part is the OCM process simulation and modeling. Then the study and analysis on the effect of variables is determined in the second part. The third part is the performance comparison between fixed bed reactor and membrane reactor while the last part is the optimum condition of each modeling. The works done in this study can be summarized in the following diagram (Figure 4.1);

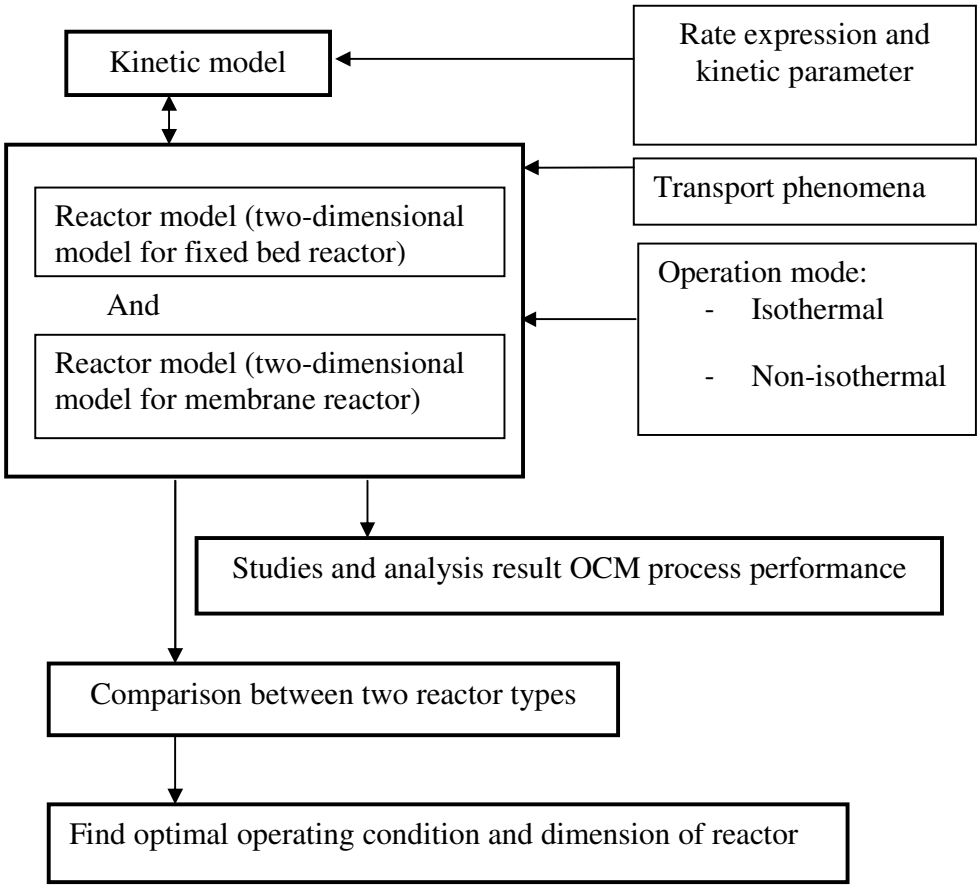

Figure 4.1 Diagrams of the work

4.1 Simulation and modeling of OCM process

4.1.1 Kinetic model

Numerous kinetic reaction models have been presented to describe the performance of the OCM process over several catalysts. Li/MgO, La_2O_3/CaO and Na-W-Mn/SiO_2 were three of the most studied catalysts in literatures for OCM process. Li/MgO shows high catalytic activity in the low temperature range, La_2O_3/CaO was one of the most common catalysts used in OCM models and Na-W-Mn/SiO_2 was one of the most studied three-component catalyst. In the model, the kinetic mechanism and kinetic equations considered in this work were proposed by Wang and Lin over Li/MgO catalyst, Stansch *et al.* over La_2O_3/CaO catalyst and Danespayeh *et al*. over Na-W-Mn/SiO_2 catalyst. Stiochiometric equation and reaction rate of proposed models were shown in Table 4.1.

Table 4.1 Stiochiometric equation and reaction rate of proposed models

Model	Stoichiometry equation	Reaction rate
Wang and Lin	Step 1 : $CH_4+2O_2 \longrightarrow CO_2+2H_2O$ Step 2 : $2CH_4+0.5O_2 \longrightarrow C_2H_6+H_2O$ Kinetic parameters: $K_1 = 2.472 \times 10^7 e^{-49.649/RT}$ $K_2 = 10.10e^{-23.15/RT}$ $K_3 = 0.103 \times 10^{-3} e^{-4.548/RT}$ $K_4 = 0.093 \times 10^{-4} e^{27.94/RT}$	$r_1 = \frac{K_3 P_{O_2}^{1.251}}{4}\left[\left(1+\frac{8K_2\frac{C_p}{C_T}P_{CH_4}}{K_3P_{O_2}^{1.251}}\right)^{0.5}-1\right]+16S_0K_2\frac{C_p}{C_T}P_{C_2}$ $r_1 = \frac{K_3 P_{O_2}^{1.251}}{16}\left[\left(1+\frac{8K_2\frac{C_p}{C_T}P_{CH_4}}{K_3P_{O_2}^{1.251}}\right)^{0.5}-1\right]^2+8S_0K_2\frac{C_p}{C_T}P_{C_2}$ $\frac{C_p}{C_T} = \frac{K_1P_{O_2}^{0.5}}{K_1P_{O_2}^{0.5}+K_1K_2K_4+K_2(P_{CH_4}+8S_0P_{C_2})}$ $S_0 = \frac{2}{\left(1+\frac{8K_2\frac{C_p}{C_T}P_{CH_4}}{K_3P_{O_2}^{1.251}}\right)^{0.5}+1}$ $Z = \frac{K_1P_{O_2}^{0.5}}{K_1P_{O_2}^{0.5}+K_1K_2K_4+K_2(P_{CH_4}+8S_0P_{C_2})}$

Model	Stoichiometry equation	Reaction rate
Stansch *et al.* (The kinetic parameters were summarized in Table 3.2)	Step 1 :$CH_4+2O_2 \rightarrow CO_2+2H_2O$ Step 2 :$2CH_4+0.5O_2 \rightarrow C_2H_6+H_2O$ Step 3 :$CH_4+O_2 \rightarrow CO+H_2O+H_2$ Step 4 :$CO+0.5O_2 \rightarrow CO_2$ Step 5 :$C_2H_6+0.5O_2 \rightarrow C_2H_4+H_2O$ Step 6 :$C_2H_4+2O_2 \rightarrow 2CO+2H_2O$ Step 7 : $C_2H_6 \rightarrow C_2H_4+H_2$ Step 8 :$C_2H_4+2H_2O \rightarrow 2CO+2H_2O$ Step 9 :$CO+H_2O \rightarrow CO_2+H_2$ Step 10 :$CO_2+H_2 \rightarrow CO+H_2O$	$r_j = \frac{k_{0j} e^{-\frac{E_{0,j}}{RT}} P_C^{m_j} P_{O_2}^{n_j}}{(1 + K_{jCO_2} e^{-\Delta H_{od,O_2/RT}} P_{CO_2})^2} \quad j = 1,3-6$ $r_2 = \frac{k_{02} e^{-\frac{E_2}{RT}} (K_{0O_2} e^{-\Delta H_{od,O_2/RT}} P_{O_2})^{n_1} P_{CH_4}}{[1 + (K_{0O_2} e^{-\Delta H_{od,O_2/RT}} P_{O_2})^{n_1} + K_{0O_2} e^{-\Delta H_{od,O_2/RT}} P_{O_2}]^2}$ $r_7 = k_{07} e^{-E/RT} P_{C_2H_6}^{m_7}, \qquad r_8 = k_8 e^{-E/RT} P_{C_2H_6}^{m_8} P_{H_2O}^{n_8}$ $r_9 = k_{09} e^{-E/RT} P_{CO_2}^{m_9} P_{H_2}^{n_9}, \qquad r_{10} = k_{10} e^{-}$
Danespayeh *et al.* (The kinetic parameters were summarized in Table 3.3	Step 1 : $2CH_4+0.5O_2 \rightarrow C_2H_6+H_2O$ Step 2 : $CH_4+2O_2 \rightarrow CO_2+H_2O$ Step 3 :$CH_4+O_2 \rightarrow CO+H_2O+H_2$ Step 4 :$CO+0.5O_2 \rightarrow CO_2$ Step 5 :$C_2H_6+0.5O_2 \rightarrow C_2H_4+H_2O$ Step 6 :$C_2H_4+2O_2 \rightarrow 2CO+2H_2O$ Step 7 :$C_2H_4+2H_2O \rightarrow 2CO+4H_2$ Step 8 :$C_2H_6 \rightarrow C_2H_4+H_2$ Step 9 :$CO_2+H_2 \rightarrow CO+H_2O$ Step 10 :$CO+H_2O \rightarrow CO_2+H_2$	$r_1 = \frac{k_{01} e^{-\frac{E_1}{RT}} (K_{0O_2} e^{-\Delta H_{od,O_2/RT}} P_{O_2})^{n_1} P_C^{n}}{[1 + (K_{0O_2} e^{-\Delta H_{od,O_2/RT}} P_{O_2})^{n_1}]^2}$ $r_j = k_{0j} e^{-E/RT} P_C^{m_j} P_{O_2}^{n_j} \quad j = 2-6$ $r_7 = k_{07} e^{-E/RT} P_{C_2H_4}^{m_7} P_{H_2O}^{n_j}, \qquad r_8 = k_{08} e^{-E/RT} P_{C_2H_6}^{m_8}$ $r_9 = k_{09} e^{-E/RT} P_{CO_2}^{m_9} P_{H_2}^{n_9}, \qquad r_{10} = k_{10} e^{-E/RT} P_{CO}^{m_{10}} P_{H_2O}^{n_{10}}$

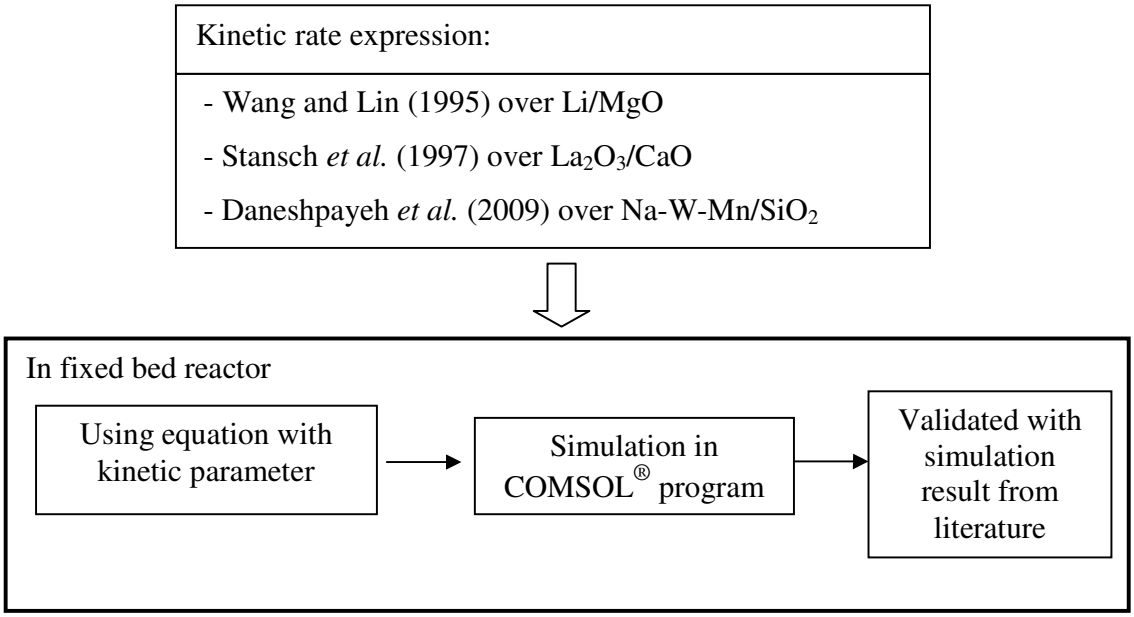

Figure 4.2 Diagrams in achieving validation of simulation

Start from using kinetic models with kinetic parameters (demonstrated in diagram) to simulate OCM in a fixed bed reactor using COMSOL® program under the same operating condition reported in the literature and then validate the model with the simulation results of the paper. Procedure for the model validation was shown in Figure 4.2;

In reactor model, the transport phenomena were coupled with reaction kinetics to develop a reactor model. The two-dimensional flow field in a fixed bed reactor and membrane reactor were coupled with the mass and heat transport for simulation performance of the OCM process. As well as, velocity, concentration and temperature profiles. Formulation of the reactor model equations was given below.

4.1.2 Reactor model

Geometry of fixed bed and membrane reactor are presented in Figures 4.3a and 4.3b respectively.

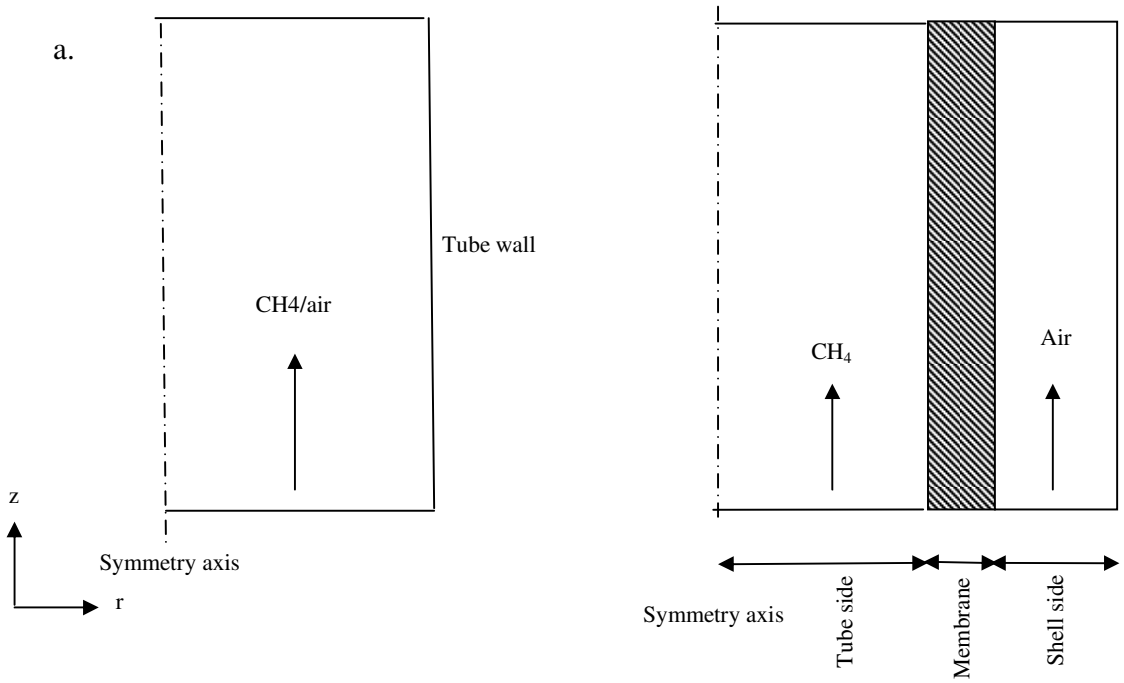

Figure 4.3 Geometry of FBR (a.) and MR (b.)

Figure 4.3 a. shows the scheme of FBR. Methane and air were mixed and co-fed to an impermeable tubular reactor; inner tube was filled with bed of catalyst. The membrane reactors in this study were double tubular reactors (resembles like a shell and tube heat exchanger) as shown in Figure 4.3 b. The tube wall was made of different membrane type i.e. porous-alumina Membranox membrane, a dense $Ba_{0.5}Sr_{0.5}Co_{0.8}Fe_{0.2}O_{3-\delta}$, and $La_{0.4}Sr_{0.6}Ga_{0.4}Fe_{0.6}O_{3-\delta}$ membrane. The tube was filled with bed of catalyst and outer shell was an impermeable wall. CH_4 was fed into the reactor from the tube side whereas mixture of oxygen and nitrogen resembling air composition were fed into the reactor from the shell side.

All the reactors were based on the following assumptions:

- Two-dimensional mathematical model
- Steady-state conditions
- Plug flow condition for all models
- Ideal gas behavior was applied for all gas components.
- Diffusivity in catalyst bed was assumed to be Knudsen mechanism.
- Membrane reactor resembles like a shell and tube heat exchanger

4.1.2.1 Governing equations

Mass balance; the mass balance for each of the eight components can be written as

$$\left(\frac{\partial^2 C_i}{\partial r^2} + \frac{1}{2}\frac{\partial C_i}{\partial r}\right) + D_i \frac{\partial^2 C_i}{\partial z^2} - u\frac{\partial C_i}{\partial z} + \rho_B r_i = 0 \qquad (4.1)$$

The rate of production was calculated for each component from the stoichiometry of the reactions.

Energy balance; the energy balance for the reactor can be written as

$$\lambda\left(\frac{\partial^2 T}{\partial r^2} + \frac{1}{2}\frac{\partial T}{\partial r}\right) + \frac{\partial^2 T}{\partial z^2} - u\rho_f C_p \frac{\partial T}{\partial z} + Q = 0 \qquad (4.2)$$

The heat source in Equation (4.2) including heat of reaction and heat flux were computed by

$$Q = \sum_{i=1}^{n} \Delta H_{rxn} r_i + U(T - T_{ex}) \qquad (4.3)$$

Momentum balance, the momentum balance for reactor describes flow in porous media. The equation extends Darcy's law combination with the continuity equation;

$$\nabla\left(-\eta(\nabla u + (\nabla u)^T)\right) + \frac{k}{\eta}u = 0 \quad (4.4)$$

The matrix of partial differential equation used in model, initial and boundary condition as described in Appendix A.

The performance of the reactor was evaluated by the conversion of reactants as well as selectivity and yield of products. The conversion was defined as the fraction of the reactant reacted to the reactant fed. For example the conversion of methane was

$$CH_4 \text{ conversion } \% = \frac{F^0_{CH_4} - F_{CH_4}}{F^0_{CH_4}} \times 100 \quad (4.5)$$

and the C_2 selectivity was defined as C_2 product formed per reactant consumed.

$$C_2 \text{ selectivity } \% = \frac{2\times(F_{C2H4}+F_{C2H6})}{(2(F_{C2H4}+F_{C2H6})+F_{CO}+F_{CO2})} \times 100 \quad (4.6)$$

Moreover, the COx selectivity was defined as COx byproduct formed per reactant consumed.

$$\text{COx selectivity } \% = \frac{F_{CO}+F_{CO2}}{(2(F_{C2H4}+F_{C2H6})+F_{CO}+F_{CO2})} \times 100 \quad (4.7)$$

While yield referred to the specific product formed per reactant fed.

$$C_2 \text{ yield } \% = \frac{2\times(F_{C2H4}+F_{C2H6})}{F^0_{CH_4}} \times 100 \quad (4.8)$$

In addition, in fixed bed reactor, the effect of operating variables under three operating modes i.e. isothermal, adiabatic, non-isothermal condition were considered.

From simulation results in fixed bed reactor, comparative simulation results of different catalyst were performed. The highest performance catalyst was selected for later use in a membrane reactor. Then different types of membranes present in literature (i.e.

Membranox (Kao *et al.* (2003)), $Ba_{0.5}Sr_{0.5}Co_{0.8}Fe_{0.2}O_{3-\delta}$ (Wang *et al.* (2003)) and $La_{0.4}Sr_{0.6}Ga_{0.4}Fe_{0.6}O_{3-\delta}$ (Shaula *et al.* (2003))) were varied. Flux equations of different membranes were shown in equation 4.8 – 4.13. The simulations were carried out by using COMSOL® program to determine a suitable model for the OCM process.

- In Membranox membrane, the diffusion flux of each species is calculated according to following equation:

$$J_i = \frac{D_{i,k}}{RT}\frac{(P^1 y_i^1 - P^2 y_i^2)}{\delta} \quad (4.9)$$

The Knudsen coefficient is calculated by the following formula :

$$D_{i,k} = \frac{2}{3}\frac{\varepsilon}{\tau} r \left(\frac{8RT}{\pi M_i}\right)^{0.5} \quad (4.10)$$

- Flux equation of $Ba_{0.5}Sr_{0.5}Co_{0.8}Fe_{0.2}O_{3-\delta}$ (BSCFO) membrane can be expressed as

$$J_{O_2} = \frac{\pi L C_i D_a}{2Sln(\frac{r_1}{r_2})} \ln\left(\frac{P_1}{P_2}\right) \quad (4.11)$$

- Flux equation of $La_{0.4}Sr_{0.6}Ga_{0.4}Fe_{0.6}O_{3-\delta}$ (LSGFO) membrane can be expressed as

$$J_{O_2} = \frac{Per_{O_2}}{d} ln \frac{P_1}{P_2} \quad (4.12)$$

Where

$$Per_{O_2} = 0.0645 \exp\left(\frac{-108400}{RT}\right) \quad (4.13)$$

4.2 Study and analysis on the effect of operating variables

In this part, we studied and analyzed the effect of operating variables such as CH_4/O_2 ratio, GHSV and temperature in the fixed bed reactor, and reactant feed flow rate, deviation in radius axis and pressure drop in the membrane reactor on the reaction performances such as conversion, selectivity, yield via expression of surface plot for each profile (concentration and temperature profiles).

4.3 Performance comparison between the two reactors

The simulation results obtained were compared between the fixed bed reactor and the membrane reactor under the same operating condition and/or same physical dimension of the reactor

4.4 Optimum conditions with 2D model

From the simulation, the results were determined to find an appropriate system at its optimum condition

CHAPTER V

RESULTS AND DISCUSSION

Simulations were carried out for OCM in fixed bed and membrane reactor. The conditions used in the simulation were summarized in Table 5.1 and, the catalyst and membrane properties were presented in Table 5.2

Table 5.1 Reactor dimension and conditions

Condition	Dimension
Fixed bed reactor	
Length of catalyst bed (m)	0.2
Diameter (m)	0.018
Temperature (K)	993-1173
Pressure (kPa)	101.325
CH_4/O_2 ratio	3.4-7.5
GHSV (h^{-1})	18000-30000
Membrane reactor	
Length (m)	0.2
Tube diameter (m)	0.018
Shell diameter (m)	0.02
Temperature (K)	993-1173
Pressure (kPa)	101.325
Volumetric flow rate in shell (m^3/s)	0.00004-0.00052
Volumetric flow rate in tube (m^3/s)	0.00014-0.0007

Table 5.2 Catalyst and membrane properties

Property	**catalyst**		
	Li/MgO	La_2O_3/CaO	Na-W-Mn/SiO_2
Average pore radius (m)	0.0005	0.01	0.00008
Porosity (-)	0.34	0.6	0.6
Totousity (-)	2.153	3	1.089
Thermal conductivity (W/m K)	10.3	1	1.35
Permeability (m^2)	2.29179×10^{-9}	8.33×10^{-7}	4.04669×10^{-10}

5.1 Model validation

The validation of the kinetic model (for Li/MgO, La_2O_3/CaO and Na-W-Mn/SiO_2 catalyst) was carried out first to ensure that the mathematics models could well predict the OCM performances. The models used were two-dimensional plug flow model.

The validity of Li/MgO catalyst using kinetic rate expression reported by Wang and Lin, (1995) was assessed by comparing our simulation results with simulation data from literature (Kao *et al.,* (1997)) in the fixed bed reactor. Figure 5.1 (a), shows yield of C_2 products versus run numbers under the condition of literature which was shown in Table 5.3. Figure 5.1 (b) shows validation results of La_2O_3/CaO catalyst by comparing our simulation results with simulation data reported by Tye *et al.,* (2002) in term of C_2 yield versus run numbers under the condition of literature which was shown in Table 5.4 and Figure 5.1 (c) shows the comparison of our results with literature reported by Daneshpayeh *et al*. (2009) for Na-W-Mn/SiO_2 catalyst providing conversion of CH_4 at space time in a range of 16.5 – 19 kg m^3/s, temperature at 1048 K. It can be seen that our simulation results agreed well with simulation data from literature.

Table 5.3 Condition for different run number (Kao *et al.,* (1997))

Condition	Run no.							
	1	2	3	4	5	6	7	8
Temperature(K)	993							
Feed flow rate (mL/s)	0.83							
Feed composition								
- He	0.8921	0.8566	0.7882	0.3347	0.8842	0.8763	0.8447	0.5592
- CH_4	0.0724	0.1118	0.1118	0.3987	0.0776	0.0763	0.1171	0.2868
- O_2	0.0355	0.0316	0.1000	0.2066	0.0382	0.0474	0.0382	0.1540

Table 5.4 Condition for different run number (Tye *et al.,* (2002))

Condition	Run no.					
	1	2	3	4	5	6
Temperature (K)	1023	1073	1103	973	1023	1103
Feed flow rate (cm^3/s)	4					
Feed molar ratio						
- CH_4	0.612	0.612	0.612	0.699	0.699	0.699
- O_2	0.051	0.051	0.051	0.095	0.095	0.095
- N_2	0.337	0.337	0.337	0.206	0.206	0.206

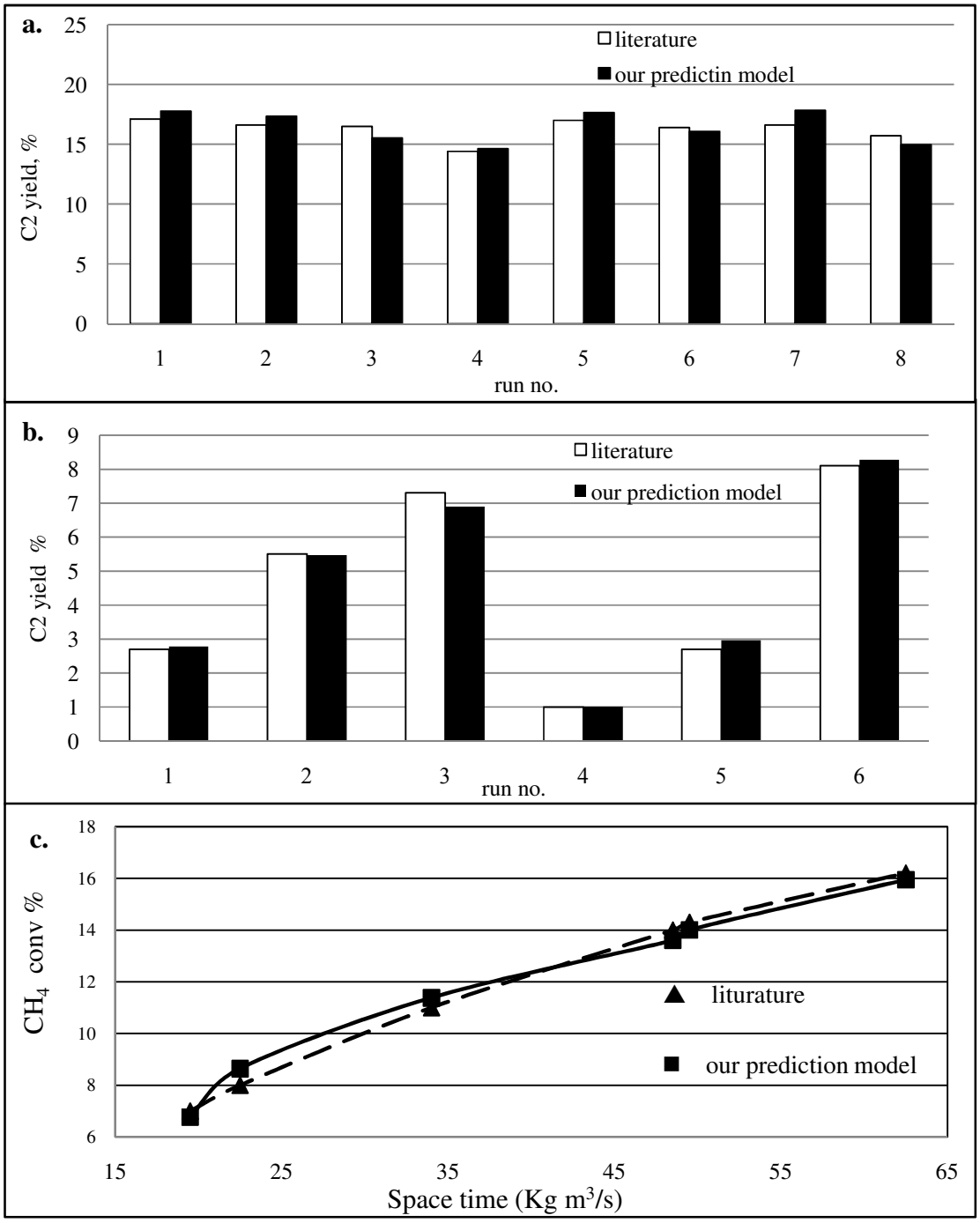

Figure 5.1 Comparison between of literature with our prediction model over Li/MgO (a.), La_2O_3/CaO (b.) and Na-W-Mn/SiO_2 (c.) catalysts.

5.2 Catalyst selection

This section present concerns the selection of a suitable catalyst among Li/MgO, La_2O_3/CaO and Na-W-Mn/SiO_2 catalysts at various conditions i.e. gas hourly space velocity (GHSV) CH_4/O_2 ratio and temperature. The system was based on a fixed bed reactor under isothermal operation mode. Summary of the operating conditions in this section was shown in Table 5.5.

Performance of OCM reaction was considered in term of CH_4 conversion and C_2 selectivity. Figure 5.2 shows activities of the three catalysts for GHSV in a range of 18000-30000 1/h. The order of CH_4 conversion follows Na-W-Mn/SiO_2 > La_2O_3/CaO > Li/MgO. The CH_4 conversion was decreased with the increase of GHSV for all catalysts.

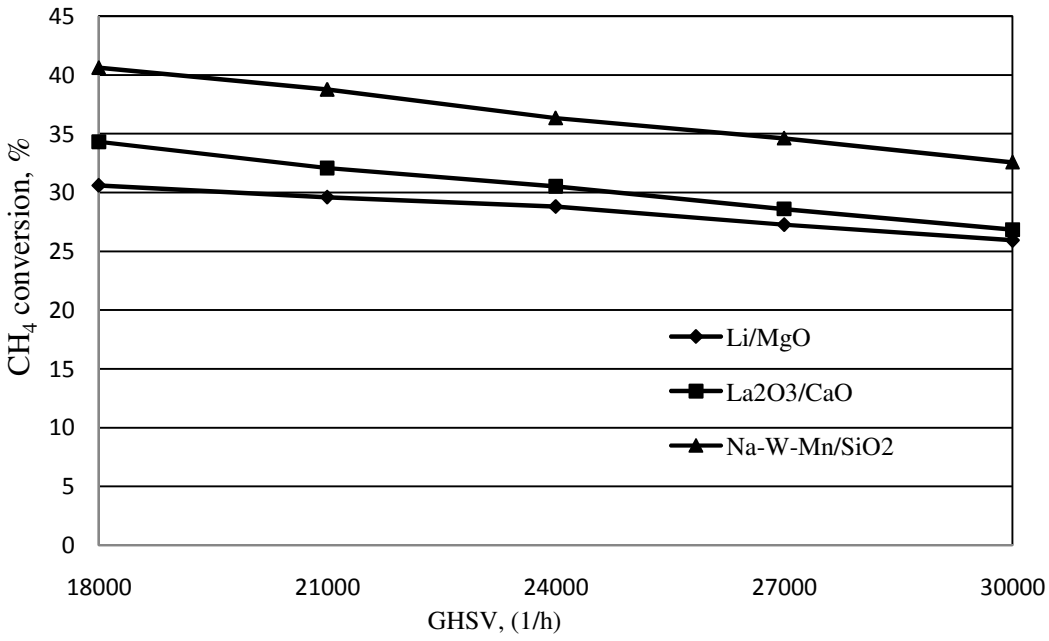

Figure 5.2 Effect of GHSV on CH_4 concentration

Figures 5.3-5.7 show results of C_2 and COx (CO and CO_2) selectivity to CH_4 conversion at position of reactor length (inlet of reactor at CH_4 conversion was set at zero) under different conditions which was summarized in Table 5.5. From all figures, CH_4 conversion was increased, C_2 selectivity was decreased and COx selectivity was increased by the distance from the inlet to the reactor for all catalysts. It was obvious that

CH_4 conversion for Na-W-Mn/SiO_2 catalyst was higher than La_2O_3/CaO and Li/MgO catalyst, respectively. Moreover, C_2 selectivity for Na-W-Mn/SiO_2 catalyst was higher than Li/MgO and La_2O_3/CaO catalysts, respectively. COx selectivity for La_2O_3/CaO catalyst was higher than Li/MgO and Na-W-Mn/SiO_2catalysts, respectively at all conditions. In addition, even La_2O_3/CaO catalyst offers CH_4 conversion higher than Li/MgO catalyst but the C_2 selectivity was lower. The comparison of OCM performance between catalysts at various CH_4/O_2 ratios was shown in Figures 5.3-5.5. The CH_4 conversion was decreased while the C_2 selectivity was increased and the COx selectivity was decreased with increasing of CH_4/O_2 ratio for all catalysts. Moreover, the comparison of OCM performance between different catalysts at various temperatures was shown in Figures 5.5-5.7. The CH_4 conversion was increased, the C_2 selectivity was decreased and the COx selectivity was increased with increasing of temperature. It should be noted that at higher temperature, rate of decreased C_2 selectivity was more than at lower temperature, for example, with Li/MgO catalyst, at 1173 K difference of C_2 selectivity between outlet to inlet was 4.43 % but at 993 K and 1073 K were 3.58 % and 3.84 % respectively. The maximum C_2 yields for all catalysts at temperature of 1173 K and CH_4/O_2 ratio of 3.4 were 30.07, 19.2 and 20.43 % for Na-W-Mn/SiO_2, La_2O_3/CaO and Li/MgO, respectively. The simulation results indicated that Na-W-Mn/SiO_2 catalyst offers the best performances among all the catalysts under isothermal mode.

Table 5.5 Summary of operating condition for catalyst selection study

Figure	condition		
	GHSV(1/h)	Temperature (K)	CH_4/O_2 ratio
5.2	18000-30000	993	3.4
5.3	-	1173	7.5
5.4	-	1173	4.2
5.5	-	1173	3.4
5.6	-	1073	3.4
5.7	-	993	3.4

a.

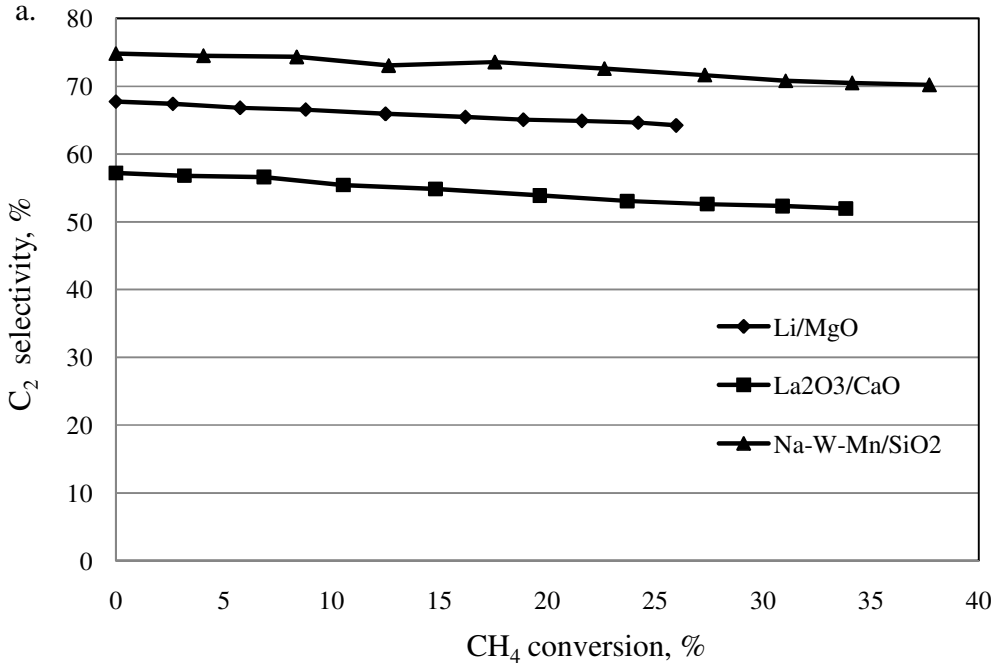

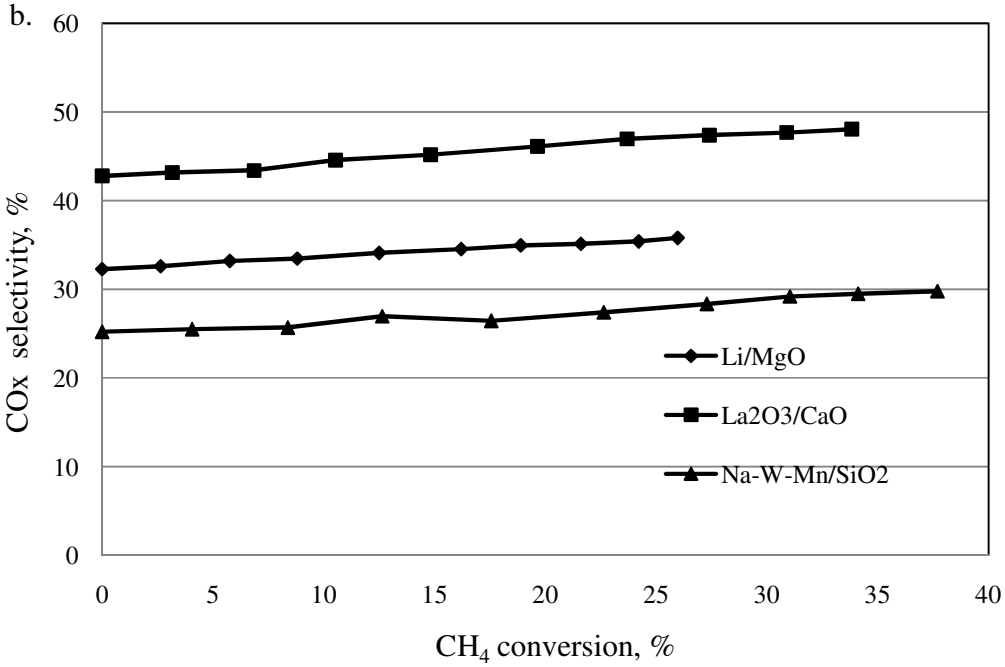

Figure 5.3 Conversion VS C_2 selectivity (a.), Conversion VS COx selectivity (b.) (T=1173 K, CH_4/O_2 ratio = 7.5)

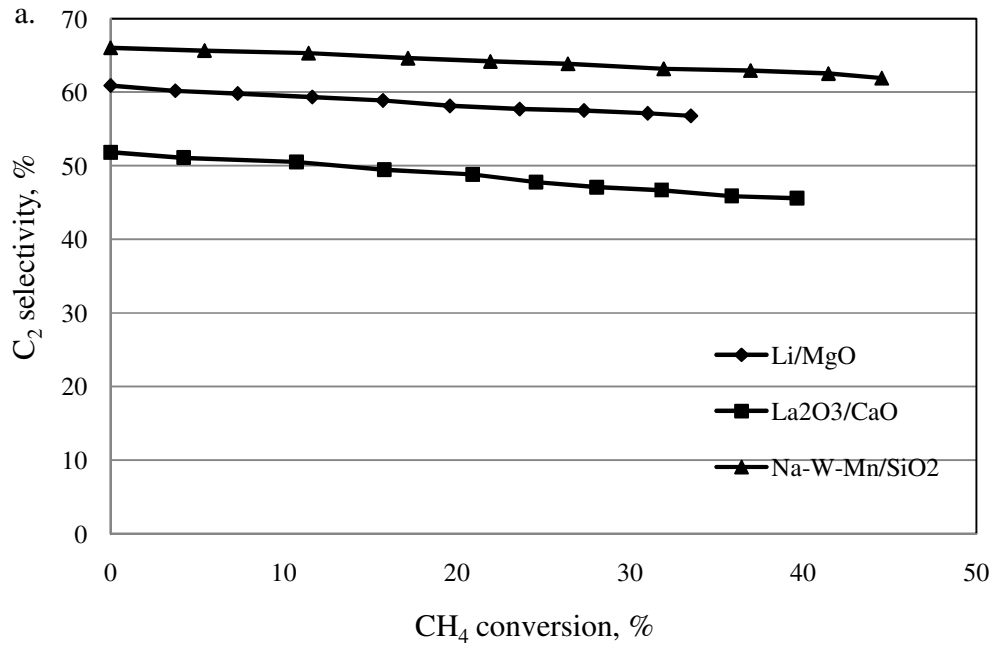

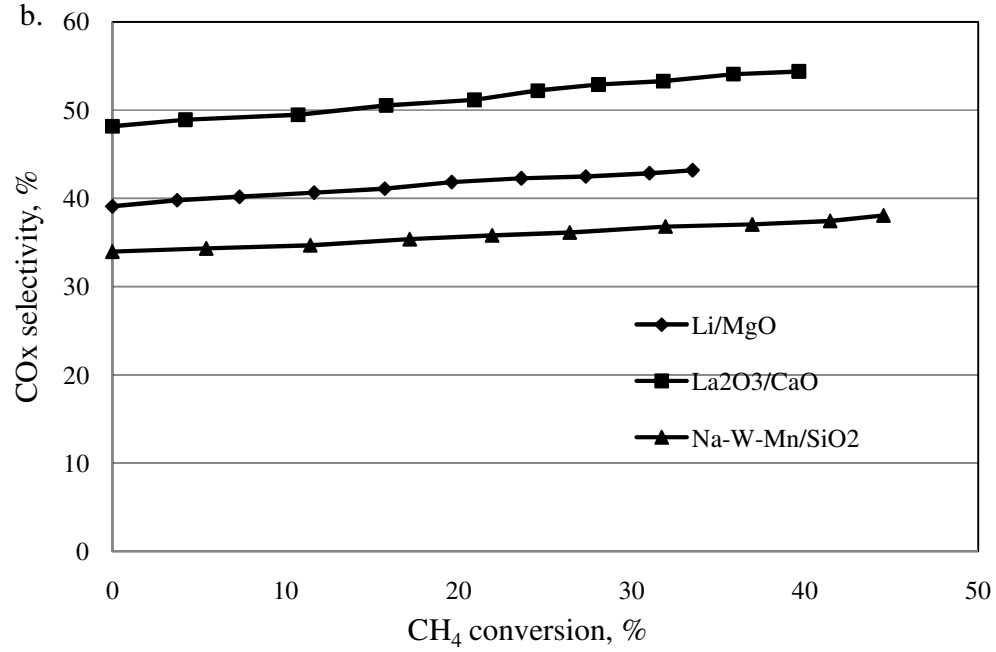

Figure 5.4 Conversion VS C_2 selectivity (a.), Conversion VS COx selectivity (b.) (T=1173 K, CH_4/O_2 ratio = 4.2)

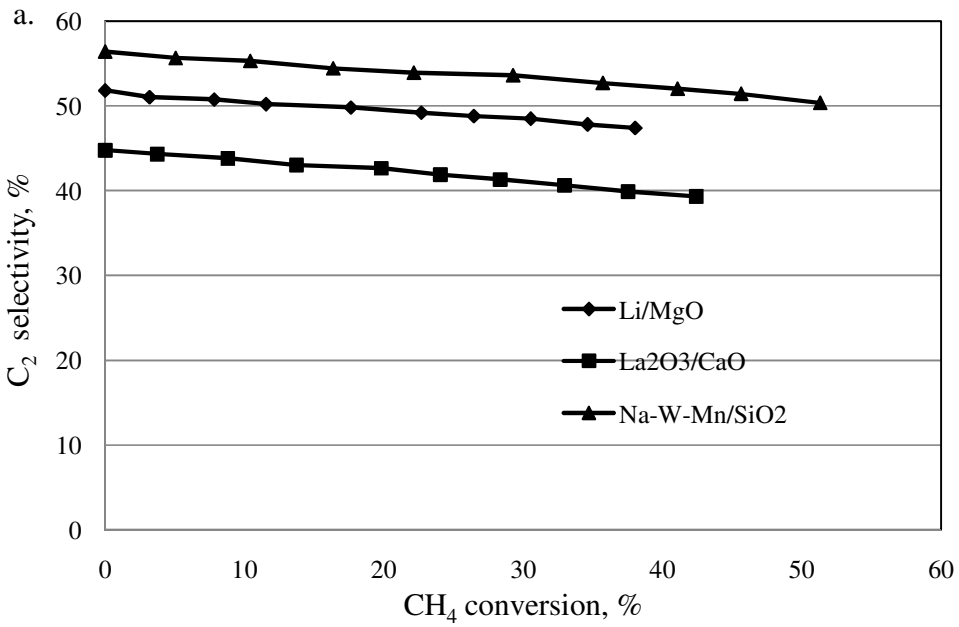

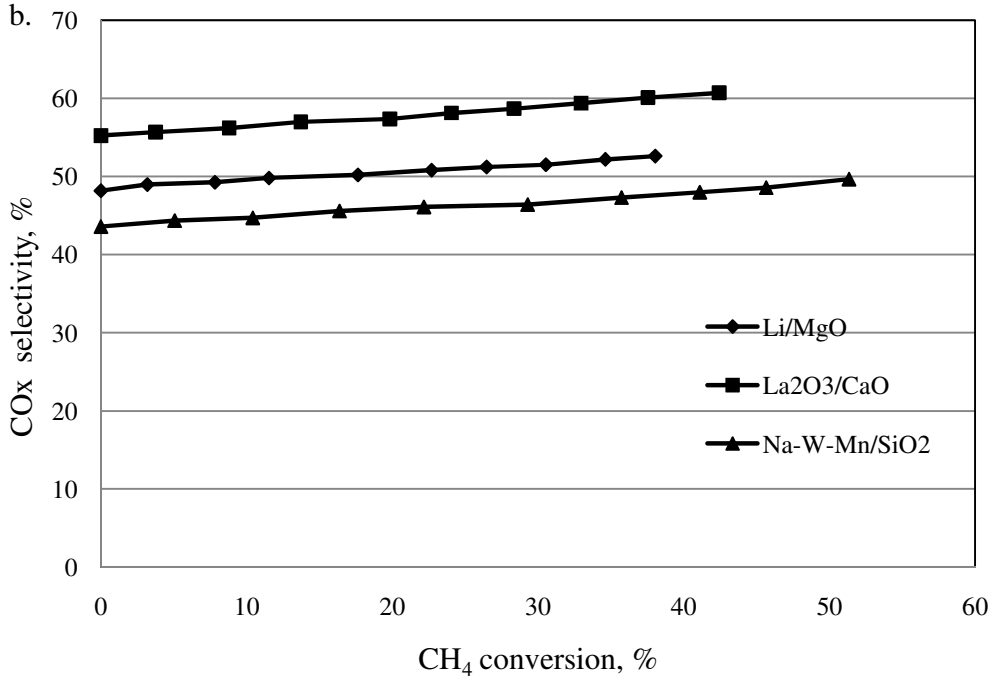

Figure 5.5 Conversion VS C_2 selectivity (a.), Conversion VS COx selectivity (b.) (T=1173 K, CH_4/O_2 ratio = 3.4)

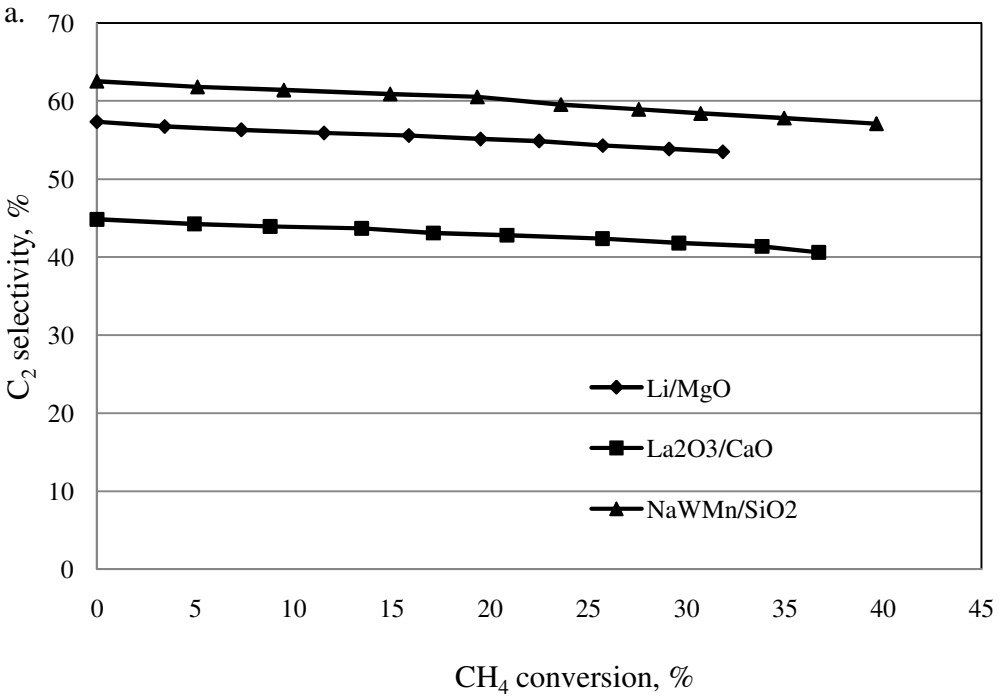

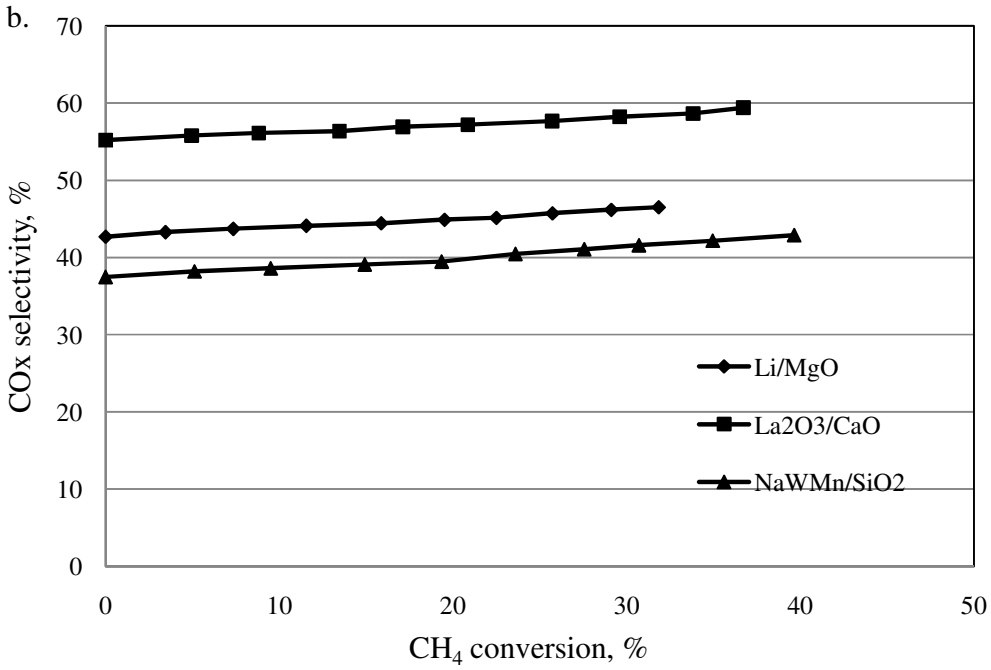

Figure 5.6 Conversion VS C_2 selectivity (a.), Conversion VS COx selectivity (b.) (T=1073 K, CH_4/O_2 ratio = 3.4)

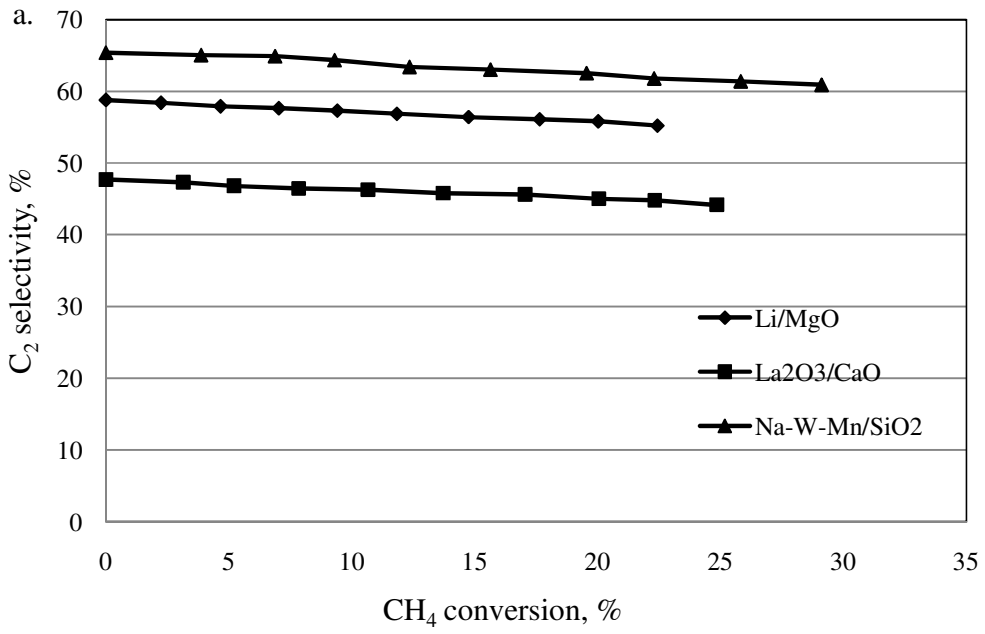

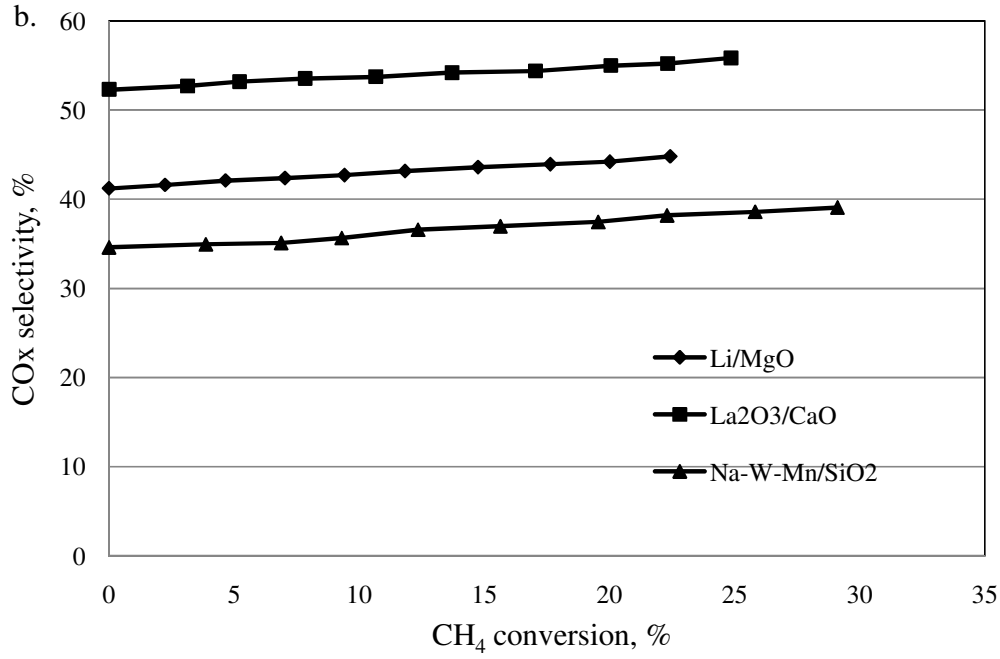

Figure 5.7 Conversion VS C_2 selectivity (a.), Conversion VS COx selectivity (b.) (T=993 K, CH_4/O_2 ratio = 3.4)

5.3 Fixed bed reactor study

From the previous section, we know that the Na-W-Mn/SiO_2 catalyst shows the best performance for OCM reaction. In the present study, this catalyst was selected for this study. Effect of operating condition i.e. GHSV, temperature, CH_4/O_2 ratio and air flow rate was investigated in a fixed bed reactor under non-isothermal mode. The 2-dimensional model was employed to explore the profiles of temperature and concentration in the axial and radial directions.

5.3.1 Effect of GHSV

The effect of GHSV in a range 9000-33000 1/h, CH_4/O_2 ratio of 2 and temperature at 1073 K on CH_4 conversion and C_2 selectivity was presented in Figure 5.8. CH_4 conversion was decreased, whereas, C_2 selectivity was increased with the increase of GHSV. Increasing GHSV results in lower contact time and hence, CH_4 and O_2 conversions were decreased (Figure 5.9 for O_2 conversion). However, it was more favorable for the C_2 hydrocarbon production because shortening contact time between C_2 products with the oxygen can limit the formation of carbon oxides.

Figure 5.10 shows ethylene concentration profile. The GHSV was considered at 9720 (a.), 16197.3 (b.), 25915.7 (c.) and 32394.6 (d.) 1/h. temperature and CH_4/O_2 were fixed at 1073 and 2, respectively. From Figures 5.10a – 5.10b, ethylene was decreased in the middle of a reactor because it reacts with oxygen to carbon oxides. However, when GHSV increases, observed decrease in the amount of ethylene was less as shown on Figures 5.10 (b.) - (d.), respectively. Figure 5.11 shows temperature profile under this condition. For a lower GHSV results (a. and b), dissipation of the hot spot along axis of the reactor was observed because OCM reaction and oxidation of hydrocarbons was highly exothermic. The reactor temperature increases as the reaction heat was accumulated. In this study, the hot spot disappears when operating at high GHSV as shown in Figure 5.11 (c. and d).

All of the results indicate that the GHSV has significant influences on both OCM performance and the thermal management of the reactors.

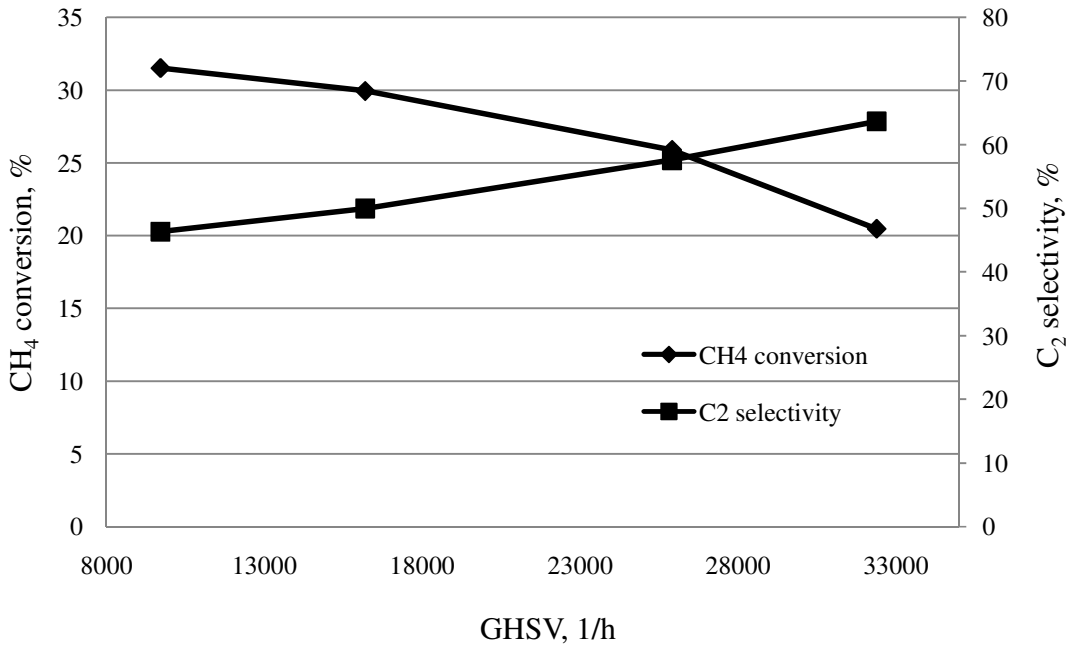

Figure 5.8 Effect of GHSV on CH_4 conversion and C_2 selectivity

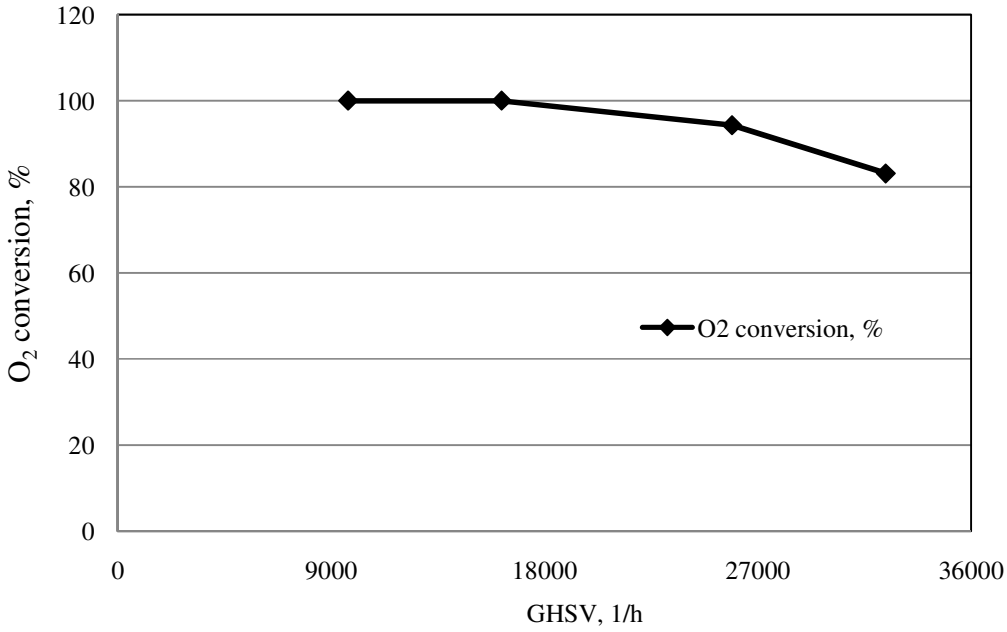

Figure 5.9 Effect of GHSV on O_2 conversion

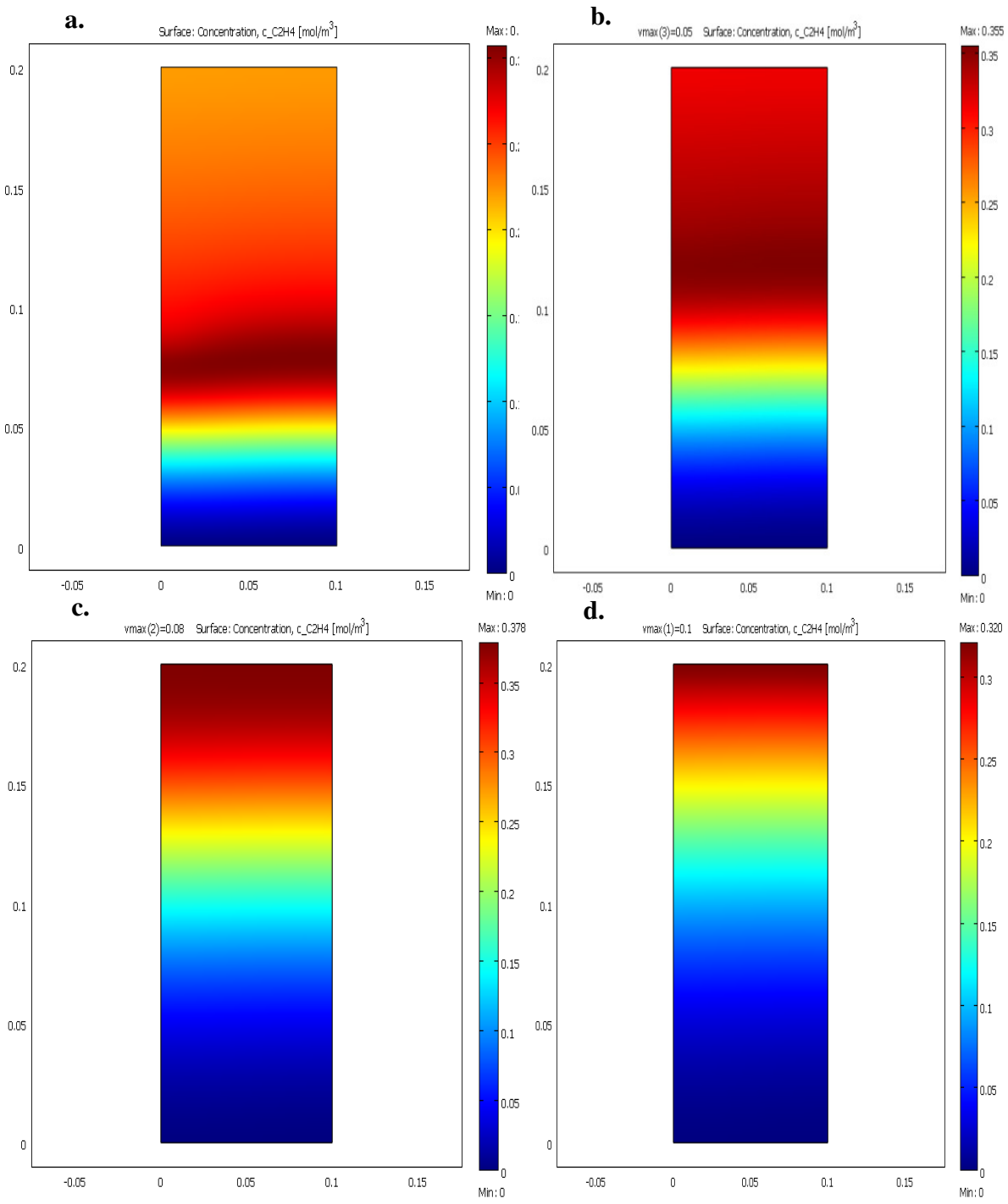

Figure 5.10 Effect of GHSV on ethylene concentration profile at 9720 (a.), 16197.3 (b.), 25915.7 (c.) and 32394.6 (d.) 1/h (CH_4/O_2= 2, *T*= 1073 K)

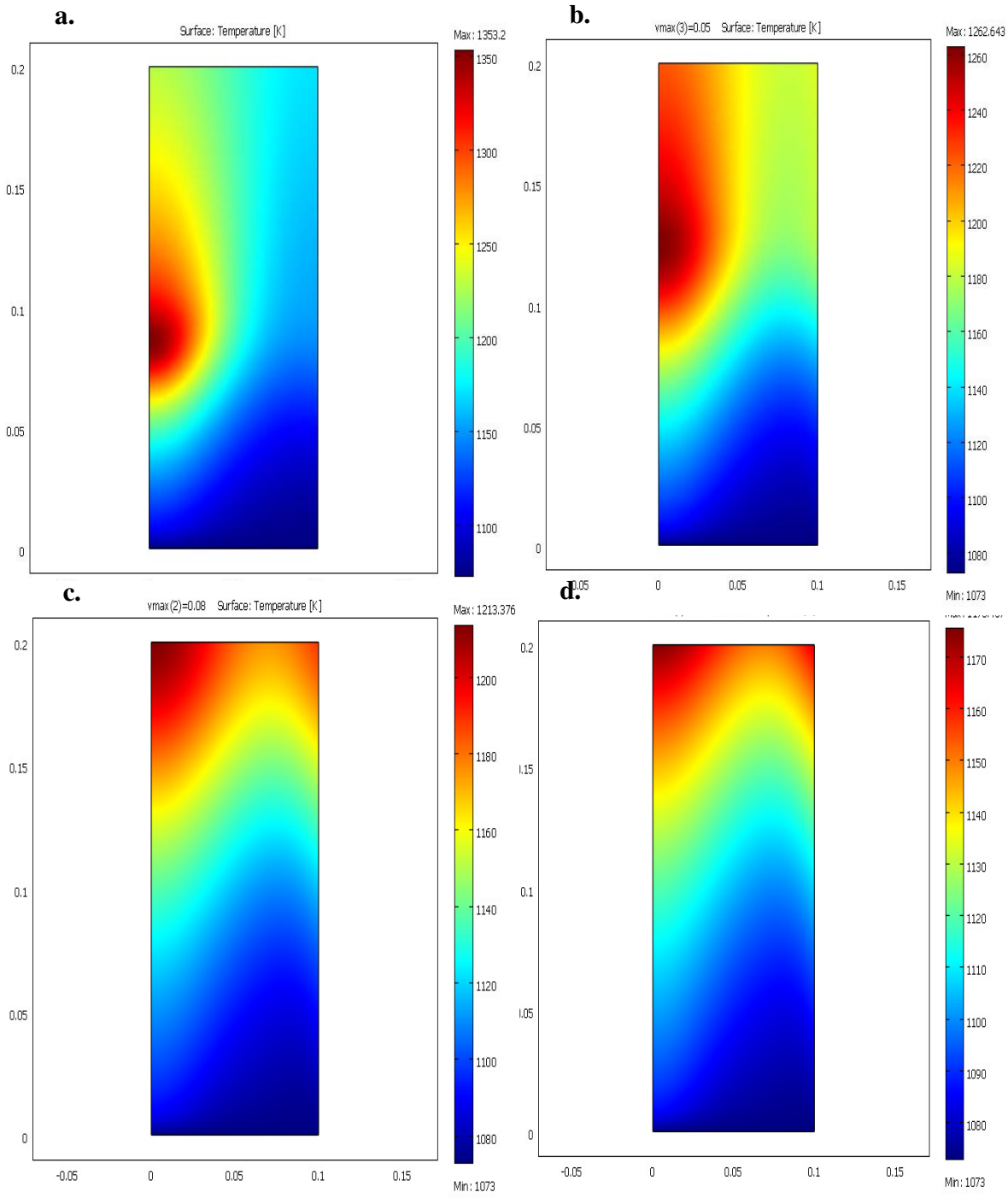

Figure 5.11 Effect of GHSV temperature profile (a.), 16197.3 (b.), 25915.7 (c.) and 32394.6 (d.) (CH_4/O_2= 2, *T*= 1073 K)

5.3.2 Effect of temperature

The effect of temperature on CH_4 conversion and C_2 selectivity was presented in Figure 5.12. The temperature was considered in a range of 993- 1173 K, CH_4 /O_2 ratio was 2 and GHSV was 9720 1/h. It was found that when increasing feed temperature; CH_4 conversion and CO_x selectivity were increased, thus decreasing C_2 selectivity. Hence, too high or too low temperature was not beneficial for C_2 yield. From the result, the best feed temperature would be 1073 K that represents highest C_2 yields.

Figure 5.13 shows temperature profile on feed temperature at 993 (a.), 1023 (b.), 1073 (c.) and 1123(d.) K, CH_4 /O_2 ratio was 2 and GHSV was 9720 1/h. when increasing feed temperature, maximum temperature was found to increase as well.The maximum temperature up to 1543.7 K on inlet temperature was 1123 K. The heat of reaction released in OCM increased with reaction temperature along the reactor. The higher temperature profiles for 1073 K and 1123 K show hot spot occurring along the axis of the reactor. Temperature variation in the radial direction as the same plane in range of 100-150 K hence; safety was a factor should be considered. The wall temperature was an important parameter which was related to the heat removal.

This suggests finding an optimum condition in order to obtain the best system in this FBR study.

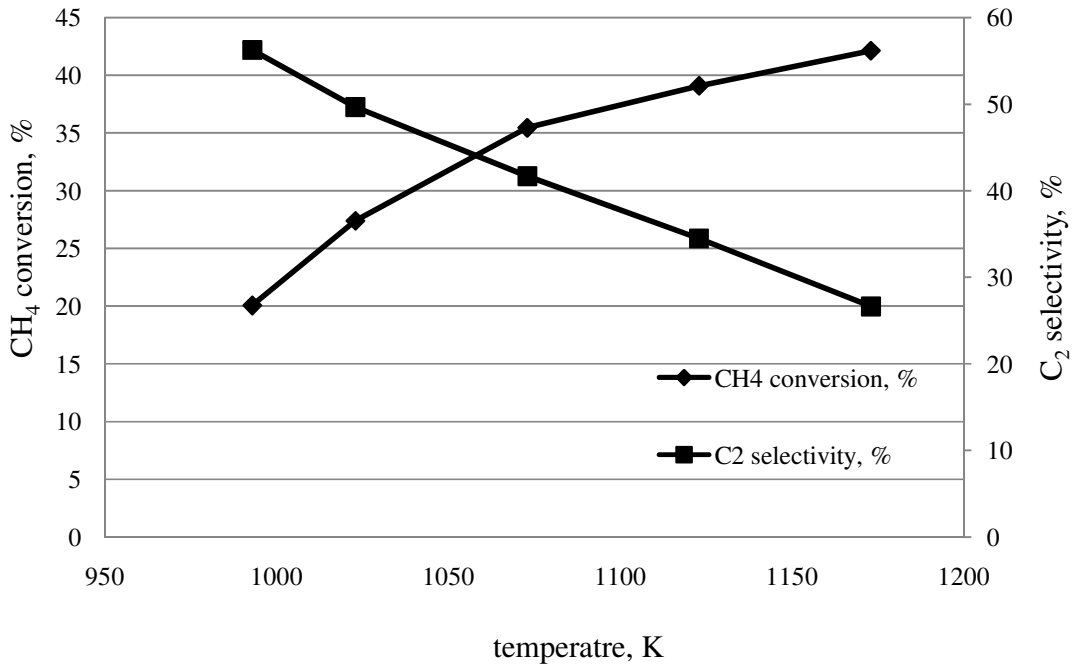

Figure 5.12 Effect temperatures on CH_4 conversion and C_2 selectivity

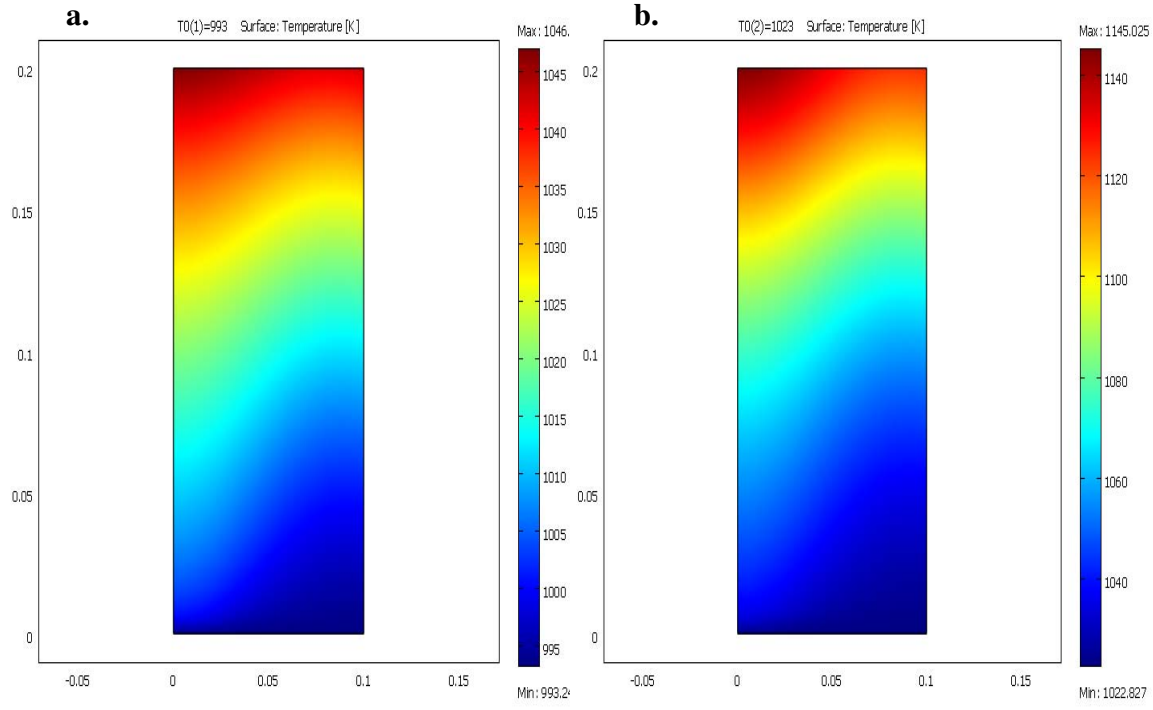

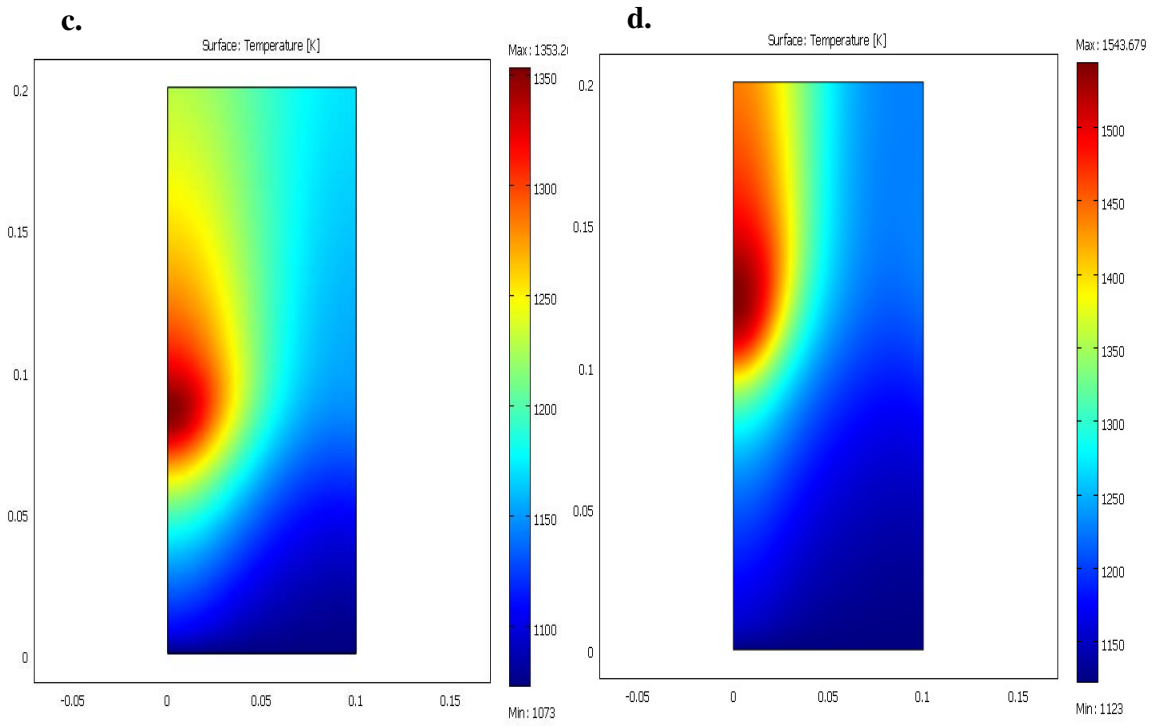

Figure 5.13 Temperature profile at T = 993 (a.), 1023 (b.), 1073 (c.) and 1123(d.) K (CH_4/O_2 = 2, GHSV = 9720 1/h)

5.3.3 Effect of CH_4/O_2 ratio

The effect of CH_4/O_2 ratio in a range 2-7.5 at GHSV of 9720 1/h and temperature of 1073 K on CH_4 conversion and C_2 selectivity were presented in Figure 5.14. CH_4 conversion was decreased, whereas, C_2 selectivity was increased with the increase of CH_4/O_2 ratio. The oxygen also makes the production of methyl radicals which cause the formation of C_2 hydrocarbons. As the oxygen content in feed was decreased to make insufficient oxygen in reaction thus, CH_4 conversion was decreased. However, when the oxygen concentration was high (low CH_4/O_2 ratio) the oxidation of methane and C_2 product becomes pronounced. Figure 5.15 shows oxygen and ethylene concentrations at CH_4/O_2 ratios of 2 and 3.4 in Figures 5.15a and 5.15b, respectively in order to make the comparison on OCM performance. At CH_4/O_2 ratio of 2, Figure 5.15a1 shows O_2 conversion was 100% at the first part of the reactor and CH_4 conversion was high to 55.83 %. Apart from that, Figure 5.15a2 shows that ethylene concentration starts to

decrease at same point of 100 % conversion of oxygen because it was oxidized to CO_x. It was improved with increasing CH_4/O_2 ratio to 3.4 was shown in Figure 5.15b. In addition, the effect of CH_4/O_2 ratio has influence on temperature in the reactor. Figure 5.16 shows temperature profile at CH_4/O_2 ratios of 2 (a.) and 3.4 (b.). It was observed that hot spot was disappeared when the CH_4/O_2 ratio was 3.4.

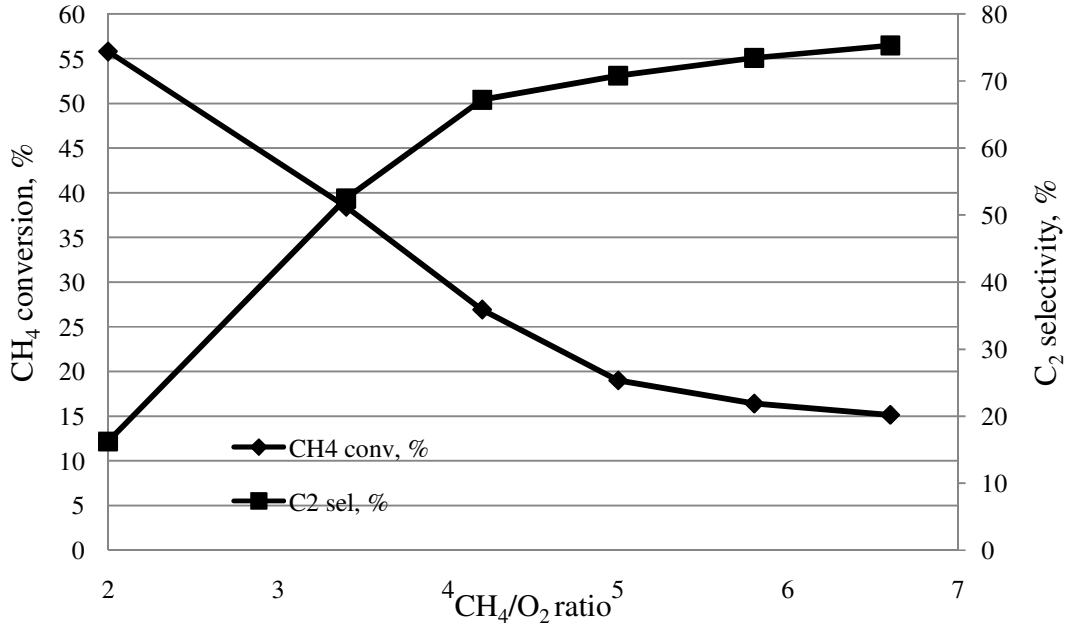

Figure 5.14 Effect CH_4/O_2 ratio on CH_4 conversion and C_2 selectivity

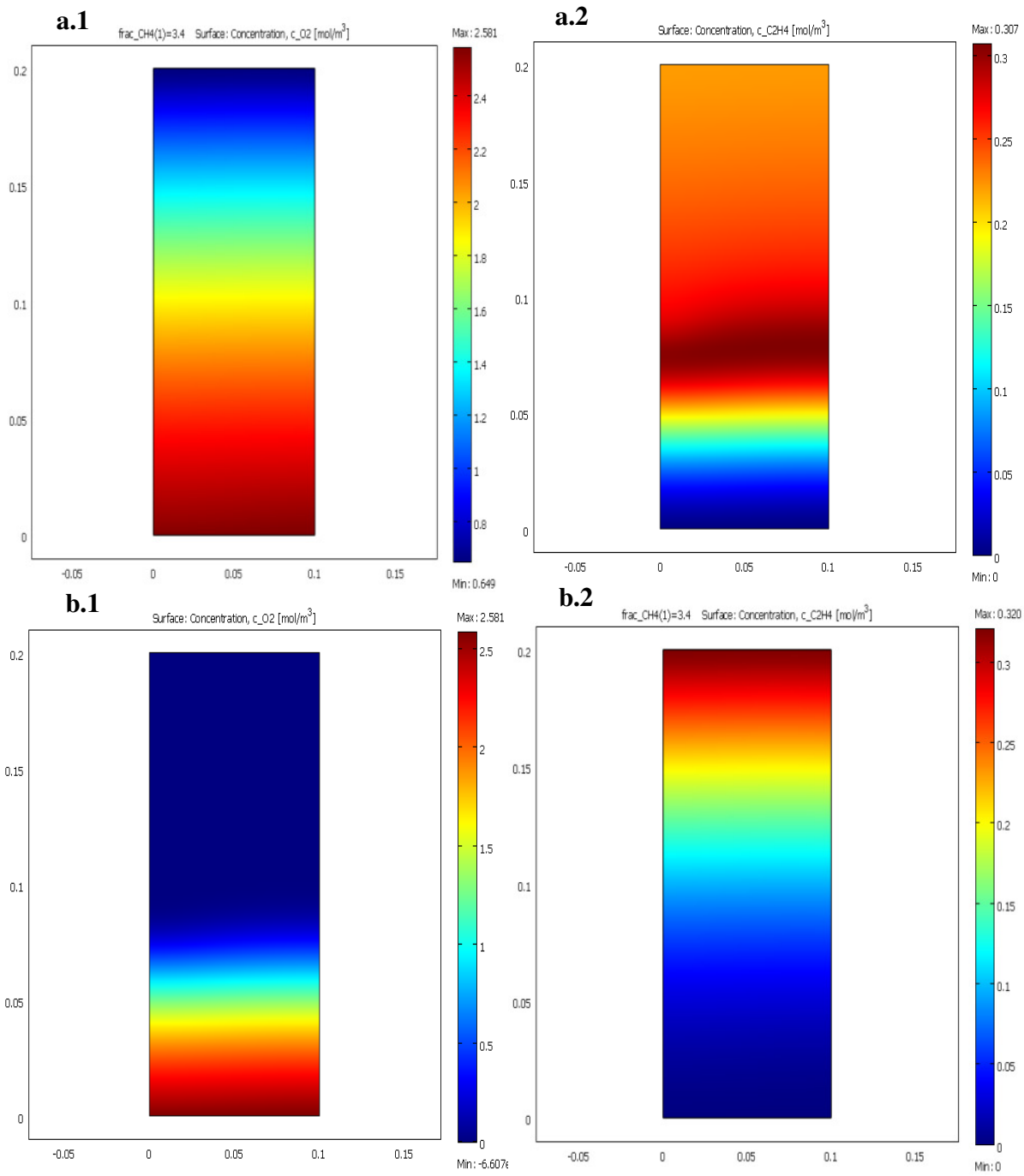

Figure 5.15 Effect of CH_4/O_2 ratio on concentration profile a. CH_4:O_2 =2, *T*=1073 K, GHSV =9720 1/h b. CH_4:O_2 =3.4, *T*=1073 K, GHSV =9720 1/h

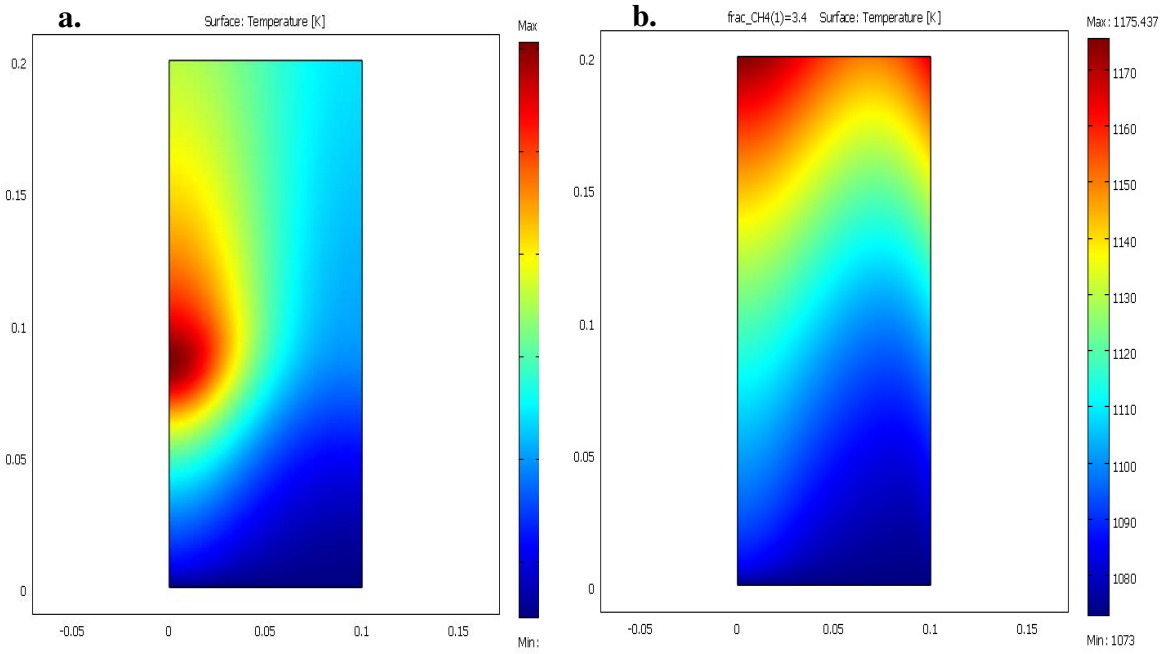

Figure 5.16 Effect of CH_4/O_2 ratio on temperature profile a. CH_4:O_2 =2, *T*=1073 K, GHSV =9720 1/h b. CH_4:O_2 =3.4, *T*=1073 K, GHSV =9720 1/h

5.3.4 Effect of air feed rate

The effect of air feed flow rate in range 0.00004 – 0.00052 m^3/ s for temperature of 1073 K and methane flow rate of 0.000816 m^3/s on CH_4 conversion and C_2 selectivity were presented in Figure 5.17. CH_4 conversion was decreased, whereas, C_2 selectivity was increased with the increase of air feed flow rate. The maximum C_2 a yield was 14.57 % appear at air feed flow rate of 0.00028 m/^{3}s.

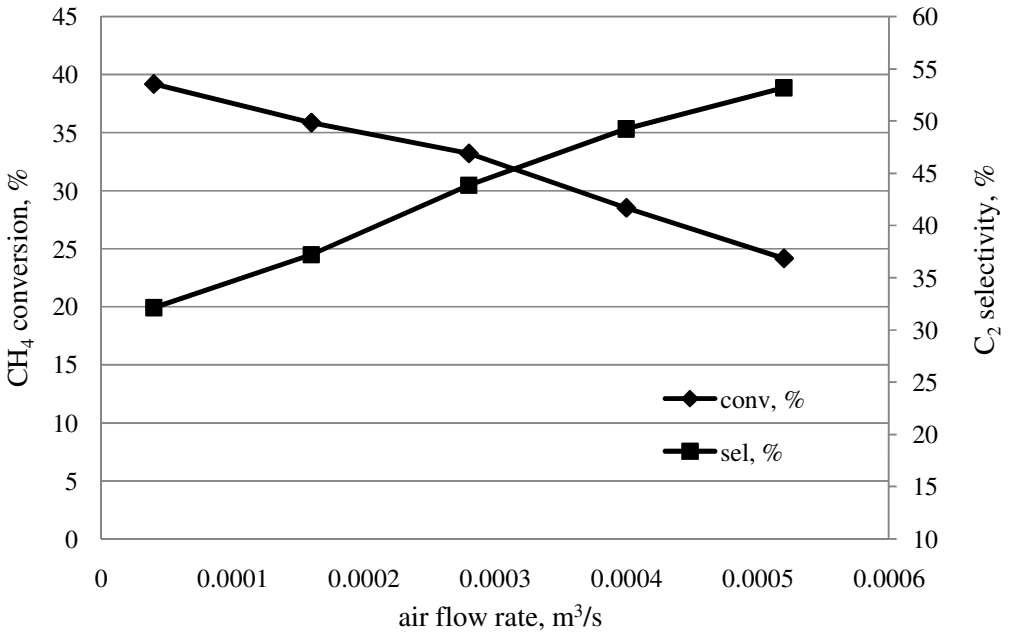

Figure 5.17 a. Effect of air flow rate on CH_4 conversion and C_2 selectivity (T=1073 K, CH_4 flow rate = 0.000816 m^3/s)

5.4 Effect of mode of operation

It was interesting to compare the effect of mode of operation including isothermal, adiabatic and non-isothermal conditions in terms of the CH_4 conversion, C_2 selectivity and C_2 yield. Table 5.6 presents the results of the comparison under the same feed conditions. The OCM process was simulated under conditions of CH_4/O_2 ratio of 3.4, feed temperature of 1073 K and GHSV of 9720 1/h. when comparing between different modes, CH_4 conversion in adiabatic mode was higher than non-isothermal mode and isothermal mode, respectively, but least C_2 selectivity. Moreover, operation in adiabatic mode shows hot spot (region) along axis of the reactor as can be seen from temperature profile in Figure 5.18a. To limit the hot spot, providing some arrangement of cooling around catalyst bed can control temperature in the reaction as demonstrated in the case of non-isothermal operation mode shown in Figure 5.18b. Other methods were proposed to solve for hot spot problem such as shortening the catalyst bed or dilution the first portion of catalyst bed (Moustafa *et al.* (2007)). The maximum yield of 20.16 % was achieved in non-isothermal mode while they were 20.003 % and 17.62 % for isothermal

and adiabatic modes, respectively. Among three different operating conditions, the best result was observed for the non-isothermal mode operation. The nature of OCM reaction was highly exothermic. Hence, to achieve this operation condition, a cooling temperature with a high heat transfer coefficient was required.

Table 5.6 OCM performance at different mode operation

Performance	**isothermal**	**adiabatic**	**Non-isothermal**
CH_4 Conversion, %	36.14	42.27.	38.43
C_2 Selectivity, %	55.35	41.68	52.46
C_2 Yield, %	20.003	17.62	20.16

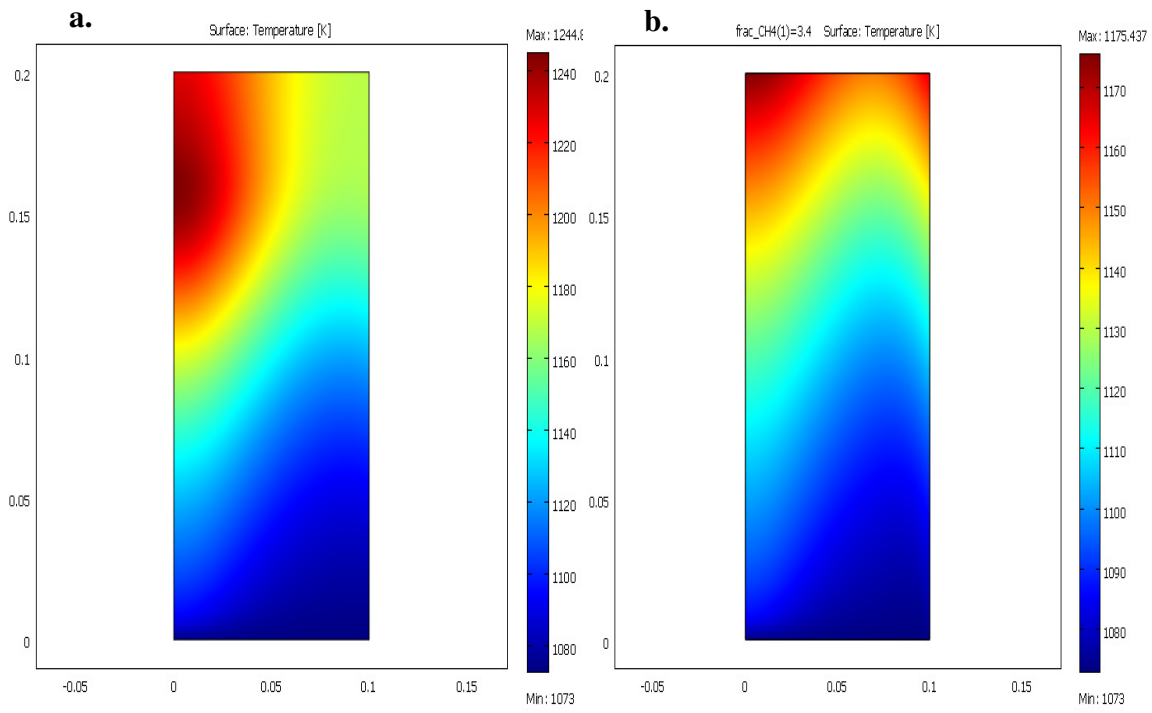

Figure 5.18 Effect of mode of operation on temperature profile a. adiabatic mode b. non-isothermal mode (CH_4:O_2 =3.4, *T*=1073 K, GHSV =9720 1/h)

Membrane reactor

From previous studies, Na-W-Mn/SiO_2 catalyst offers the best performance. In membrane reactor study, this catalyst was selected. In the first part, the characteristics of each type of membrane were investigated. The second part was a comparison of the three types of membranes at various conditions. The last past shows the effect of the variables in the operation of the membrane reactor.

5.5 Characteristics of different membrane reactors

The characteristics of membrane reactor using three different membranes were investigated. Na-W-Mn/SiO_2 OCM catalyst was packed in membrane reactor. The

condition was considered at air flow rate of 0.00028 m^3/s, CH_4 flow rate of 0.00055 m^3/s. and temperature at 993 K.

Figure 5.19 shows the concentration profiles of oxygen concentration at different MR a. $Ba_{0.5}Sr_{0.5}Co_{0.8}Fe_{0.2}O_{3-\delta}$ (BSCFO) MR, b. $La_{0.4}Sr_{0.6}Ga_{0.4}Fe_{0.6}O_{3-\delta}$ (LSGFO) MR and c. Membranox MR. It can be seen that the oxygen feed in the shell side of the reactor permeates through the membrane along the length of the reactor. The membrane acts as a distributor. Oxygen was transported through membrane in form of the lattice oxygen (O^- and O_2^-). The nature of the distribution in each position in the reactor was not uniform in radial direction. In contrast to the assumptions in the one-dimensional model report in literature (Kao *et al.* (2003) and Kiatkittipong *et al.* (2005)) that they assume uniform permeation of oxygen along reactor length. There was maximum radial oxygen concentration distribution in the middle of the reactor. Flux of oxygen in BSCFO MR was higher than those of LSGFO and Membranox MR, respectively. The BSCFO membrane exhibits higher oxygen flux and higher oxygen vacancy concentration than LSGFO due to substitution of La^{3+} by the lower valence state of Ba^{2+} and Sr^{2+}. The higher oxygen vacancy concentration in the BSCF membrane could lead to a higher C_2 formation rate (Wang *et al.* (2005)).

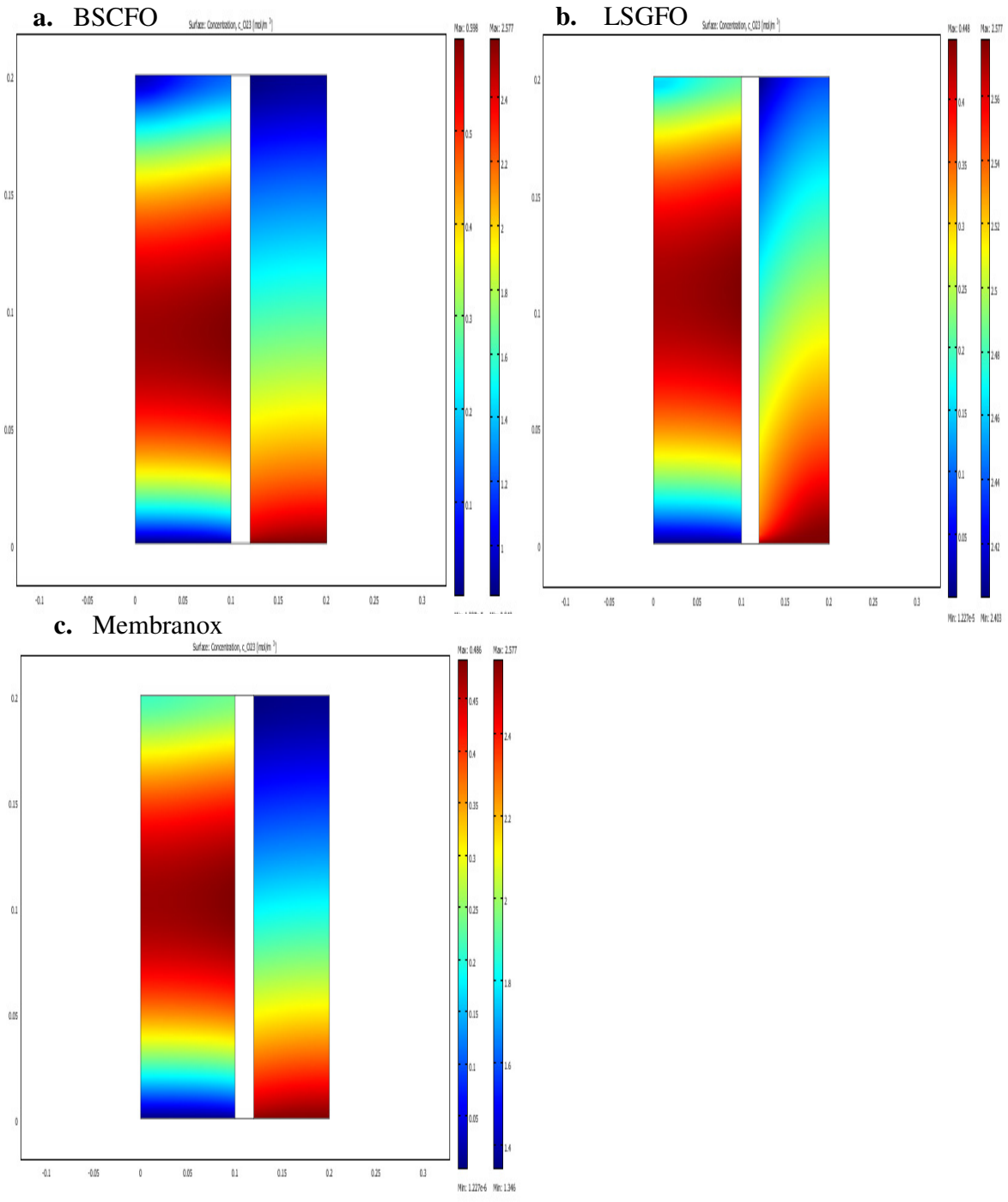

Figure 5.19 O_2 concentration profiles of three membrane reactors a. BSCFO MR, b. LSGFO MR and c. Membranox MR

Figures 5.20 and 5.21 show concentration profiles of methane (reactant) and ethylene in three MRs, a. BSCFO MR, b. LSGFO MR and c. Membranox MR. Methane was fed into tube side of reactor. Methane concentration decreases from the inlet due to reaction. In case of Membranox MR, methane (reactant) and ethylene (product) were lost from the tube side to the shell side as shown in Figures 5.20c and 5.21c. Also, the other species (C_2H_6, CO, CO_2, H_2, and H_2O) can permeate to the shell side in the same manner. Permeation of methane results in low methane conversion. Although permeation of products to the shell side could prevent the oxidation of the products but they would be present in the shell side stream at low concentration and become different to recover them. In case of dense membranes, i.e. BSCFO and LSGFO MR, no loss of products to the shell side was observed as only oxygen species could permeate through the dense membranes. The specific characteristics of the dense membrane prevent other species to the trans-membrane side.

Figure 5.22 shows temperature profiles in the three membrane reactors, a. BSCFO MR, b. LSGFO MR and c. Membranox MR. The increase of temperature was gradually increased at the center of the reactor caused by the reaction with oxygen permeable into this area of the reactor, which was observed in Figure 5.19. It shows that the reaction site was everywhere in the reactor and heat was accumulated in the bed of catalyst. Heat can transfer from the reactor to the shell side via the tube wall and therefore the temperature change near the wall becomes not significant. The temperature profiles for the different MRs were similar but there were slight differences in a rising of temperature: BSCFO > LSGFO > Membranox

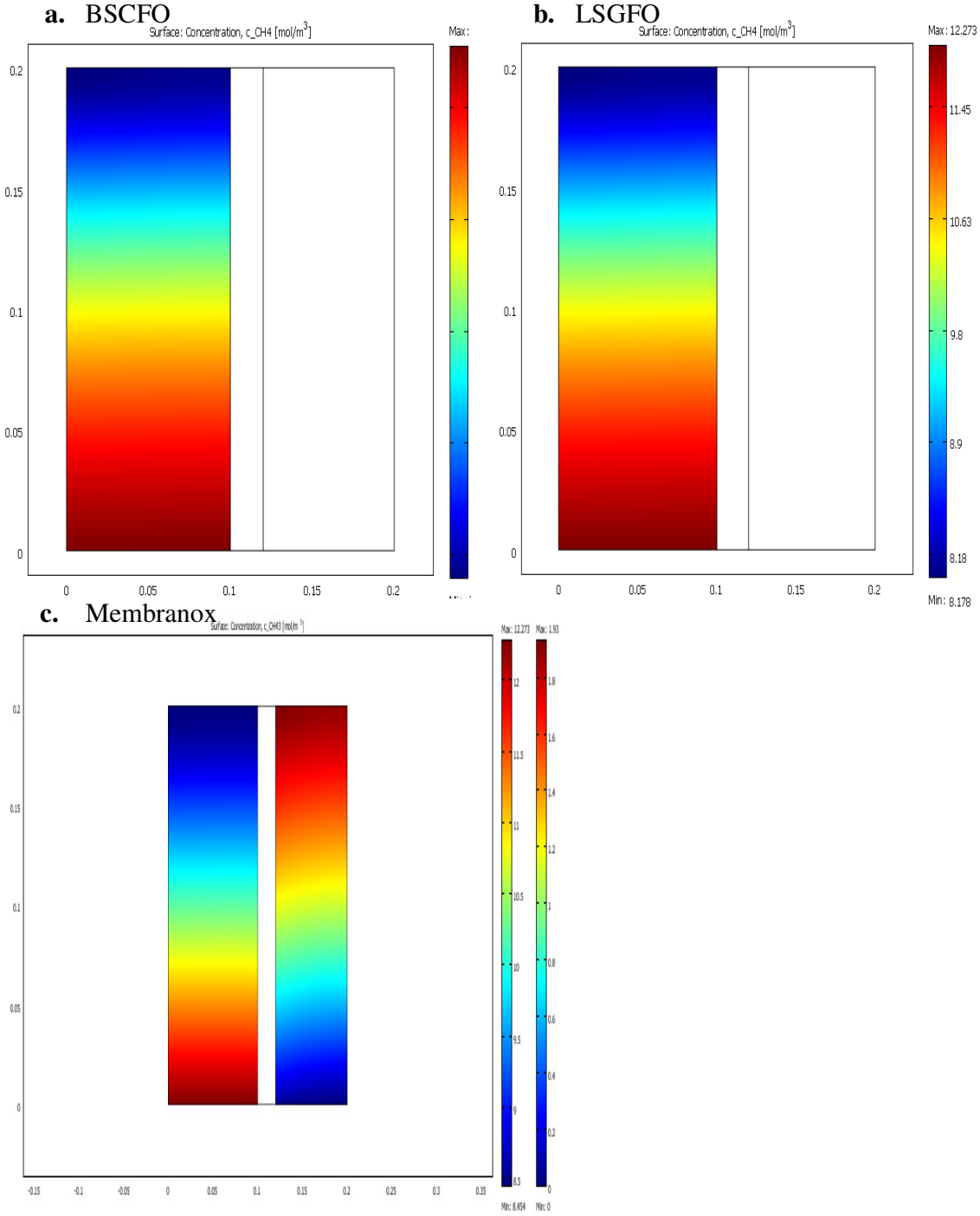

Figure 5.20 CH_4 concentration profiles of three membrane reactors a.BSCFO MR, b. LSGFO MR and c. Membranox MR

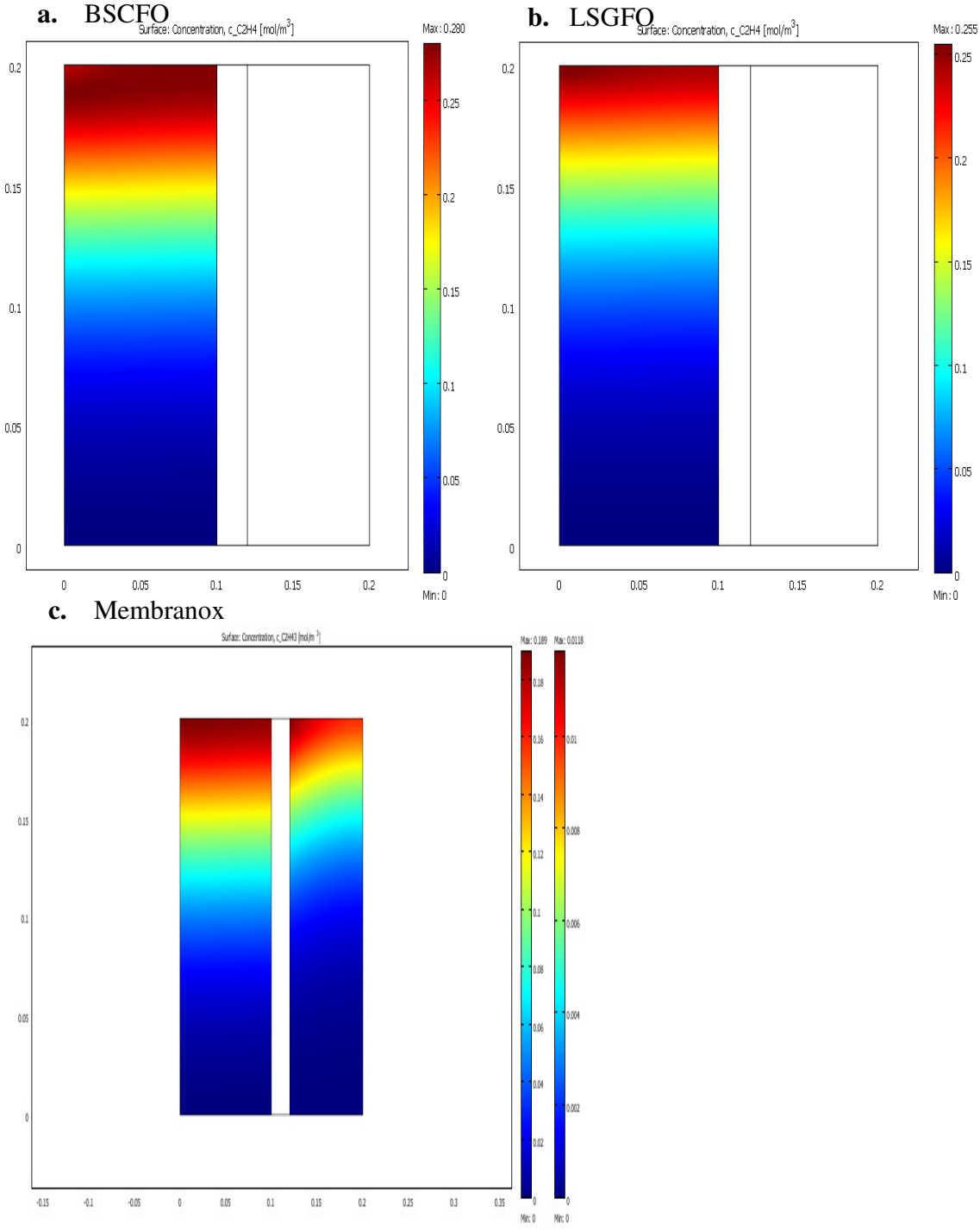

Figure 5.21 C_2H_4 concentration profiles of three membrane reactors a. BSCFO MR, b. LSGFO MR and c. Membranox MR.

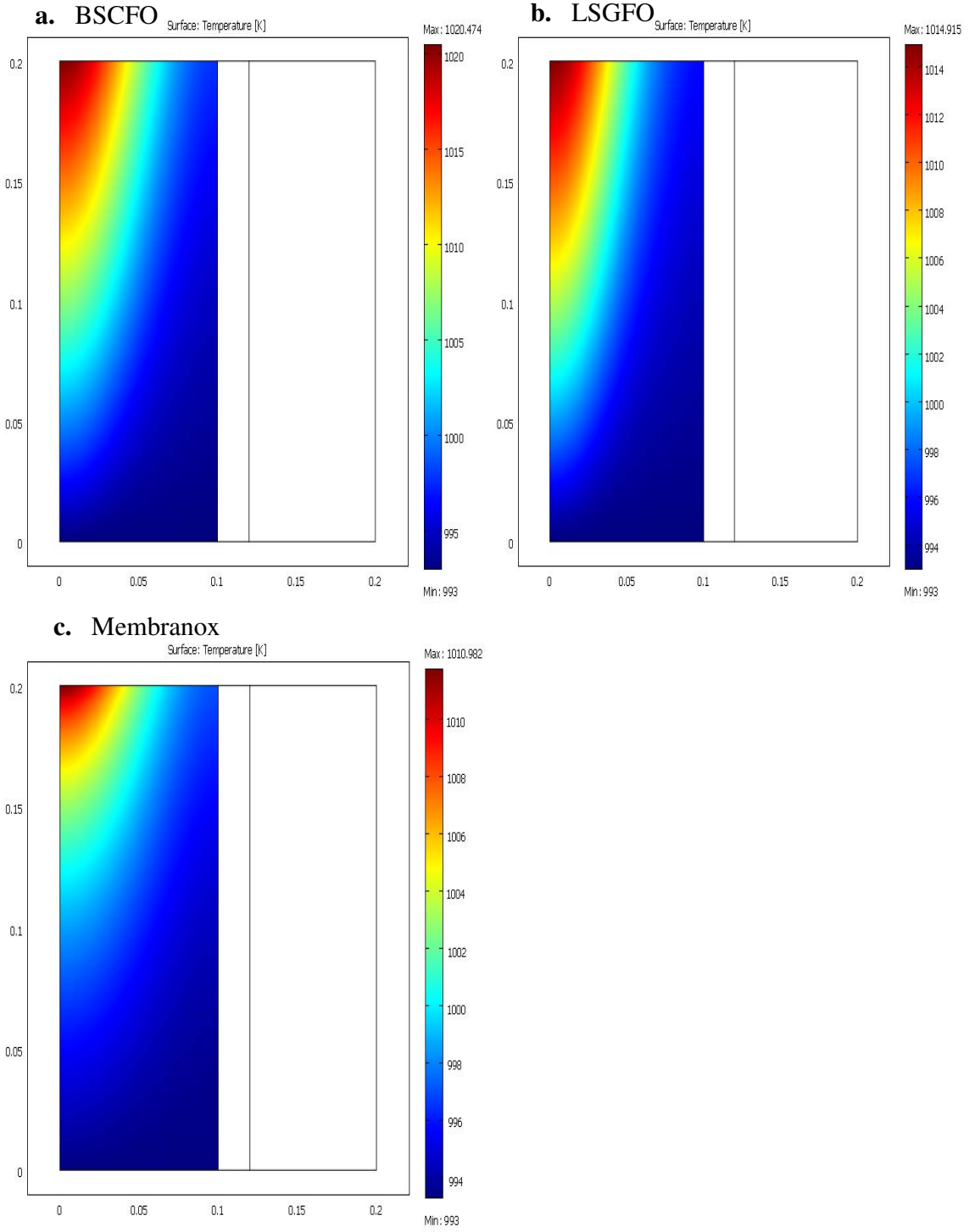

Figure 5.22 Temperature profiles of three membrane reactors a. BSCFO MR, b. LSGFO MR and c. Membranox MR

Table 5.7 Summary OCM performance at different membrane reactor (*T*=993 K, air flow rate = 0.00028 m^3/s, CH_4 flow rate = 0.00055 m^3/s)

Performance	Membrane types		
	Membranox	BSCFO	LSGFO
CH_4 conversion, %	28.39	36.03	33.37
C_2 selectivity, %	78.93	70.59	74.34
C_2 yield, %	22.41	25.43	24.81

Table 5.7 shows summary of OCM performances between three membrane types in membrane reactor at air flow rate of 0.00028 m^3/s, methane flow rate of 0.00055 m^3/s and temperature of 993 K. The C_2 yield of BSCFO membrane was 25.43 %, the highest compared to 24.81 % for LSGFO and 22.41 % for Membranox membrane. More detailed studies on the comparison of the three types of membrane and other conditions were provided in the following section.

5.6 Membrane selection

This section focuses on selecting a suitable type of membrane among Membranox (alumina membrane), a dense $Ba_{0.5}Sr_{0.5}Co_{0.8}Fe_{0.2}O_{3-\delta}$ (BSCFO) membrane and $La_{0.4}Sr_{0.6}Ga_{0.4}Fe_{0.6}O_{3-\delta}$ (LSGFO) membrane at various conditions i.e. air flow rate, CH_4 flow rate and temperature in membrane reactor.

Table 5.8 Summary of operating condition for catalyst selection study

Figure	**condition**		
	Air flow rate (m^3/s)	CH_4 flow rate (m^3/s)	Temperature (K)
5.23	0.00016	0.00055	993
5.24	0.00028	0.00055	993
5.25	0.00040	0.00055	993
5.26	0.00028	0.00055	1023
5.27	0.00028	0.00055	1073
5.28	0.00028	0.000668	993

Figures 5.23-5.28 show results of C_2 selectivity and CH_4 conversion along reactor length under different conditions as summarized in Table 5.8. From all figures, CH_4 conversion was increased and C_2 selectivity was decreased by the distance from the inlet to the reactor for all MR. It was obvious that CH_4 conversion for BSCFO MR was higher than those achieved by LSGFO and Membranox MR respectively. Moreover, C_2 selectivity for Membranox MR was higher than LSGFO and BSCFO MRs, respectively for all conditions. It was obvious that both BSCFO and LSGFO membrane show slight difference in C_2 selectivity and CH_4 conversion but the more difference in Membranox membrane. The effect of air flow rate was shown in Figures 5.23-5.25. The CH_4 conversion was increased and the C_2 selectivity was decreased with increasing of air flow rate. The effect of CH_4 flow rate was shown in Figures 5.24 and 5.28. The CH_4 conversion was decreased and the C_2 selectivity was increased with increasing of CH_4 flow rate. Finally, the effect of temperature was shown in Figures 5.24 5.26 and 5.27. The CH_4 conversion was increased and the C_2 selectivity was decreased with increasing of temperature. At higher temperature (1173 K), the rate of reduction of C_2 selectivity was more than that at lower temperatures (1073 and 993 K) which shows the same characteristics as the changes in fixed bed reactor. The maximum C_2 yields for all membranes appear at temperature of 1023 K, CH_4 flow rate of 0.00055 $m/^3s$ and air flow

rate of 0.00028 m^3/s. The values were 25.85, 24.43 and 21.71 % for BSCFO, LSGFO and Membanox, respectively. The simulation results indicated that BSCFO membrane offers the best performances among all the membranes. Further discussion on the effect of parameters was provided in the next section.

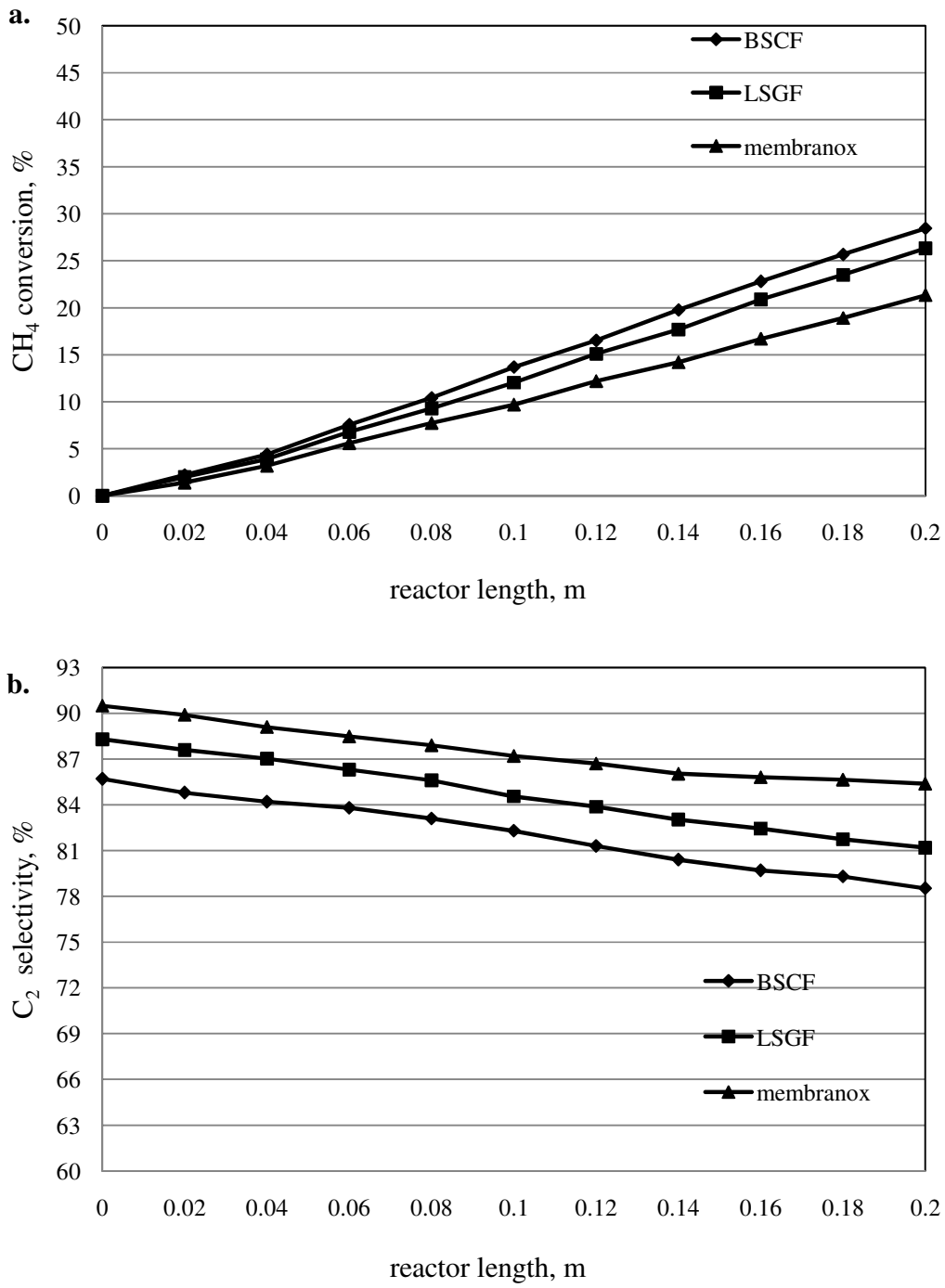

Figure 5.23 a. CH_4 conversion, b. C_2 selectivity along reactor length (T=993, air flow rate = 0.00016 m^3/s, CH_4 flow rate = 0.00055 m^3/s)

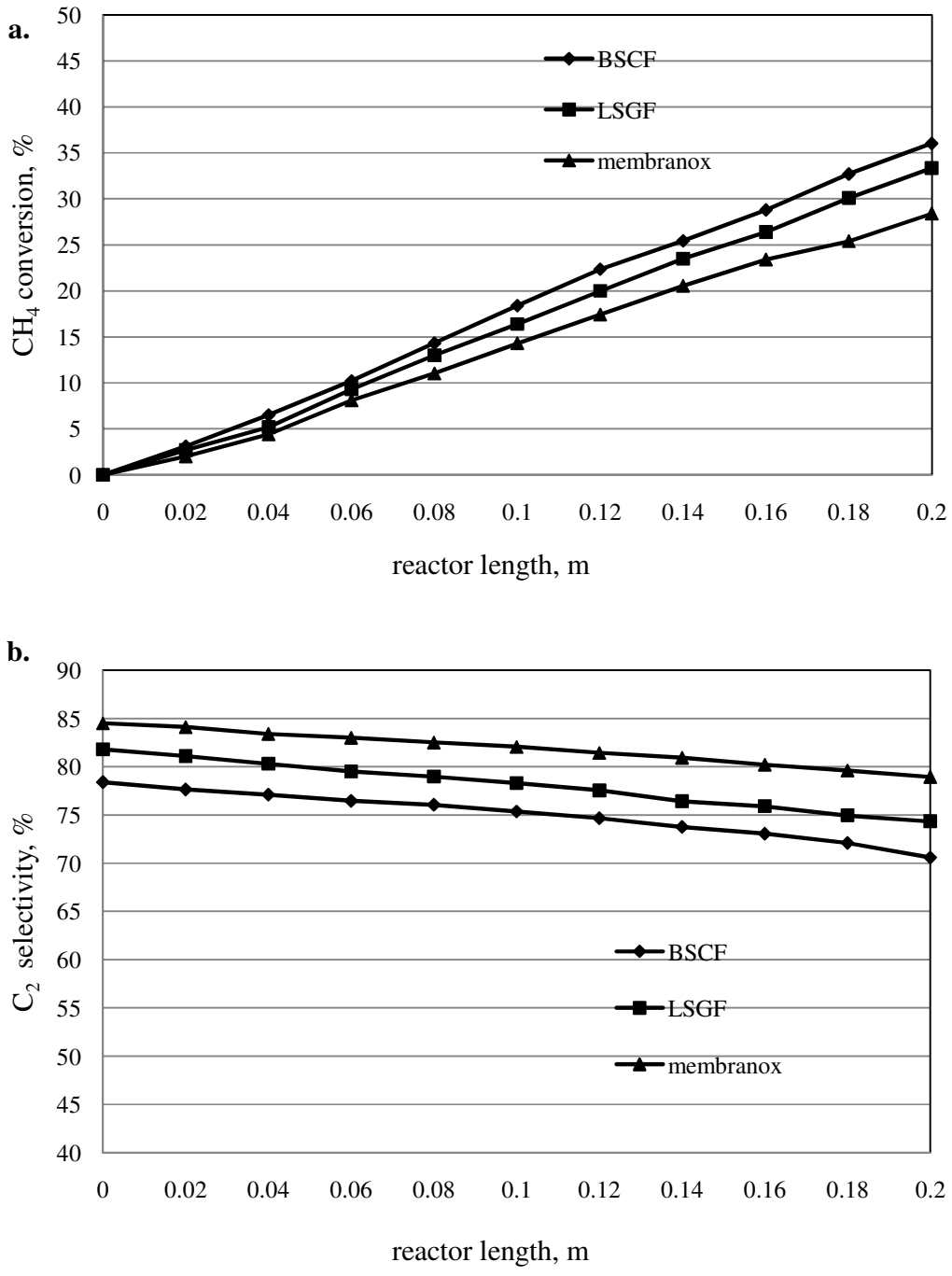

Figure 5.24 a. CH_4 conversion, b. C_2 selectivity along reactor length (T=993, air flow rate = 0.00028 m^3/s, CH_4 flow rate = 0.00055 m^3/s)

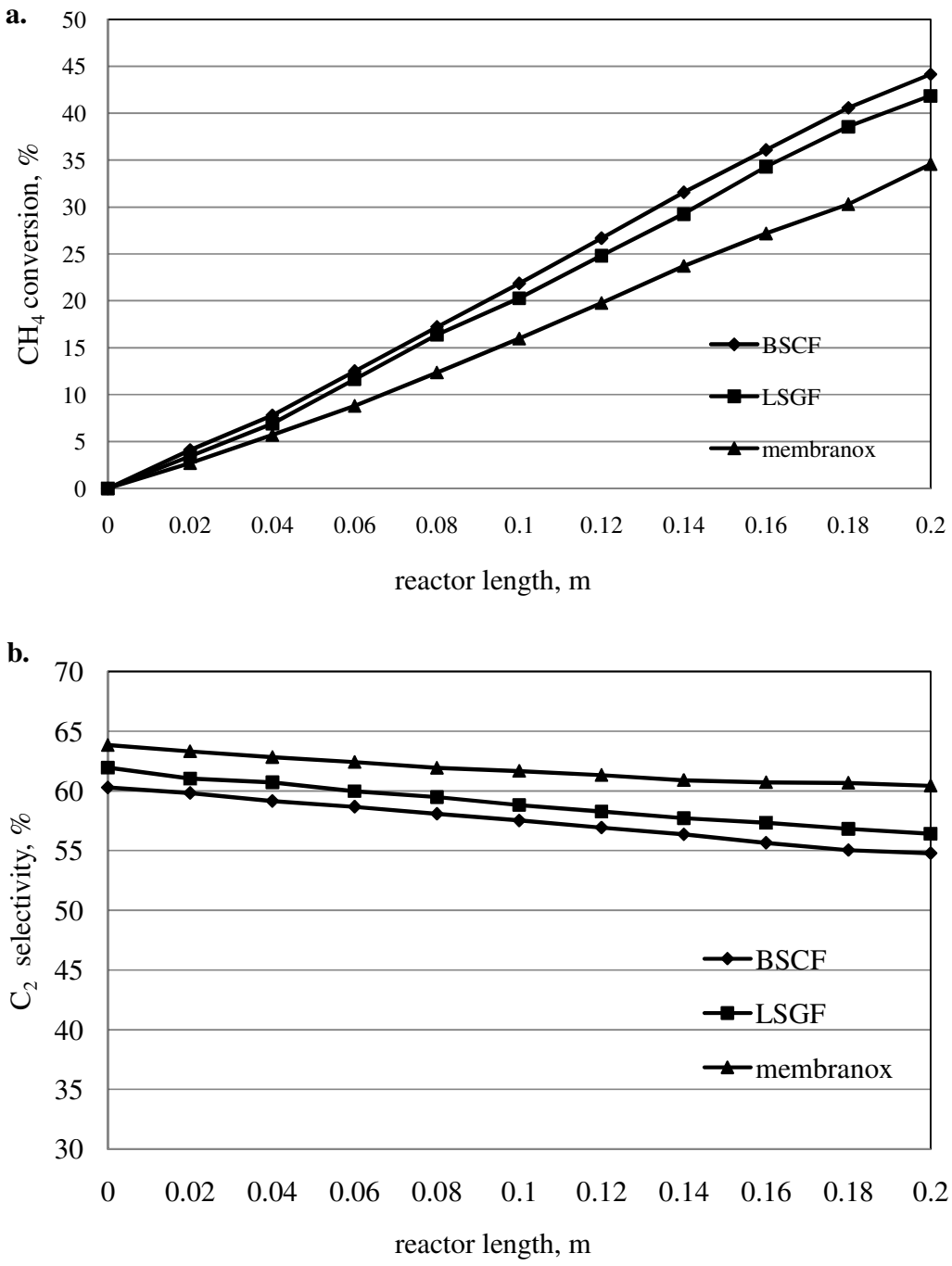

Figure 5.25 a. CH_4 conversion, b. C_2 selectivity along reactor length (T=993, air flow rate = 0.0004 m^3/s, CH_4 flow rate = 0.00055 m^3/s)

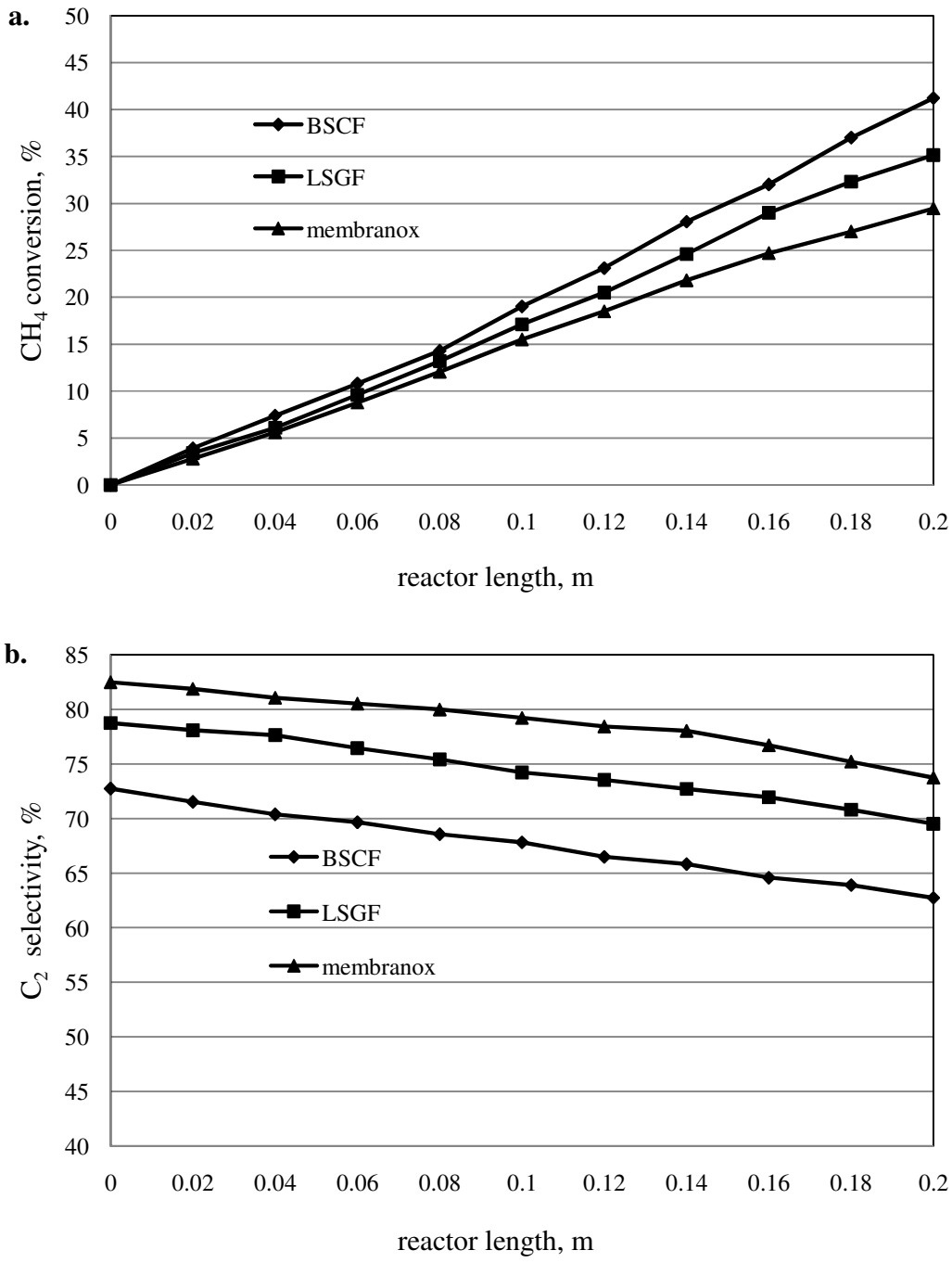

Figure 5.26 a. CH_4 conversion, b. C_2 selectivity along reactor length (T=1023 K, air flow rate = 0.00028 m^3/s, CH_4 flow rate = 0.00055 m^3/s)

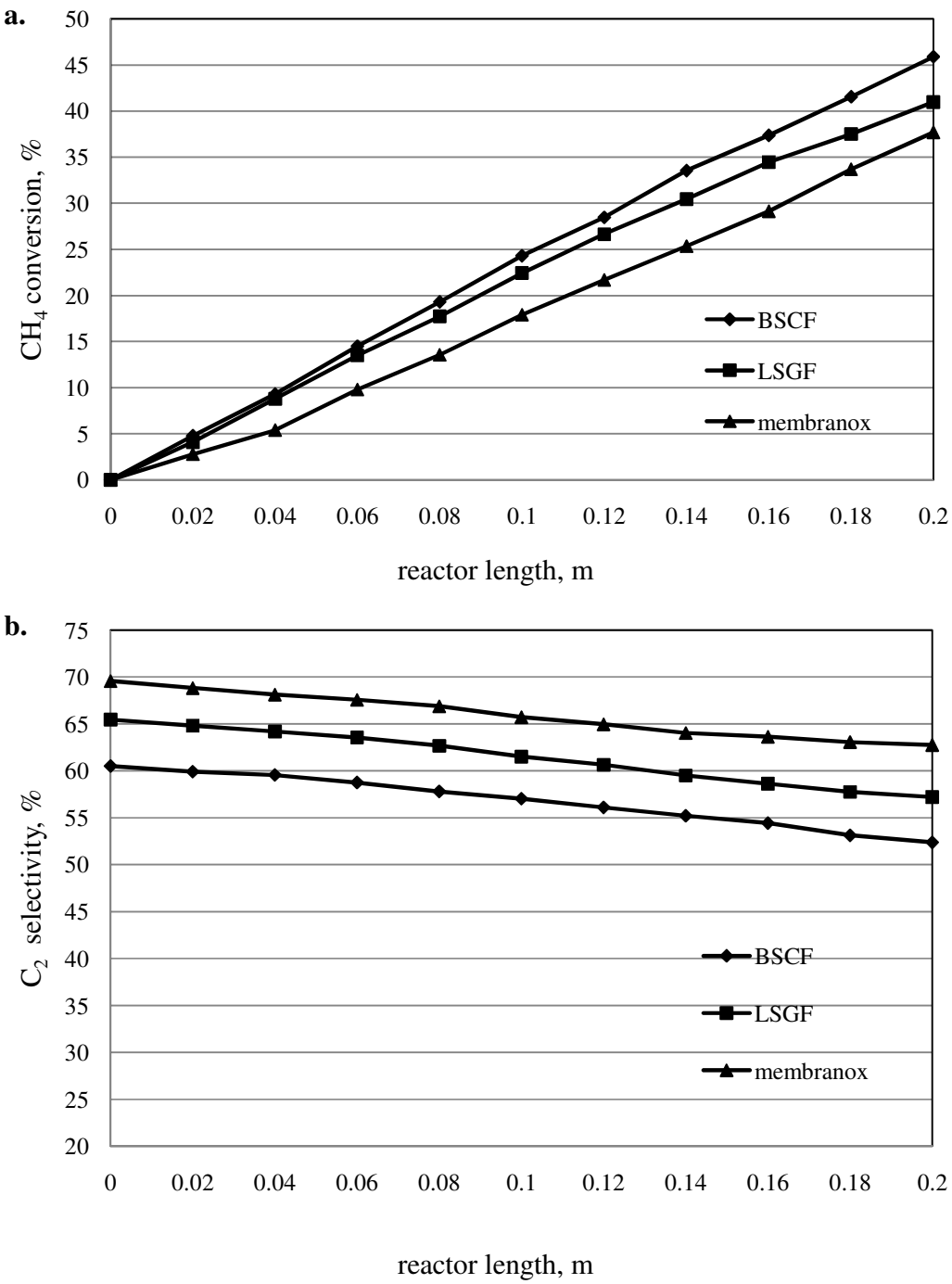

Figure 5.27 a. CH_4 conversion, b. C_2 selectivity along reactor length (T=1073 K, air flow rate = 0.00028 m^3/s, CH_4 flow rate = 0.00055 m^3/s)

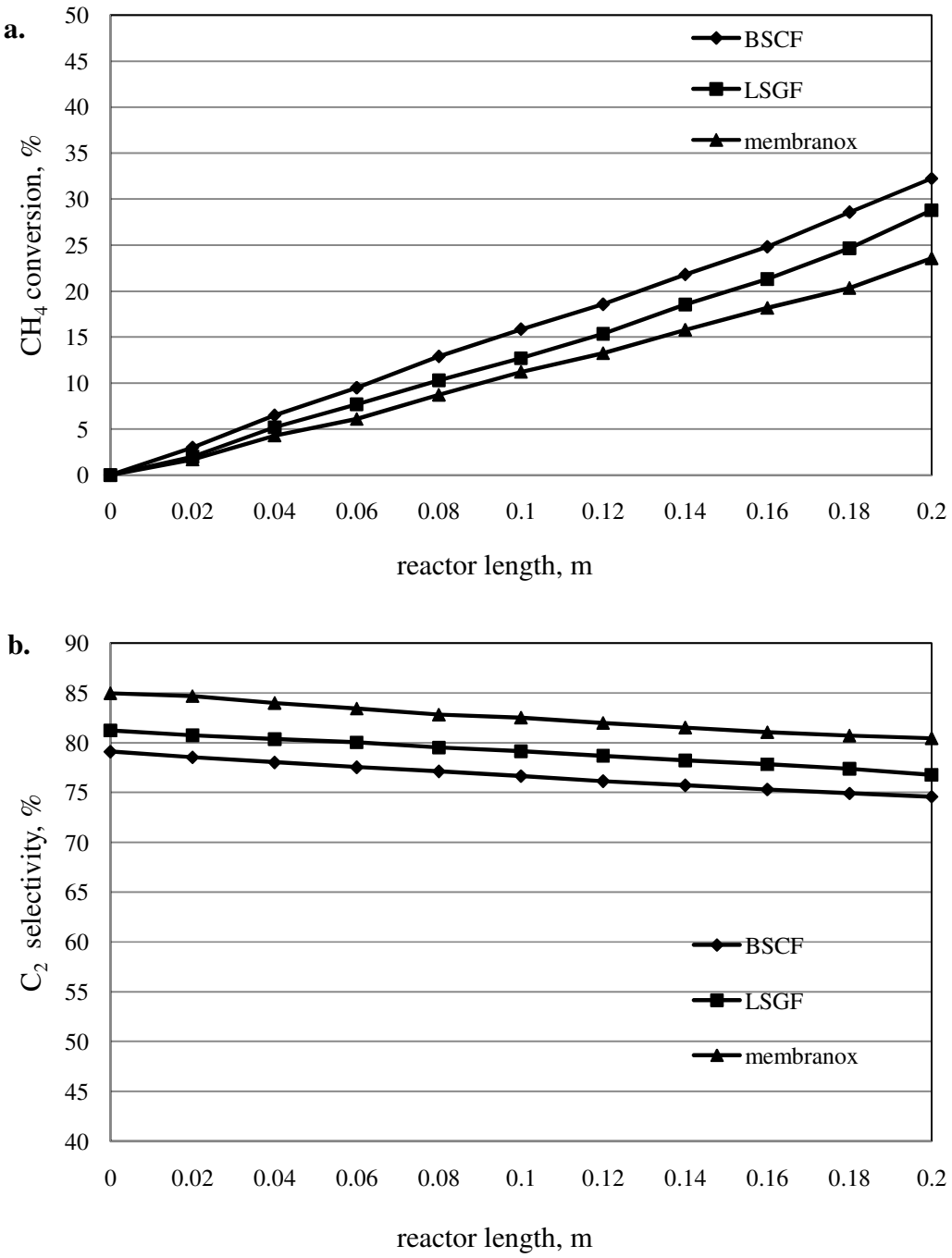

Figure 5.28 a. CH_4 conversion, b. C_2 selectivity along reactor length (T=993, air flow rate = 0.00028 m^3/s, CH_4 flow rate = 0.000668 m^3/s)

5.7 Membrane reactor study

From the previous section, we know that BSCFO membrane provides the best performance for MR and therefore it was selected in this present study. Effect of operating condition i.e. air flow rate, methane flow rate and temperature were investigated. The models were used to explore the profiles of temperature and concentration in the axial and radial directions.

5.7.1 Effect of methane feed rate

The effect of methane feed flow rate in a range 0.000138 – 0.000688 m^3/s at temperature 993 K and air flow rate of 0.00028 m^3/s on CH_4 conversion and C_2 selectivity were presented in Figure 5.29. CH_4 conversion was decreased, whereas, C_2 selectivity was increased with the increase of methane feed flow rate. Increasing methane feed flow rate results in lower contact time, and hence, CH_4 conversion was decreased. Besides, the methane feed rate also affects the permeation of oxygen into the tube side as shown in Figure 5.30 As show O_2 concentration profile at different methane feed flow rate. At lower methane feed flow rate (Figures 5.30a and 5.30b), oxygen-permeable membrane into the first part of the reactor. It completes conversion at position of permeation into tube side. On the other hand, at higher methane feed rate (Figures 5.30c – 5.30e); oxygen-permeable membrane into tube side in same position in the previous case but it to conversion lower and slower than the previous case which was observed from the higher oxygen flow rate along length of the reactor. Because of at higher methane feed flow rate, methane feed rate taking oxygen flow rate which was permeated in tube side was higher as well. As a result, lower contact between methane and oxygen. This was to make CH_4 conversion less.

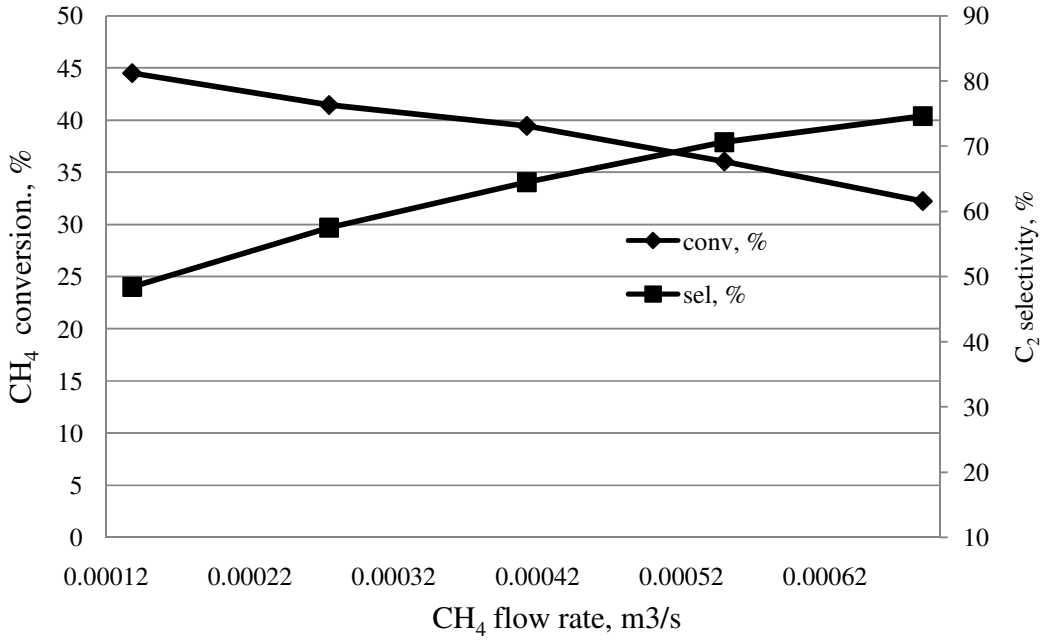

Figure 5.29 The effect of CH_4 feed rate on CH_4 conversion and C_2 selectivity (T=993 K, air flow rate = 0.00028 m^3/s

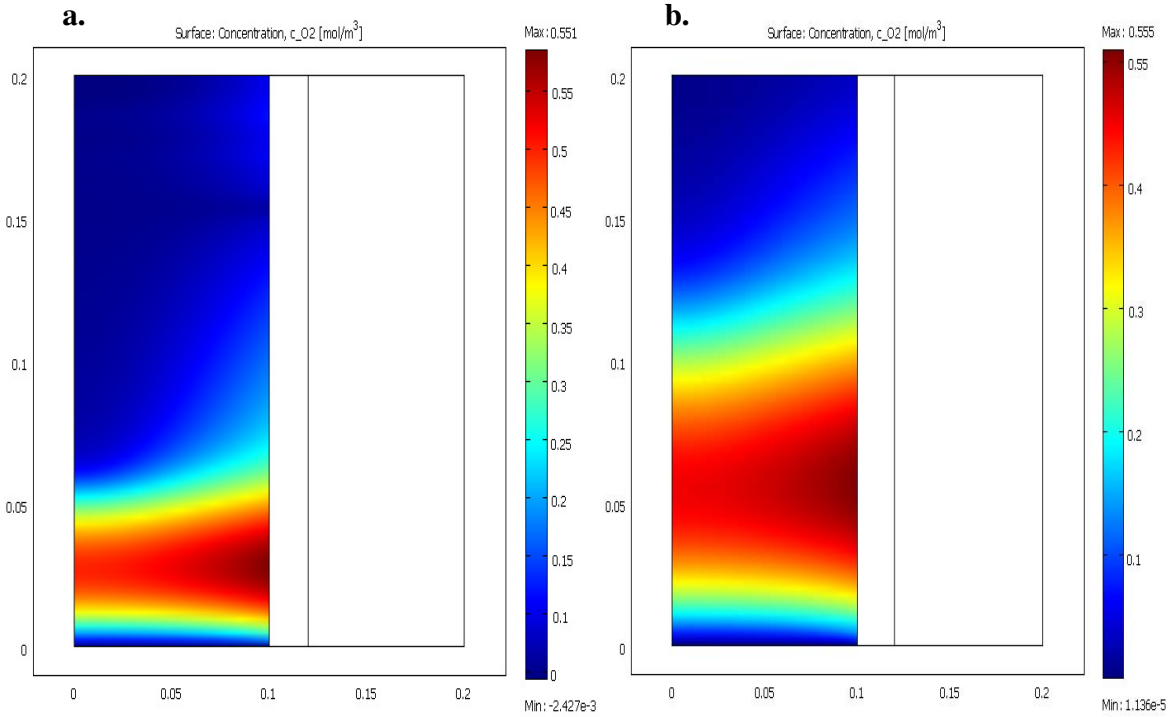

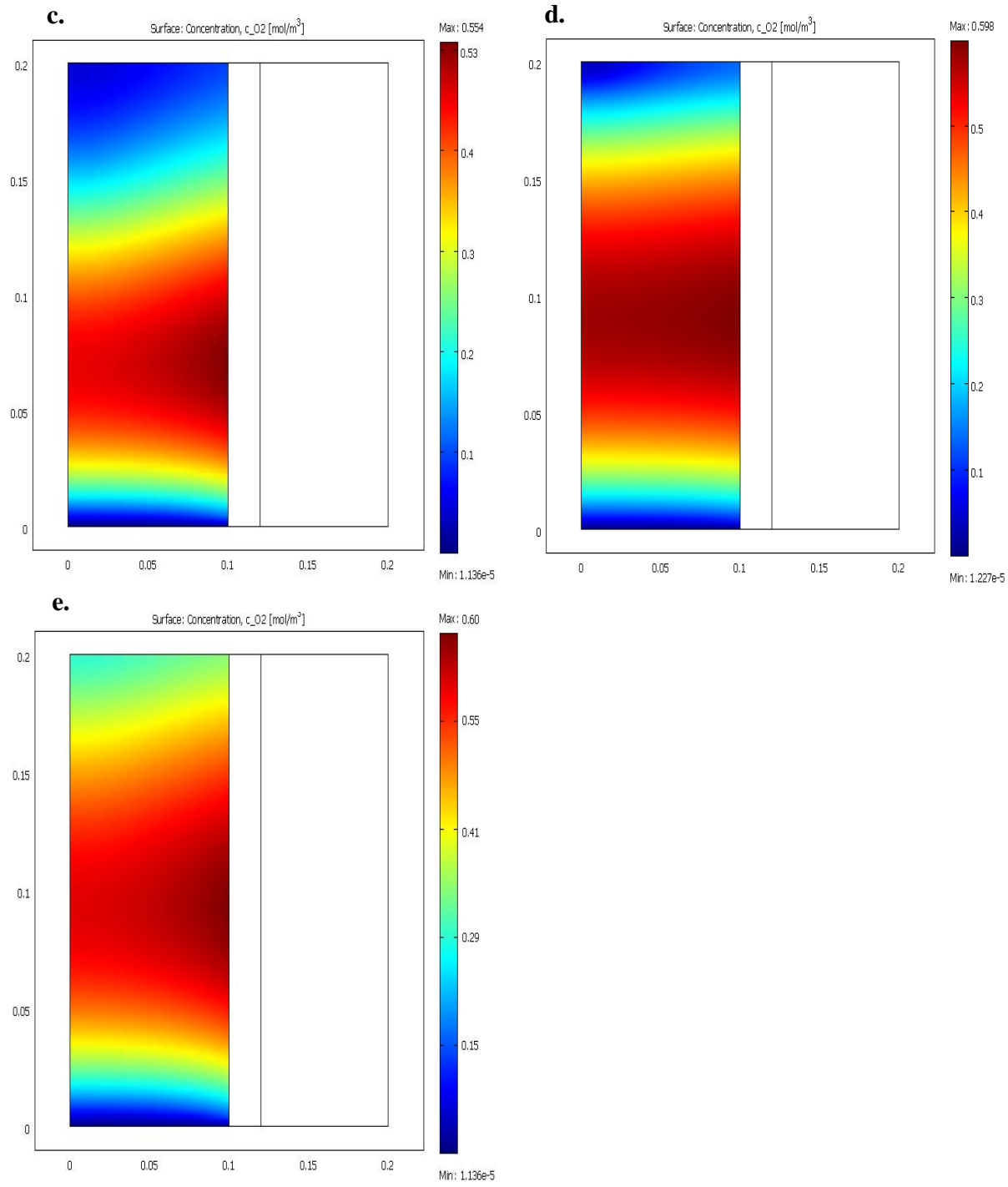

Figure 5.30 Effect of CH_4 feed rate on O_2 concentration profile at CH_4 feed rate = (a.) 0.000138, (b.) 0.000275, (c.) 0.000413, (d.) 0.00055, (e.) 0.000688 m^3/s

5.7.2 Effect of air feed rate

The effect of air feed flow rate in range 0.00004 – 0.0052 m^3/ s for temperature of 993 K and methane flow rate of 0.00055 m^3/s on CH_4 conversion and C_2 selectivity were presented in Figure 5.31. CH_4 conversion was increased, whereas, C_2 selectivity was decreased with the increase of air feed flow rate. When increasing air feed rate, the flux of oxygen permeation increases due to higher driving force of oxygen across the membrane. As a result, CH_4 conversion increases. C_2 selectivity was decreased because higher amount of oxygen could react with the methyl radical and C_2 product to carbon oxides.

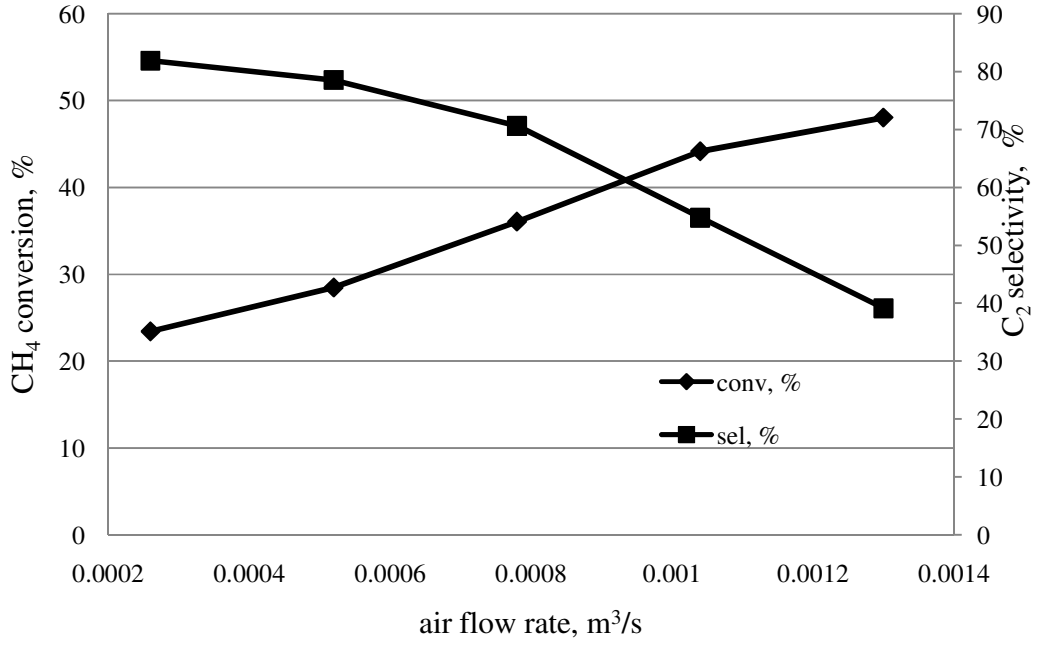

Figure 5.31 a. Effect of air flow rate on CH_4 conversion and C_2 selectivity (*T*=993 K, CH_4 flow rate = 0.0055 m^3/s)

5.7.3 Effect of temperature

The effect of temperature between 993 - 1173 K for air feed rate of 0.00028 m^3/s and methane feed rate of 0.00055 m^3/s on CH_4 conversion and C_2 selectivity were presented in Figure 5.32. CH_4 conversion was increased, whereas, C_2 selectivity was decreased with the increased temperature. Figure 5.33 shows the temperature profiles. The hot sport temperature was always observed due to the accumulation of heat of reaction along the reactor. Figure 5.33e shows temperature profiles for both of the shell and tube sides. Temperature increases gradually in the tube side from the inlet to along reactor especially at the center of the reactor, while the shell side temperature was slightly increased. The trend of temperature in the tube side was more than the shell side due to heat released from exothermic reaction. However, at higher temperature (1173 K) it was unfavorable for C_2 yield. It seems to be the hot spot takes place in the middle of the reactor, This suggests that the MR configuration from packed bed membrane reactor should be changed to a catalytic membrane reactor with a membrane tube coated with catalyst at inner tube wall in order to prevent hot spot problem.

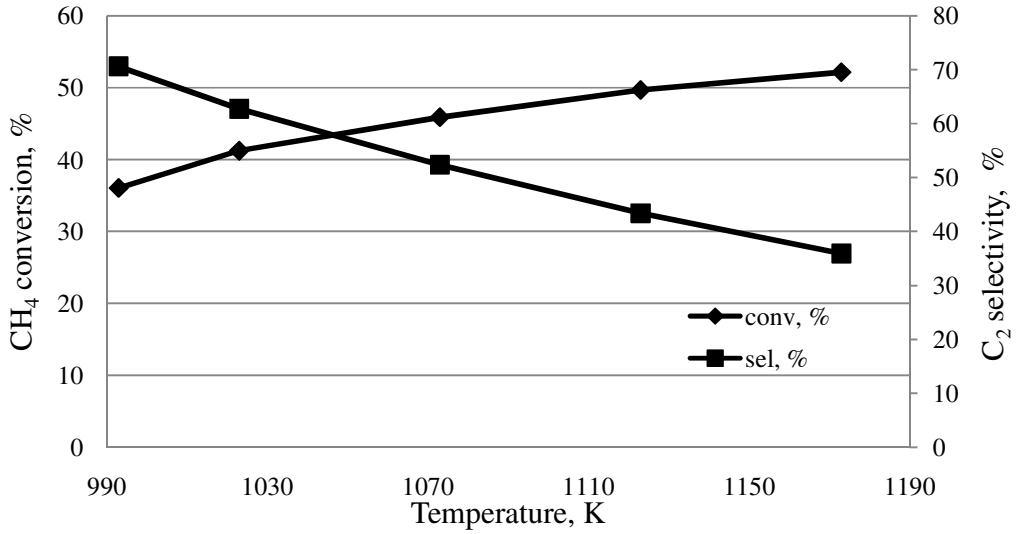

Figure 5.32 Effect of temperature on CH_4 conversion and C_2 selectivity (air flow rate = 0.00028 m^3/s, CH_4 flow rate = 0.0055 m^3/s)

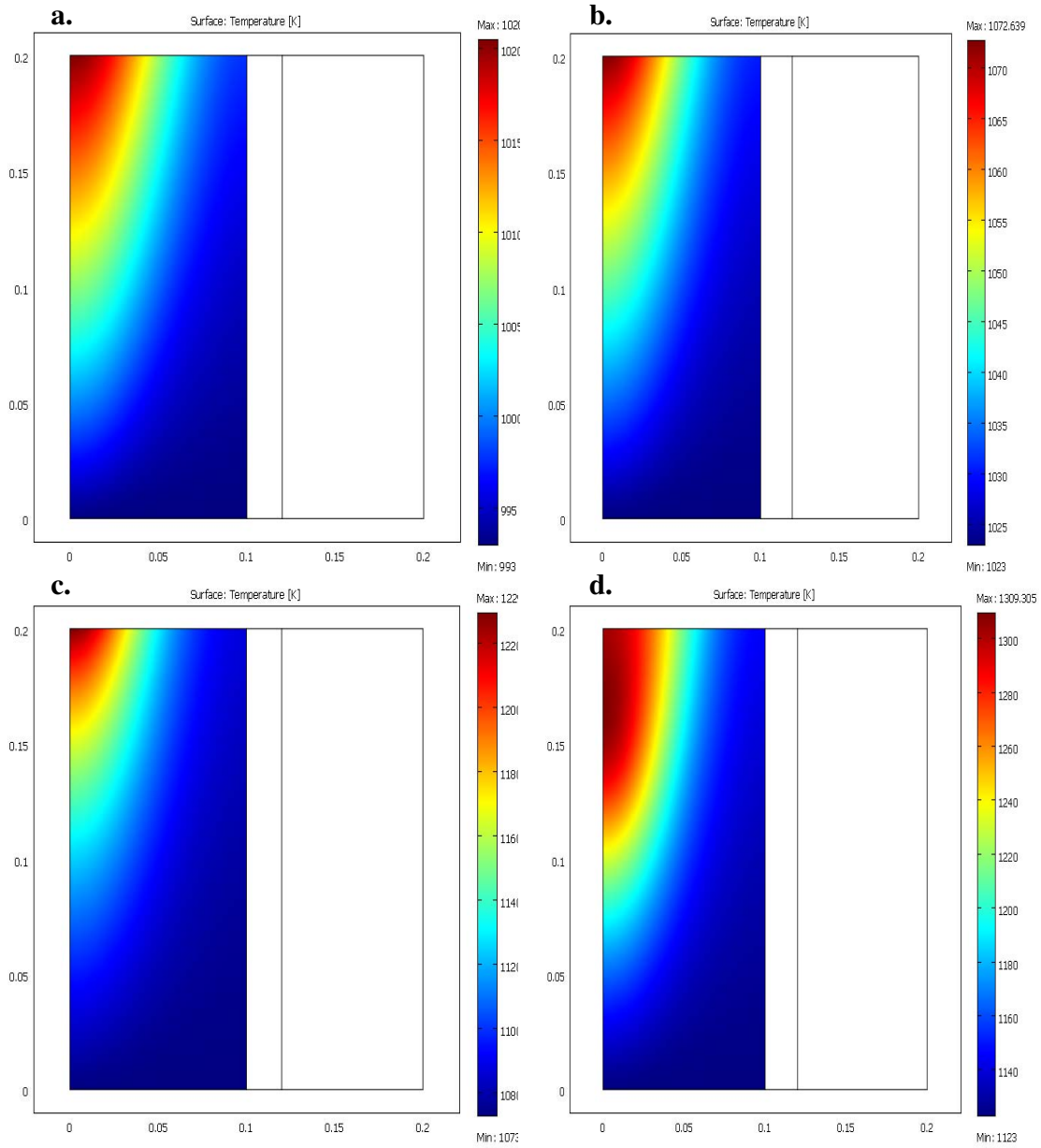
a.
Surface: Temperature [K]
Max: 102
Min: 993
b.
Surface: Temperature [K]
Max: 1072.639
Min: 1023
c.
Surface: Temperature [K]
Max: 122
Min: 107
d.
Surface: Temperature [K]
Max: 1309.305
Min: 1123

e.

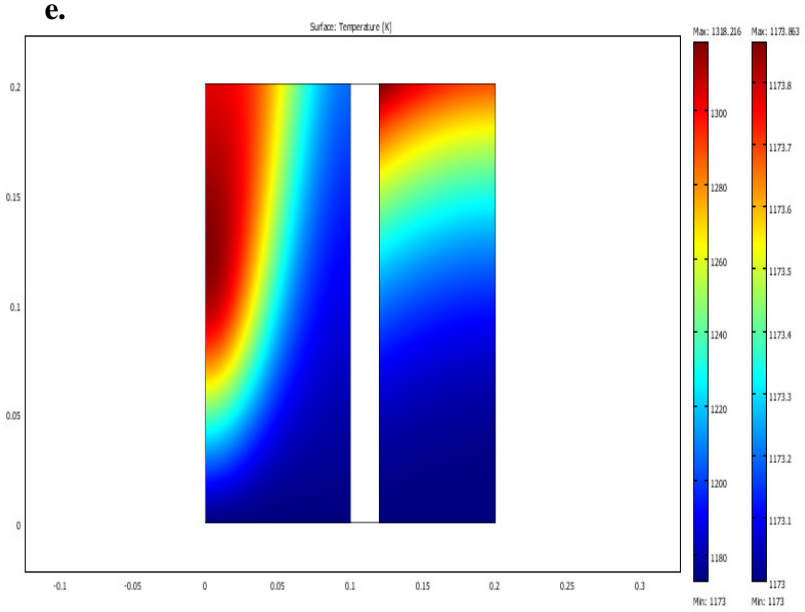

Figure 5.33 Temperature profiles at different feed temperatures at T_{inlet} = (a.) 993, (b.) 1023, (c.) 1073, (d.) 1123, (e.) 1173 K

5.8 Comparisons between fixed bed and membrane reactor

In this section, the performance comparison between FBR and MR was considered based on the same physical dimension and operating condition; Na-W-Mn/SiO_2 catalyst loading of 55.983 g, air flow rate of 0.0028 m^3/s in FBR (in MR, The flux of oxygen to permeated in tube side equal to the amount of oxygen that feed into the FBR.), methane flow rate of 0.000816 m^3/s and temperature of 1123 K. The maximum yield was found to be 13.5 % for FBR and 20.11 % for MR. A comparison of these two reactors was summarized in Table 5.9. The main reason for this low performance of FBR was because the methane and oxygen were fed together to the reactor. Although the CH_4 conversion was high, it was likely to have further oxidation of C_2 products to carbon oxides which lowers the C_2 selectivity. This behavior was different when operating in a membrane reactor. Oxygen concentration in the reactor was controlled and distributed along the length of the membrane. Formation of C_2 products

was more preferable than formation of CO_x. The MR shows higher C_2 selectivity than FBR. Figure 5.34 shows that the oxygen concentration profiles in the FBR and the MR were different. Figure 5.35 indicates the different profiles of temperature in FBR and MR. It was obvious that the temperature increase in the FBR was higher than that of the MR. The maximum temperature in reactor was 1543 K and 1309 K in FBR and MR respectively. Moreover, Figure 5.3shows the temperature effect between 993 - 1173 K on the C_2H_4/C_2H_6 ratio in the C_2 products for air feed rate of 0.00028 m^3/s and methane feed rate of 0.00055 m^3/s. The C_2H_4/C_2H_6 ratio increased with increasing temperature and reached a value of 0.6 in FBR and 0.8 in MR at 1173 K. The C_2H_4/C_2H_6 ratio in MR was much higher than that in the FBR, which was an advantage of the membrane reactor.

From result in this section, Shows that the membrane reactor performance was better than the fixed bed reactor. Therefore, in the next study focus on particularly in the membrane reactor.

Table 5.9 Comparison between two types of reactor at condition: *T*= 1123 K, *P*= 1 atm, air flow rate = 0.00028 m^3/s, methane flow rate= 0.000816 m^3/s)

Performance	**FBR**	**MR (BSCFO)**
CH_4 conversion, %	38.46	37.58
C_2 selectivity, %	35.25	57.23
C_2 yield, %	13.56	21.51

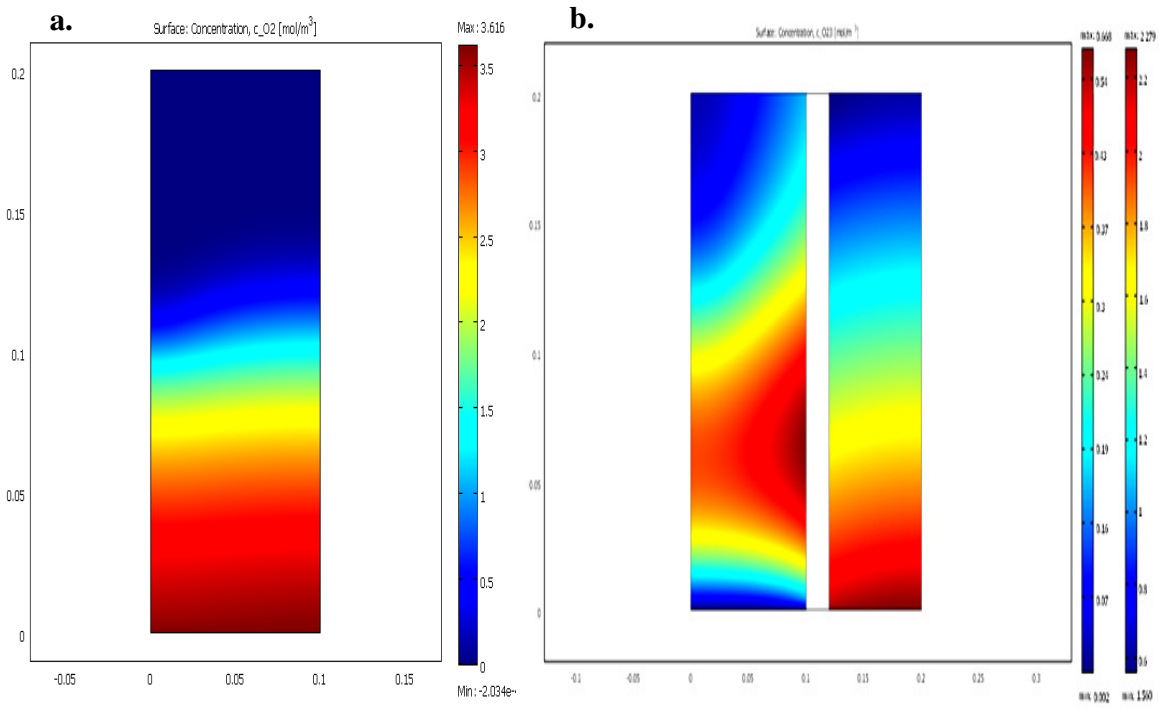

Figure 5.34 O_2 concentration profiles for different reactors a.) FBR, b.) MR

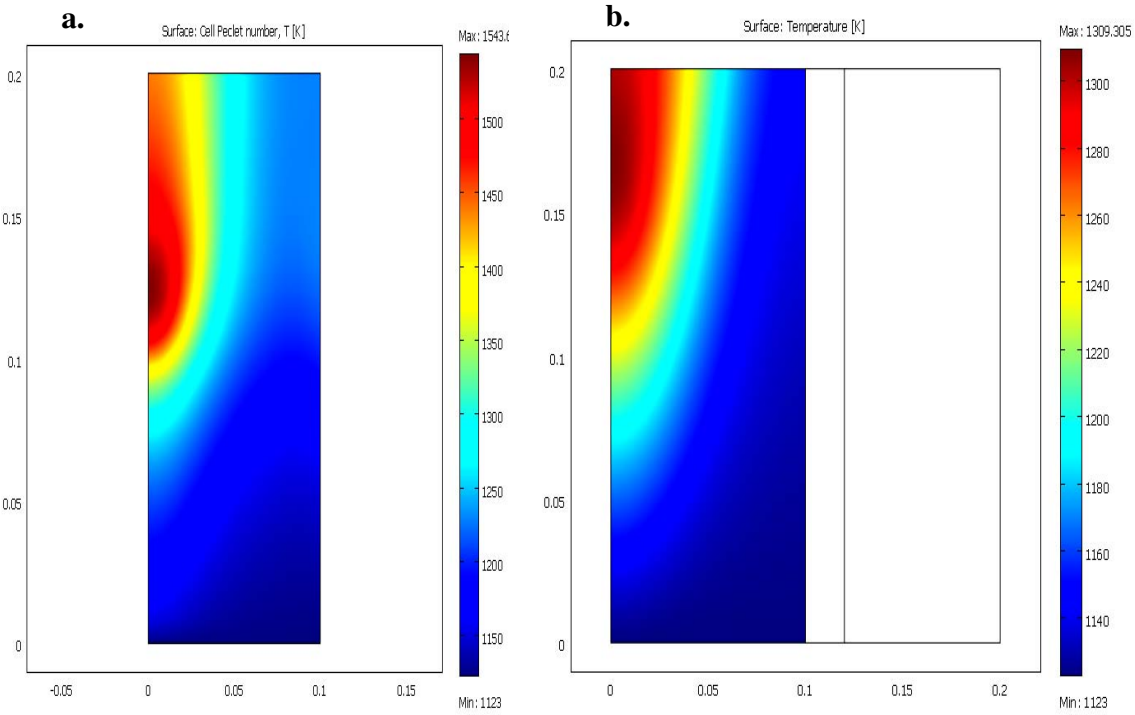

Figure 5.35 Temperature profiles for different reactors a.) FBR, b.)MR

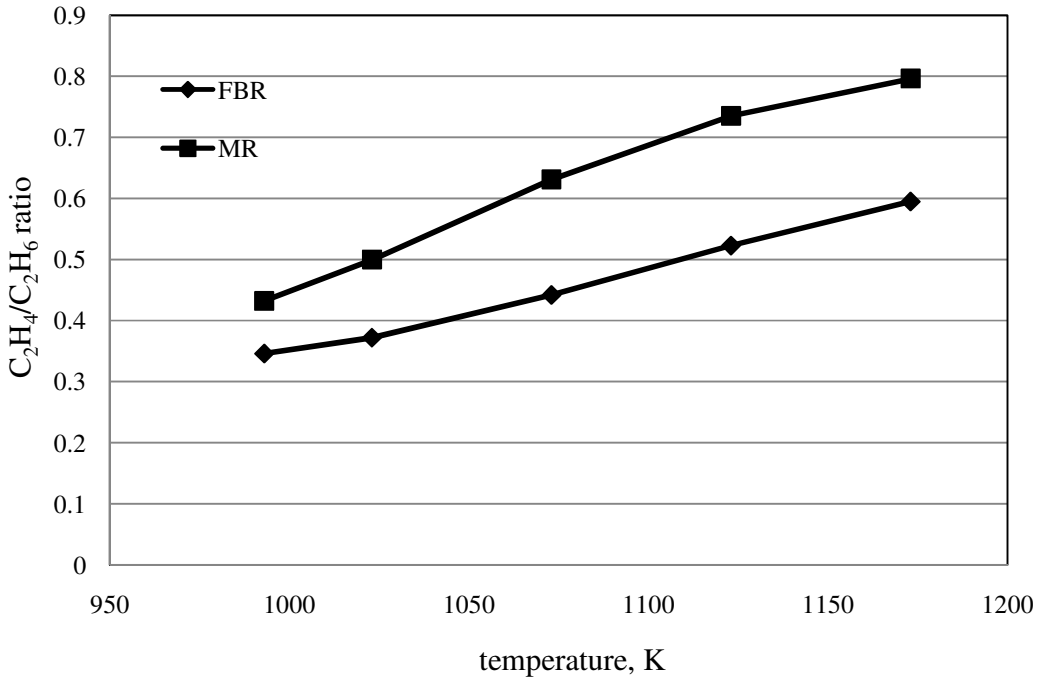

Figure 5.36 Comparison of the C_2H_4/C_2H_6 ratio obtained in FBR and BSCFO MR over Na-W-Mn/SiO_2 catalyst. (Air flow rate of 0.00028 m^3/s., methane flow rate of 0.000816 m^3/s.)

5.9 Sizing of reactor

In the last section, we focus on determining an optimum dimension of MR to provide the best performance in OCM process. The simulations were carried out using membrane reactors with different diameters as summarized in Table 5.10. The GHSV was kept at the same value for all cases. Table 5.11 summarizes the different operating conditions used in the simulations of reactors with different sizes.

Table 5.10 Dimension of different sizes of membrane reactor

model	dimension		
	r_{tube}(m)	r_{shell}(m)	h(m)
a.	0.0045	0.010	0.8
b.	0.006	0.013	0.45
c.	0.009	0.020	0.2
d.	0.0135	0.030	0.089
e.	0.018	0.040	0.05
f.	0.0225	0.050	0.032
g.	0.027	0.060	0.022

Table 5.11 Condition for sizing of reactor study

condition	GHSV (1/h)	Temp. (K)	Figure
1	58427.55	993	5.38
2	38904.54	993	5.39
3	19452.27	993	5.40
4	38904.54	1073	5.41
5	38904.54	1173	5.42

First, we focus on characteristics of different diameters of reactor at GHSV of 38904.54 1/h and temperature of 993 K. Figure 5.35 shows membrane area/volume of different diameters of reactor. It was observed that membrane area/volume decreases and therefore oxygen permeation would decrease with increasing reactor diameter. The oxygen permeation has an influence on reaction rate and OCM performance. Moreover,

the tube diameter affected variation of oxygen profile such as axial and radial dispersion in the tube side as shown in Figure 5.36. For membrane reactors with a small diameter (Figure 5.36a-5.36b), the oxygen permeation was high especially near the feed inlet and oxygen was present even at the center of the reactor. For medium diameters (Figures 5.36c – 5.36e), the oxygen could permeate through the membrane along the reactor length. It was observed that oxygen conversion was lower than the small diameter case. In addition, the oxygen concentration in tube side was still high. Furthermore, for larger diameter (Figures 5.36f –5.36g), oxygen concentration varies significantly along both the axial and radial directions. The concentration of oxygen was not well-distributed throughout in the radius direction. It was only present near the membrane area (tube wall).

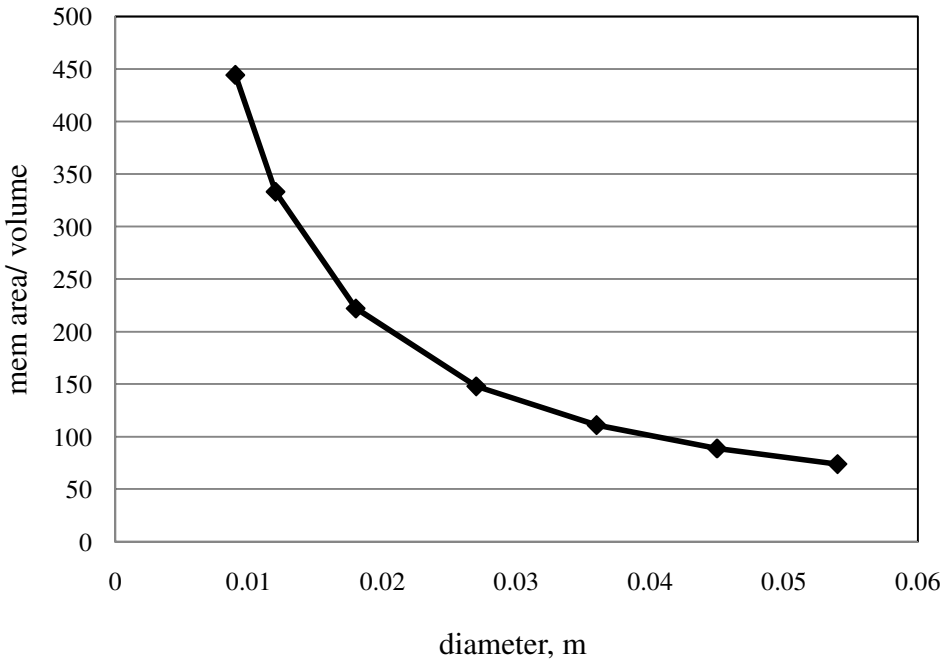

Figure 5.37 Membrane/volume with different reactor diameter

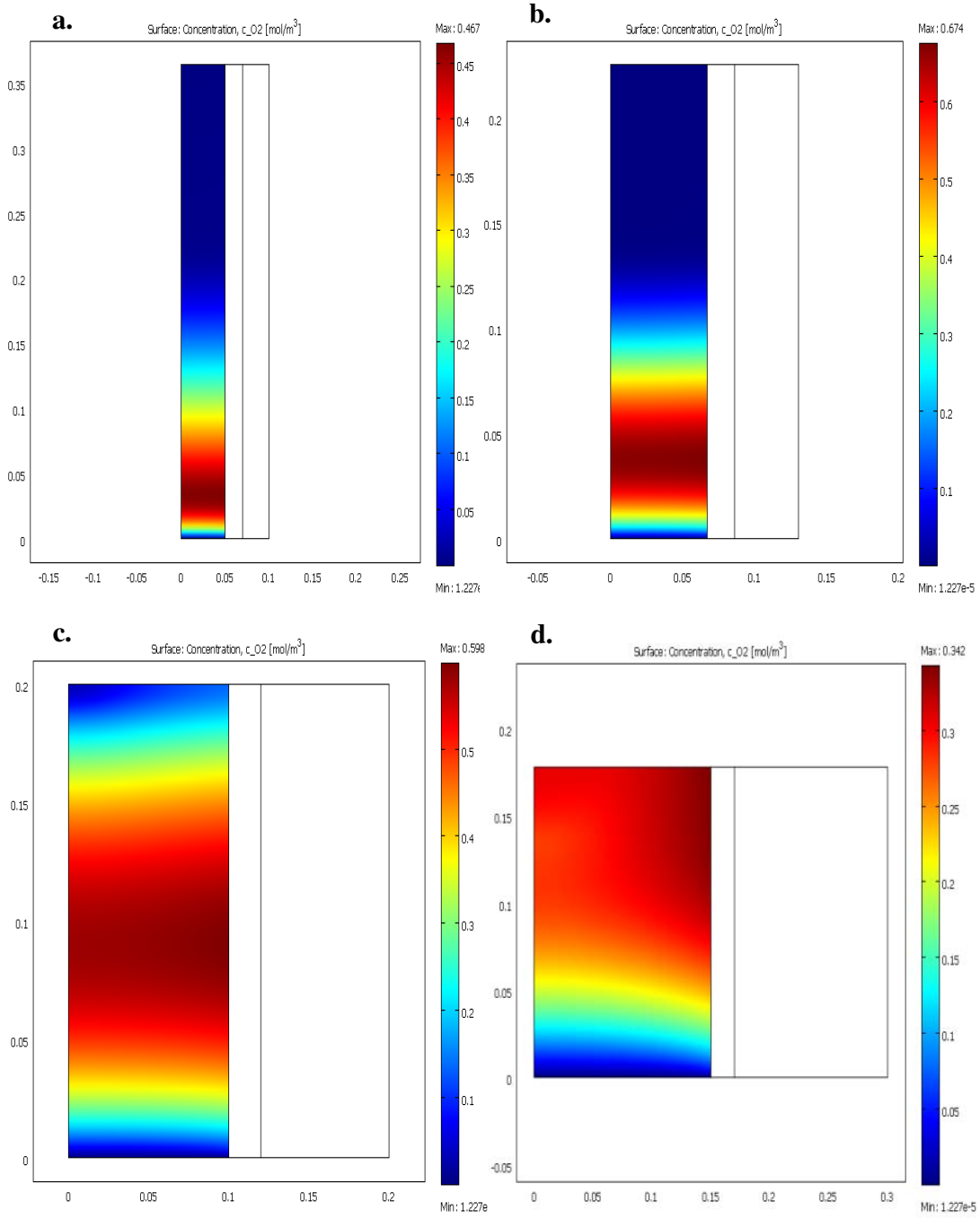
a.
Surface: Concentration, c_O2 [mol/m3]
Max: 0.467
Min: 1.227e
b.
Surface: Concentration, c_O2 [mol/m3]
Max: 0.674
Min: 1.227e-5
c.
Surface: Concentration, c_O2 [mol/m3]
Max: 0.598
Min: 1.227e
d.
Surface: Concentration, c_O2 [mol/m3]
Max: 0.342
Min: 1.227e-5

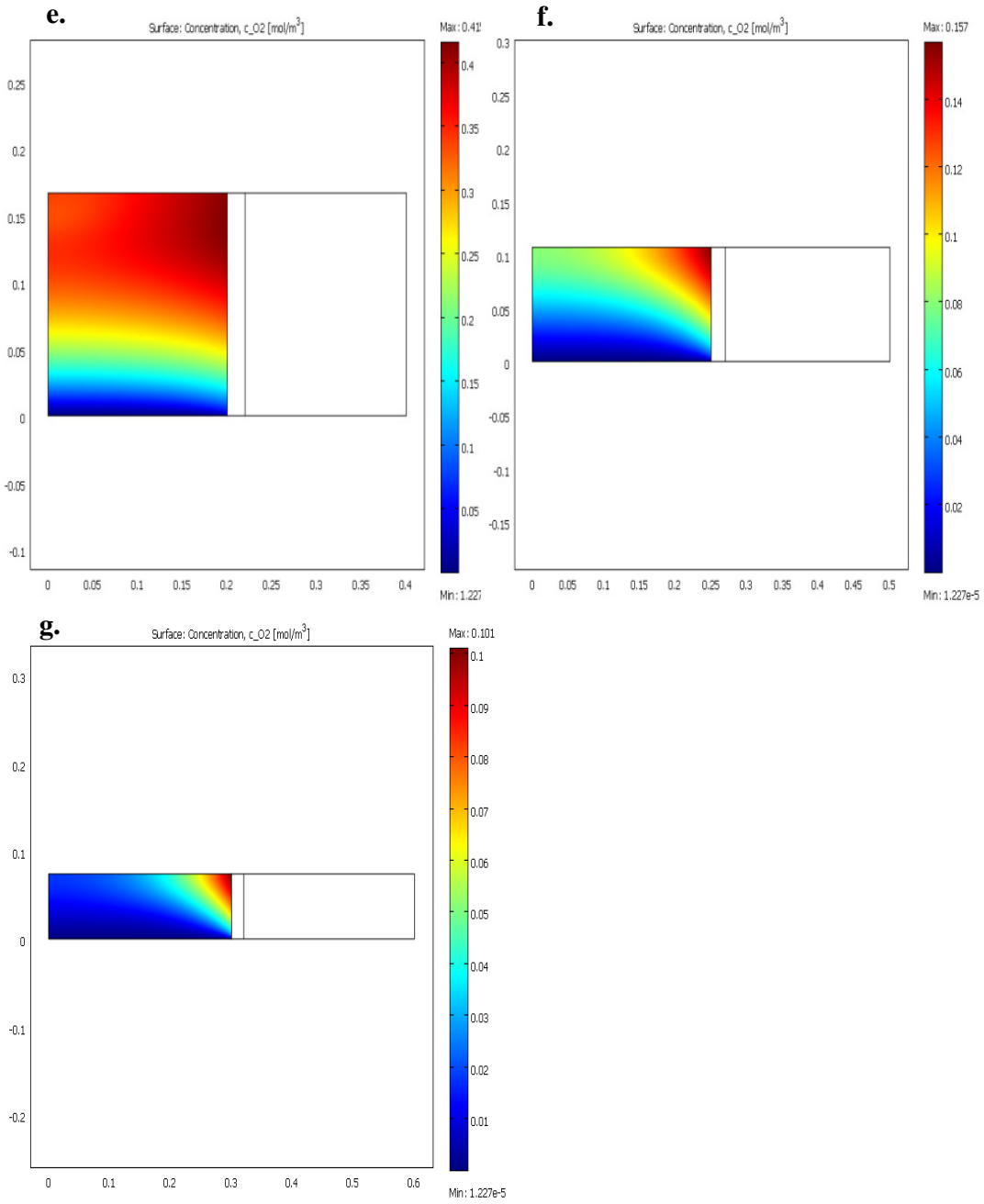

Figure 5.38 O_2 concentration profile with different reactor tube diameter

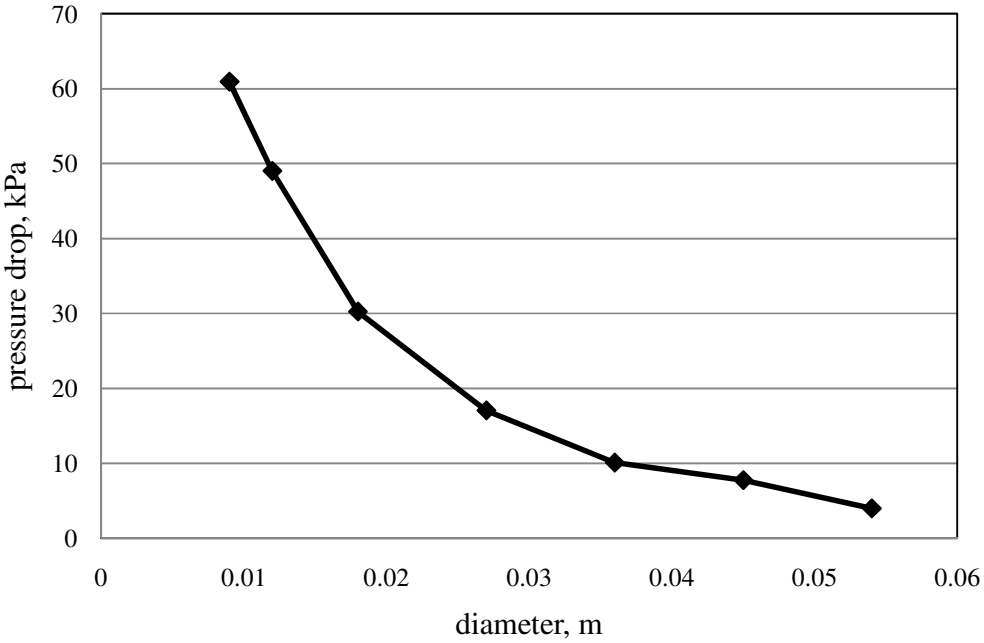

Figure 5.39 Pressure drop with different reactor tube diameter (GHSV = 38904.54 1/h and *T*= 993 K)

Figure 5.37 shows pressure drop over the catalyst bed for the reactors with different diameters. It shows that decreasing the reactor diameter causes the increased pressure drop. It was obvious that the difference in size of the membrane reactor influences the oxygen concentration within the reactor as well as the pressure drop across the catalyst bed.

Figures 5.38 – 5.42 show CH_4 conversion and C_2 yield for different sizes of the reactor (Table 5.10) and conditions (Table 5.11). From the simulations, the maximum CH_4 conversion and C_2 yield appear at the reactor diameter of 0.018 m (model c.) except when GHSV was 58427.55 1/h at 993 K (Figure 5.38) whose maximum CH_4 conversion and C_2 yield occurs at the reactor diameter of 0.027 m (model d.). It was suggested that there is an optimal dimension of the reactor. At a smaller diameter, the membrane area was higher and more oxygen can permeate to the catalyst bed. Variation of oxygen concentration along the radial direction was not pronounced. These lead to higher methane conversion but lower selectivity. However, at too large diameter, the lower membrane area allows less oxygen permeation and the catalyst was not efficiently

utilized due to the large variation of oxygen along the radial direction, thus resulting in the lower methane conversion. Therefore, an optimum reactor diameter was observed.

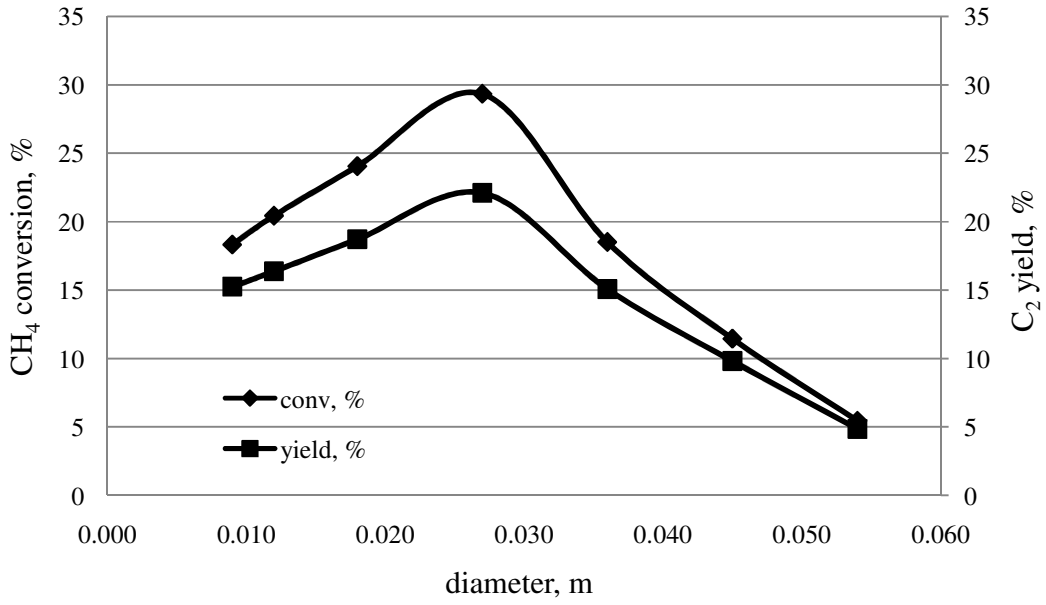

Figure 5.40 CH_4 conversion and C_2 selectivity with different tube diameter (T=993 K, GHSV= 58427.55 1/h

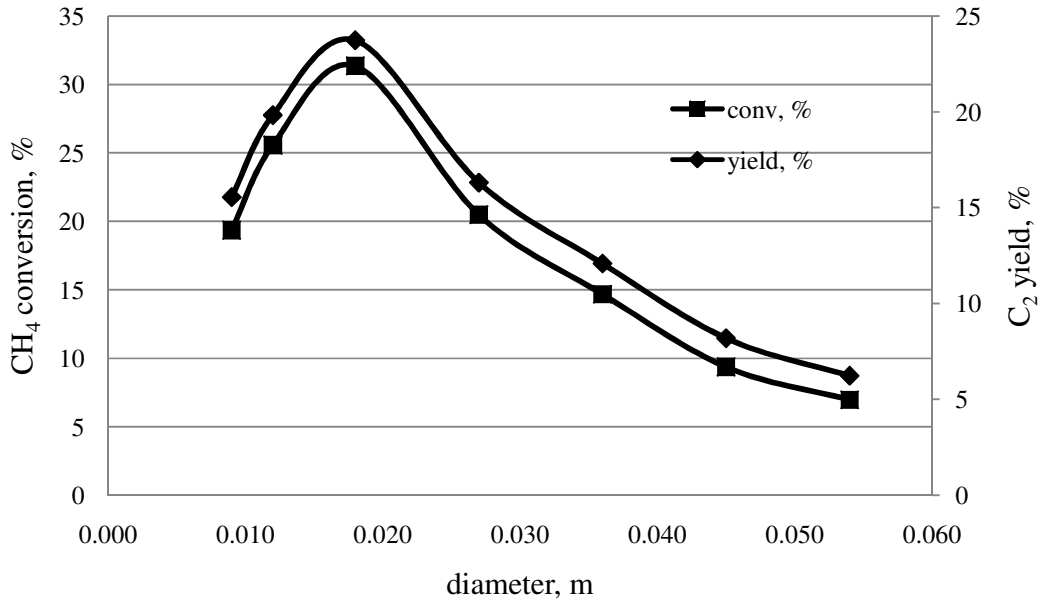

Figure 5.41 CH_4 conversion and C_2 selectivity with different tube diameter (*T*=993 K, GHSV= 38904.54 1/h)

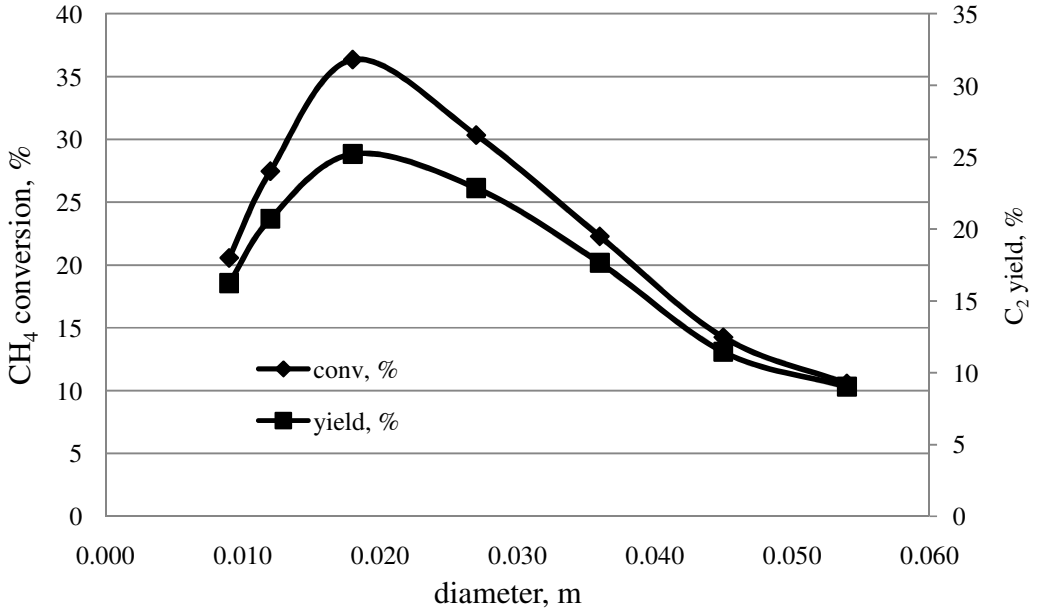

Figure 5.42 CH_4 conversion and C_2 selectivity with different tube diameter (*T*=993 K, GHSV= 194552.27 1/h)

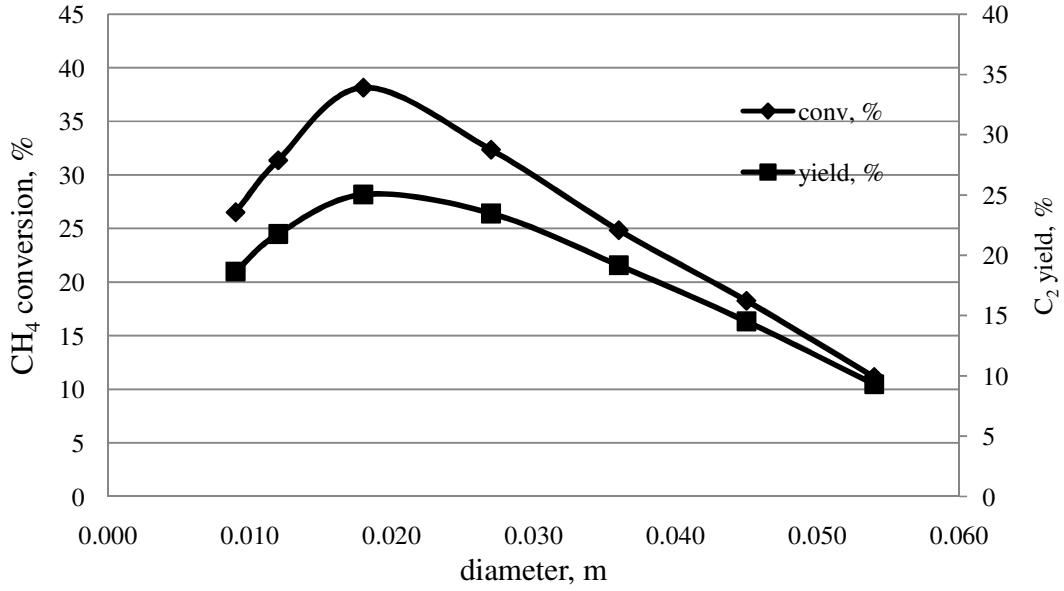

Figure 5.43 CH_4 conversion and C_2 selectivity with different tube diameter (T=1073 K, GHSV= 38904.54 1/h)

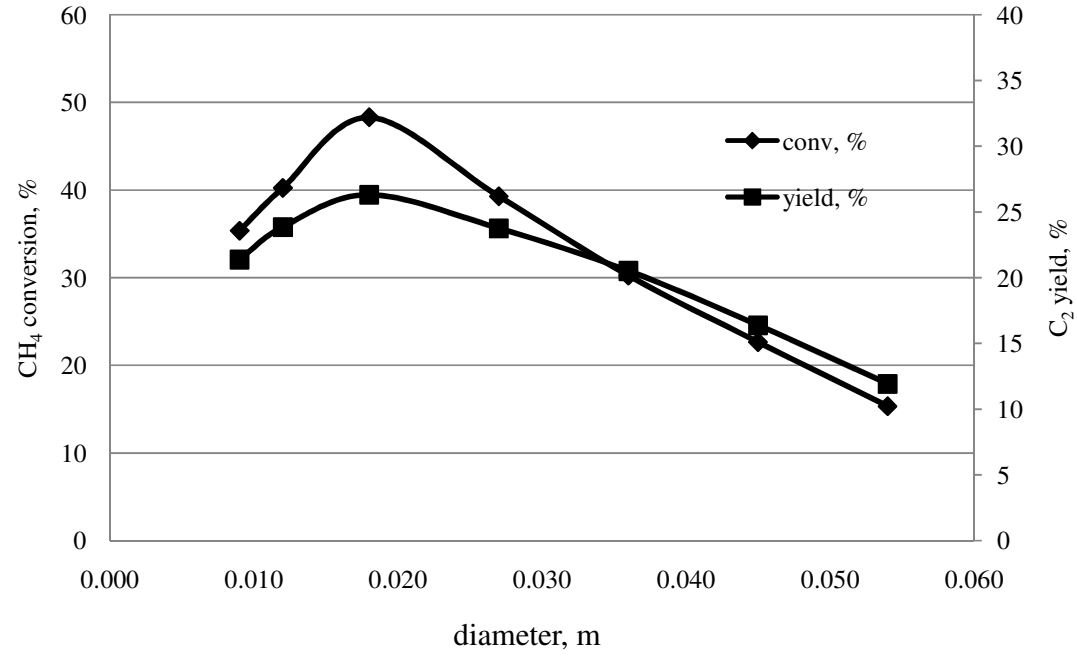

Figure 5.44 CH_4 conversion and C_2 selectivity with different tube diameter (T=1173 K, GHSV= 38904.54 1/h)

Once we know appropriate dimension of the reactor and then more simulations were performed under various conditions to find the best result. Performance of OCM at different conditions was summarized in Table 5.12. The best performance was found at GHSV of 38904.54 1/h and temperature of 1073 K, offering the highest C_2 yield of 26.82 %.

Comparison of our simulation results with the experimental results shown in Table 5.13. In same our membrane type, OCM in packed bed BSCFO membrane reactor using La-Sr/CaO catalyst report by Wang *et al*. and Oliver *et al*. that the best C_2 yield was 15 % and 18 % respectively. In same our catalyst type, OCM in packed bed $Ba_{0.5}Ce_{0.4}Gd_{0.1}Co_{0.8}Fe_{0.2}O_{3-\delta}$ (BCGCFO) membrane reactor using Na-W-Mn/SiO_2 catalyst reported by Bhatia *et al*. that the C_2 yield was 14.4 %. From all of results in packed bed membrane reactor that both case of same catalyst and same membrane case , our simulation was higher than reported in literatures. On the contrary, when compare with result of catalytic $Ba_{0.5}Ce_{0.4}Gd_{0.1}Co_{0.8}Fe_{0.2}O_{3-\delta}$ (BCGCFO) membrane reactor using Na-W-Mn/SiO_2 catalyst report by Bhatia *et al***.** They reported C_2 yield was 34.7 %. This result demonstrates that the performance at operation in the catalytic membrane reactor was better than our results.

Table 5.12 Summary OCM performance on optimum reactor at different condition

Operating condition		OCM performance		
GHSV (1/h)	T (K)	CH_4 conv, %	C_2 sel, %	C_2 yield, %
58427.55	993	24.051	77.81	18.720
38904.54	993	31.355	75.673	23.272
19452.27	993	36.361	69.412	25.283
38904.54	1073	38.132	65.630	25.026
38904.54	1173	48.285	54.467	26.231
38904.54	1223	52.465	49.653	26.050
38904.54	1273	57.820	43.373	25.087
19452.27	1073	43.713	61.352	26.818
19452.27	1173	50.34	52.973	26.667
19452.27	1223	58.325	41.854	24.241

Table 5.13 Highest C_2 yield reported for OCM in literature

Catalyst	Membrane	Type of reactor	Temperature (K)	CH_4 flow rate (m^3/s)	C_2 yield, %	Reported by
Na-W-Mn/SiO_2	BSCFO	PBMR	1073	1.95×10^{-1}	26.82	This work
La-Sr/CaO	BSCFO	PBMR	1123	3.33×10^{-7}	15	Wang *et al.*
La-Sr/CaO	BSCFO	PBMR	1223	1.41×10^{-6}	18	Oliver *et al.*
Na-W-Mn/SiO_2	BCGCFO	PBMR	1123	7.5×10^{-6}	14.4 %	Bhatia *et al.*
Na-W-Mn/SiO_2	BCGCFO	CMR	1123	7.5×10^{-6}	34.7 %	Bhatia *et al.*

*$Ba_{0.5}Ce_{0.4}Gd_{0.1}Co_{0.8}Fe_{0.2}O_{3-\delta}$ (BCGCFO)

Chapter VI

CONCLUSIONS AND RECOMMENDATIONS

1. Conclusions

Two-dimensional mathematical modeling of oxidative coupling of methane (OCM) in a fixed bed reactor and a membrane reactor was studied in this research. The simulations were carried out using Comsol multiphysics program. The present study showed that the models were well-validated with previous results reported in literatures. In the fixed bed reactor, suitable catalysts were selected by comparing between Na-W-Mn/SiO_2, La_2O_3/CaO and Li/MgO catalysts under isothermal mode. The simulation results indicated that Na-W-Mn/SiO_2 catalyst offers the best performances among all the catalysts at various conditions. Different operating conditions, such as temperature, CH_4/O_2 ratio and GHSV have influences on performance of OCM reactors packed with Na-W-Mn/SiO_2 and operated under non-isothermal mode. Increasing operating temperature resulted in increasing CH_4 conversion but decreasing C_2 selectivity However, the effects of CH_4/O_2 ratio and GHSV showed the contrary results. Especially in regard of hot spots in the reactor, it was found that the three operating variables (CH_4/O_2 ratio, GHSV and temperature) affect the occurrence of hot spots. A suitable condition to achieve the best performance was at CH_4/O_2 ratio of 3.4, feed temperature of 1073 K and GHSV of 9720 1/h. The maximum C_2 yield was 20.16%. In addition, from the studies of the three modes, isothermal, adiabatic and non-isothermal, it can be seen that the best results appeared in non-isothermal mode, heat management can make a better performance of the OCM reactor, which can be used in a real operation in the reactor design.

In membrane reactor, characteristics of three membranes including BSCFO, LSGFO and Membranox membranes were investigated. Flux of oxygen in BSCFO MR was higher than those of LSGFO and Membranox MR, respectively. In case of Membranox MR, reactant and products were lost from the reaction side to the shell side by permeating through the membrane. On the other hand, in case of dense membranes

i.e. BSCFO and LSGFO, no reactant and product loss was present due to the high selectivity. The specific characteristics of the dense membrane prevent other species to the trans-membrane side. Suitable membranes were selected by comparing between BSCFO, LSGFO and Membranox membrane. The simulation results indicated that BSCFO membrane offers the best performances among all the membranes at various conditions. Various operating conditions, such as methane flow rate, air flow rate and temperature have influences on performance of OCM reaction operated in BSCFO membrane reactor. Increasing operating temperature resulted in increasing CH_4 conversion but decreasing C_2 selectivity. However, hot spot temperature of about 1173 K was still observed in membrane reactor. Moreover, increasing of methane feed flow rate results in lower CH_4 conversion but increased C_2 selectivity. The effect of air flow rate showed the contrary results.

The performance of both FBR and MR were compared with the same physical dimension in term of catalyst loading and operating condition (air flow rate = 0.00024 m^3/s, methane flow rate = 0.000816 m^3/s and temperature = 1123 K). The maximum yield was about 13.5 % for FBR and 20.11 % for MR. The temperature profiles of FBR and MR revealed that significant hot spot temperature was observed for the FBR unlike that of the MR.

Finally, optimum dimension of MR was determined. The simulation results indicated that optimum dimension was 0.018 m diameter and 0.2 m length. The best performance was found at GHSV of 38904.54 1/h and temperature of 1073 K, offering CH_4 conversion of 43.713 %, C_2 selectivity of 61.352 % and C_2 yield of 26.82 %.

2. Recommendation

Performance of OCM may be improved when changing reactor configuration such as catalytic membrane reactor or fluidized bed reactor. The design of OCM system by combination between reactors type and separation unit with OCM process to increase C_2 yield and performance of OCM process should be considered. Moreover, in the simulation study using three-dimensional model taking into account hydrodynamics within the reactor was recommended for future work. It should represent more realistic phenomena with better prediction accuracy.

REFERENCES

Ahari, J.S., Ahmadi, R., Mikami, H., Inazu, K. and Zarrinpashne, S., Application of a simple kinetic model for the oxidative coupling of methane to the design of effective catalysts. Catalysis Today 145 (2009): 45–54.

Akin, F.T., Lin, Y.S., Selective oxidation of ethane to ethylene in a dense tubular membrane reactor. Journal of Membrane Science 209 (2002): 457–467.

Akin, F.T., Lin, Y.S. and Zeng, Y., Comparative Study on oxygen permeation and oxidative coupling of methane on disk-shaped and tubular dense Ceramic membrane reactors. Chemical Engineering Journal 40 (2001): 5908-5916.

Al-Zahrani, S.M., The effects of kinetics, hydrodynamics and feed conditions on methane coupling using fluidized bed reactor. Catalysis Today 64 (2001): 217–225.

Amin, N.A.S. and Pheng, S.E., Influence of process variables and optimization of ethylene yield in oxidative coupling of methane over Li/MgO catalyst. Chemical Engineering Journal 116 (2006): 187–195.

Bart, A., Hassel, V., Kawada, T., Sakai, N., Yokokawa, H. and Doldya, M., Oxygen permeation modeling of perovskites. Solid State Ionics 66 (1993): 295-305.

Bonnie, J.M., Sanford, G. and Martin, A. R., Coefficients for calculating thermodynamics and transport properties of individual species. NASA Technical Memorandum 4513 (1993).

Bhatia, S, Thien, C. Y., Rahman A., MohamedOxidative coupling of methane (OCM) in a catalytic membrane reactor and comparison of its performance with other catalytic reactors. Chemical Engineering Journal 148 (2009): 525–532.

Carreiro, J. A. S. P. and Baerns, M., Oxidative coupling of methane : I. Alkaline earth compound catalysts Journal of Catalysis 117 (1989): 258-265.

Chou, L., Cai, Y., Zhang, B., Niu, J., Ji, S. and Li, S., Oxidative Coupling of Methane over Na-W-Mn/SiO_2 Catalysts at Elevated Pressures Journal of Natural Gas Chemistry 11 (2002): 131-136.

Coronas, J., Menéndez, M. and Santamaria, J., Methane oxidative coupling using porous ceramic membrane reactors - II. Reaction. Chemical Engineering Science 49 (1994): 2015-2025.

Daneshpayeh, M., Abbasali, K., Navid, M., Yadolah, M., Rahmate, S. and Alireza, T., Kinetic modeling of oxidative coupling of methane over $Mn/Na_2WO_4/SiO_2$ catalyst. Fuel Processing Technology 90 (2009): 403–410.

Elshof, J.E., Bouwmeester, H.J.M. and Verweij, H., Oxidative coupling of methane in a mixed-conducting perovskite membrane reactor. Applied Catalysis 130 (1995): 195-212.

Etchegoyen, G., Chartier, T. and Gallo, P.D., An architectural approach to the oxygen permeability of a $La_{0.6}Sr_{0.4}Co_{0.8}Fe_{0.9}Ga_{0.1}O_{3-\delta}$ perovskite membrane. Journal of the European Ceramic Society 26 (2006): 2807–2815.

Haag, S., Andre, C., Veen, V. and Mirodatos, C., Influence of oxygen supply rates on performances of catalytic membrane reactors Application to the oxidative coupling of methane. Catalysis Today 127 (2007): 157–164.

Hutchings, G. J., Scurrell, M.S. and Woodhouse, J. R., Oxidative coupling of methane using oxide catalysts Chemical Society Reviews 18 (1989): 251-283.

Istadi, N.A., Saidina, A., Optimization of process parameters and catalyst compositions in carbon. Fuel Processing Technology 87 (2006): 449 – 459.

Jamal, C., Ali, G., Christophe, G. and Danilo, K., Two-phase model for a catalytic turbulent fluidized-bed reactor: Application to ethylene synthesis. Chemical Engineering Science 54 (1999): 2039-2045.

Jeffrey, A.L., Jay, P., Jyh-Yih, R., Fokion, N.E. and Theodore, T., The use of OCM reactors for ignition enhancement of natural gas combustion for practical applications: Reactor design aspects. Chemical Engineering Science 61 (2006): 6637 – 6645.

Jianjun, S., Joris, W. and Guy B.M., Microkinetics of methane oxidative coupling. Catalysis Today 137 (2008): 90–12.

Julbe, A., Farrusseng, D. and Guizard, C., Porous ceramic membranes for catalytic reactors-overview and new ideas. Journal of Membrane Science 181 (2001): 3-20.

Karimi, A., Ahmadi, R., Bozorg, Z., Jebreili, J. and Barkhordarion, A., Catalytic oxidative coupling of methane experimental investigation and optimization of operational condition. Petroleum & Coal 49 (2007): 36-40.

Keller, G.E., Bhasin, M.M., Synthesis of ethylene via oxidative coupling of methane 1.Determination of active catalysts. Journal of Catalysis 73 (1982): 9-19.

Kiatkittipong, W., Tagawa, T., Goto, S., Assabumrungrat, S., Silpasup, K. and Praserthdam, P., Comparative study of oxidative coupling of methane modeling in various types of reactor. Chemical Engineering Journal 115 (2005): 63–71.

Kiyoshi, O., Kiyotaka, J. and Akira, M., Active and selective catalysts for the synthesis of C_2H_4 and C_2H_6 via oxidative coupling of methane. Journal of catalysis 108 (1986): 353-359.

Kao, Y.K., Lei, L., and Lin, Y. S., A comparative simulation study on oxidative coupling of methane in fixed-bed and membrane reactors. Industrial & Engineering Chemistry Research 36 (1997): 3583-3593.

Kao, Y.K., Lei, L. and Lin, Y.S., Optimum operation of oxidative coupling of methane in porous ceramic membrane reactors. Catalysis Today 82 (2003): 255–273.

Lacombe, S., Durjanova, Z. and Mleczko, L., Kinetic modeling of the oxidative coupling of methane over lanthanum oxide in connection with mechanistic Studies. Chemical Engineering Technology 18 (1995): 216 – 223.

Lafarga, D., Lafuente, A., MeneÂndez, M. and SantamarõÂ, J., Thermal stability of g-Al_2O_3/a-Al_2O_3 mesoporous membranes. Journal of Membrane Science 147 (1998): 173-185.

Lane, G.S. and Wolf, E.E., Methane utlilization by oxidative coupling, I, A Study of Reactions in the Gas phase during the Co-feeding of methane and oxygen. Journal of Catalyst 113 (1988): 144.

Langille, J.A., Pasaleb, J., Renb, J.Y., Egolfopoulosa, F.N. and Tsotsisb, T.T., The use of OCM reactors for ignition enhancement of natural gas combustion for practical applications: Reactor design aspects. Chemical Engineering Science 61 (2006): 6637 – 6645.

Li, S.J., Reaction Chemistry of W-Mn/SiO_2 catalyst for the Oxidative coupling of methane. Natural gas Chemistry 12 (2003): 1-9.

Liu, H., Wang, X., Yung, D., Gao, R., Wang, Z. and Jung, J., Scale up and stability test for oxidative coupling of methane over $Na2WO_4$-Mn/SiO_2 catalyst in a 200 ml fixed-bed reactor. Natural gas Chemistry 17 (2008): 59-63.

Louis, O., Stephane, H., Claude, M. and Andre C.V.V., Oxidative coupling of methane using catalyst modified dense perovskite membrane reactors. Catalysis Today 142 (2009): 34 –41.

Lu, Y. , Dixon, A. G., Moser W. R., Ma Y. H., Balachandran, U., Oxidative coupling of methane using oxygen-permeable dense membrane reactors. Catalysis Today 56 (2000): 297–305.

Lunsford, J.H. The catalytic coupling of methane Angewandte Chemie International Edition in English 34 (1995): 970–980.

Lunsford, J.H., catalytic conversion of methane to more useful chemical and fuel: a challenge for the 21 century. Catalysis Today 63 (2000): 165-174.

Marcano S.J.G. and Tsotsis T. T., (2002) "Catalytic membranes and catalytic membrane reactors", 1st edition, Wiley-VCH, New York, USA

Maria, T., Nadka, D., Jeng-Shiang, T. and Alvin, H.W., Oxidative coupling of methane the transition from reaction to transport control over La_2O_3/MgO catalyst. Applied Catalysis 169 (1998): 237-247.

Morteza, S., Bahram, D. and Asghar, E., Some aspects of kinetics and mechanism of the oxidative coupling of methane. Journal of Chemical Technology and Biotechnology 67 (1996): 15-20.

Moustafa, T.M., Abou-Elreesh, M. and Fateen, S., Modeling, simulation and optimization of the catalytic reactor for methanol oxidation dehydrogenation. COMSOL conference (2007).

Nagaoka, K., Karasuda, T. and Aika, K., The effect of SnOz addition to LiMgO catalysts for the oxidative coupling of methane. Journal of Catalysis 181 (1999): 160-164.

Olivier, L., Haag, S.P., Mirodatos, C. and Veen, A.C.V., Oxidative coupling of methane using catalyst modified dense perovskite membrane reactors. Catalysis Today 142 (2009): 34 – 41.

Pak, S., Qia, P. and Lunsford, J.H., Elementary reactions in the Oxidative coupling of methane over Na_2WO_4-Mn/SiO_2 and Na_2WO_4-Mn/SiO_2 . Journal of catalysis 179 (1998): 220-230.

Pekediz, A. and Lasa, H.I., Methane oxidative coupling in a novel riser simulator reactor. Chemical Engineering Science 49 (1994): 4759-4770.

Prodip, K., Yan, Z. and Ajay, K.R., Multi-objective optimization of simulated countercurrent moving bed chromatographic reactor for oxidative coupling of methane. Chemical Engineering Science 64 (2009): 4137 – 4149.

Quddus, M. R., Zhang, Y., Ray, A.K., Multi-objective optimization in solid oxide fuel cell for oxidative coupling of methane. Chemical Engineering Journal 165 (2010): 639–648.

Reid, R.C., Prausnitz, J.M. and Poling B.E., (1987), "The Properties of Gases and Liquids", 4th Edition, McGraw-Hill, New York, USA

Ruxton, H.V. and Richard, H.W., Knudsen flow-diffusion in porous pellets. Industrial and Engineering Chemistry 53 (1961): 837- 840.

Shahri, M.K.S., Alavi, S.M., Kinetic studies of the oxidative coupling of methane over the Mn/Na_2WO_4/SiO_2 catalyst. Journal of Natural Gas Chemistry 18(2009): 25–34.

Shaula, A.L., Yaremchenko, A.A., Kharton, V.V. Logvinovich, D.I., Naumovich, E.N., Kovalevsky, A.V., Frade, J.R. and Marques, F.M.B., A Oxygen permeability of $LaGaO_3$-based ceramic membranes. Journal of Membrane Science 221 (2003): 69–77.

Shao, Z., Dong, H., Xiong, G., Cong, Y. and Yang, W., Performance of a mixed-conducting ceramic membrane reactor with high oxygen permeability for methane conversion. Journal of Membrane Science 183 (2001): 181–192.

Simon, Y., Baronne, F., and Marquaire, P.M., Kinetic modeling of the oxidative coupling of methane. Industrial & Engineering Chemistry Research 46 (2007): 1914- 1922.

Stansch, Z., Mleczko, L., and Baerns, M.,Comprehensive kinetics of oxidative coupling of methane over the La_2O_3/CaO Catalyst. Industrial & Engineering Chemistry Research 36*(*1997): 2568-2579.

Subhash, B., Chua, Y.T. and Rahman, M.A., Oxidative coupling of methane (OCM) in a catalytic membrane reactor and comparison of its performance with other catalytic reactors. Chemical Engineering Journal 148 (2009): 525–532.

Sunarso, J., Baumann, S., Serrac, J.M., Meulenberg, W.A., Liua, S., Lind, Y.S. and Diniz, C., Mixed ionic–electronic conducting (MIEC) ceramic-based membranes for oxygen separation. Journal of Membrane Science 320 (2008): 13–41.

Takenaka, S., Kaburagi, T., Yamanaka, I. and Otsuka, K., Oxidative coupling of methane over Li^+-added Y_2O_3 catalyst prepared from $Y(OH)_3$ Catalysis Today 71 (2001): 31-36.

Tye, C.T., Mohamed, A.R. and Bhatia, S., Oxidative Coupling of Methane in a catalyst bed reactor and membrane reactor: modeling and simulation. Chemical engineering Journal 5 (2004): 834-844.

Tye, C.T., Mohamed, A.R. and Bhatia, S., Modeling of catalytic reactor for oxidative coupling of methane using La2O3/CaO catalyst. Chemical Engineering Journal 87 (2002): 49–59.

Thien, C.Y., Mohamed, A.R. and Bhatia, S., Process optimization of oxidative coupling of methane for ethylene production using response surface methodology. Journal of Chemical Technology and Biotechnology 82 (2007):81–91.

Todd, B. and Young, J.B., Thermodynamic and transport properties of gases for use in solid oxide fuel cell modeling. Journal of Power Sources 110 (2002):186-200.

Tonkovich, A.L.Y., Jimenez, D.M., Zilka, J.L., Roberts, G.L. Inorganic membrane reactors for the oxidative coupling of methane. Chemical Engineering Science 51 (1996): 3051-3056**.**

Unnl, O., Guy, D. and Joachim, J.K., A kinetic study of the oxidative coupling of methane over a $BaCO_3$ /La_2On $(CO_3)_{3-n}$ catalyst. Catalysis Today 13 (1992): 209-218.

Wang, W. and Lin, Y.S., Analysis of oxidative coupling of methane in dense oxide membrane reactors. Journal of Membrane Science 103 (1995): 219-233.

Wang, H., Rong, W., David, T.L. and Weishen, Y., Experimental and modeling studies on $Ba_{0.5}Sr_{0.5}Co_{0.8}Fe_{0.2}O_{3-\delta}$ (BSCF) tubular membranes for air separation. Journal of Membrane Science 243 (2004): 405–415.

Wang, H., You, C. and Yung, W., Oxygen permeation study in a tubular $Ba_{0.5}Sr_{0.5}Co_{0.8}Fe_{0.2}O_{3-\delta}$ oxygen permeable membrane. Journal of Membrane Science 210 (2002): 259–271.

Wang, H., You, C. and Yung, W., Oxidative coupling of methane in $Ba_{0.5}Sr_{0.5}Co_{0.8}Fe_{0.2}O_{3-\delta}$ (BSCF) tubular membrane reactors. Catalysis Today 104 (2005): 160–167.

Xu ,S. J., Thomson , W. J., Perovskite-type oxide membranes for the oxidative coupling of methane. AIChE Journal 43 (1997): 2731–2740.

Yaghobi, N., Ghoreishy, M.H.R., Oxidative coupling of methane in a fixed bed reactor over perovskite catalyst: A simulation study using experimental kinetic model. Journal of Natural Gas Chemistry 17(2008): 8–16.

Yaghobi, N., Ghoreishy M.H.R., Modeling the oxidative coupling of methane: Heterogeneous chemistry coupled with 3D flow field simulation. Journal of Natural Gas Chemistry 18(2009): 39–44.

Yakabe, H., Hishinuma, M., Uratani, M., Matsuzaki, Y. and Yasuda, I., Evaluation and Modelling of Performance of Anode-supported Solid Oxide Fuel Cell, Journal of Power Sources 86(2000): 423-431.

Yaping, L., Oxygen-permeable dense membrane reactor for the oxidative coupling of methane. Journal of Membrane Science 170 (2000): 27–34.

Yentekakis, I.V., Jiang, Y., Makri, M. amd Vayenas, C.G., Oxidative coupling of methane to ethylene with 85% yield in a gas recycle electrolytic or catalytic reactor separator. Surface Science and Catalysis 107 (1997): 307-312.

Yves, S., Franois, B. and Marie, M.P., Kinetic modeling of the oxidative coupling of methane. Chemical Engineering Journal (2007): 1914-192.

Zenga, Y., Lina, Y.S. and Swartzb, S.L., Perovskite-type ceramic membrane: synthesis, oxygen permeation and membrane reactor performance for oxidative coupling of methane. Journal of Membrane Science 150 (1998): 87-98.

APPENDICES

APPENDIX A

Use of COMSOL Multiphysics

The finite element method was proposed to formulate the PDE problem. The developed finite element model the reactor was solved with quadratic finite element basis functions, using a commercial finite element simulation environment COMSOL. The software runs the finite element analysis together with meshing which was a partition of the geometry model into small units of simple shapes and error control using a variety of numerical solvers. Three application modes were needed; heat transfer by conductive and convective was used to model. Mass transfer by convective and diffusion was used to show the concentration and transport of eight species of interest. Brinkman equation was applied to describe fluid flow.

The matrix of partial differential equation used in model described in equation (A.1)-(A.12)

(Example of OCM over Na-W-Mn/ SiO_2 in BSCFO membrane reactor) Stiochiometric equation and reaction rate of this model was shown in Table 4.1.

- **Multi-component species transport**

- Variable = c_CH4, c_O2, c_C2H4, c_C2H6, c_CO, c_CO2, c_H2, c_H2O
  Active domain: tube side

$$\left(\frac{\partial^2 c\_CH4}{\partial r^2}+\frac{1}{2}\frac{\partial c\_CH4}{\partial r}\right)+D_{i,k}^{eff}\frac{\partial^2 c\_CH4}{\partial z^2}=u\frac{\partial c\_CH4}{\partial z}-\rho_B(-2\times r_1-r_2-r_3) \quad (A.1)$$

$$\left(\frac{\partial^2 c\_O2}{\partial r^2}+\frac{1}{2}\frac{\partial c\_O2}{\partial r}\right)+D_{i,k}^{eff}\frac{\partial^2 c\_O2}{\partial z^2}=u\frac{\partial c\_O2}{\partial z}-\rho_B(-0.5\times r_1-2\times r_2-r_3-0.5\times r_4-0.5\times r_5-2\times r_6) \quad (A.2)$$

$$\left(\frac{\partial^2 c\_C2H4}{\partial r^2}+\frac{1}{2}\frac{\partial c\_C2H4}{\partial r}\right)+D_{i,k}^{eff}\frac{\partial^2 c\_C2H4}{\partial z^2}=u\frac{\partial c\_C2H4}{\partial z}-\rho_B(r_5-r_6-r_7+r_8) \quad (A.3)$$

$$\left(\frac{\partial^2 c\_C2H6}{\partial r^2}+\frac{1}{2}\frac{\partial c\_C2H6}{\partial r}\right)+D_{i,k}^{eff}\frac{\partial^2 c\_C2H6}{\partial z^2}=u\frac{\partial c\_C2H6}{\partial z}-\rho_B(r_1-r_5-r_8) \quad (A.4)$$

$$\left(\frac{\partial^2 c\_CO}{\partial r^2}+\frac{1}{2}\frac{\partial c\_CO}{\partial r}\right)+D_{i,k}^{eff}\frac{\partial^2 c\_CO}{\partial z^2}=u\frac{\partial c\_CO}{\partial z}-\rho_B(r_3-r_4+2\times r_6+2\times r_7+r_9-r_{10}) \quad (A.5)$$

$$\left(\frac{\partial^2 c\_CO2}{\partial r^2}+\frac{1}{2}\frac{\partial c\_CO2}{\partial r}\right)+D_{i,k}^{eff}\frac{\partial^2 c\_CO2}{\partial z^2}=u\frac{\partial c\_CO2}{\partial z}-\rho_B(r_2+r_4-r_9+r_{10}) \quad (A.6)$$

$$\left(\frac{\partial^2 c\_H2}{\partial r^2}+\frac{1}{2}\frac{\partial c\_H2}{\partial r}\right)+D_{i,k}^{eff}\frac{\partial^2 c\_H2}{\partial z^2}=u\frac{\partial c\_H2}{\partial z}-\rho_B(r_3+4\times r_7+r_8-r_9+r_{10}) \quad (A.7)$$

$$\left(\frac{\partial^2 c\_H2O}{\partial r^2}+\frac{1}{2}\frac{\partial c\_H2O}{\partial r}\right)+D_{i,k}^{eff}\frac{\partial^2 c\_H2O}{\partial z^2}=u\frac{\partial c\_H2O}{\partial z}-\rho_B(r_1+2\times r_2+r_3+r_5+2\times r_6-2\times r_7+r_9-r_{10}) \quad (A.8)$$

- Variable = c_O23

  Active domain: shell side

$$\left(\frac{\partial^2 c\_O23}{\partial r^2}+\frac{1}{2}\frac{\partial c\_O23}{\partial r}\right)+D_{ij}^{eff}\frac{\partial^2 c\_O23}{\partial z^2}=u\frac{\partial c\_O23}{\partial z} \quad (A.9)$$

- **Energy transport**

- Variable = T1

  Active domain: tube side

$$\lambda\left(\frac{\partial^2 T1}{\partial r^2}+\frac{1}{2}\frac{\partial T1}{\partial r}\right)+\frac{\partial^2 T1}{\partial z^2}=u\rho_f C_p\frac{\partial T1}{\partial z}-\sum_{i=1}^{n}\Delta H_{rxn}r_i \quad (A.10)$$

- Variable = T2

  Active domain: shell side

$$\lambda\left(\frac{\partial^2 T2}{\partial r^2}+\frac{1}{2}\frac{\partial T2}{\partial r}\right)+\frac{\partial^2 T2}{\partial z^2}=u\rho_f C_p\frac{\partial T2}{\partial z} \quad (A.11)$$

- **Momentum transport**

- Variable = u, P

  Active domain: tube side

$$\frac{\eta}{\kappa}u=\nabla\cdot[-PI+\left(\frac{1}{\varepsilon_p}\right)\eta(\nabla u+(\nabla \mathrm{u})^{\mathrm{T}})] \quad (A.12)$$

- **Geometry and boundary condition**

  - **Membrane reactor**

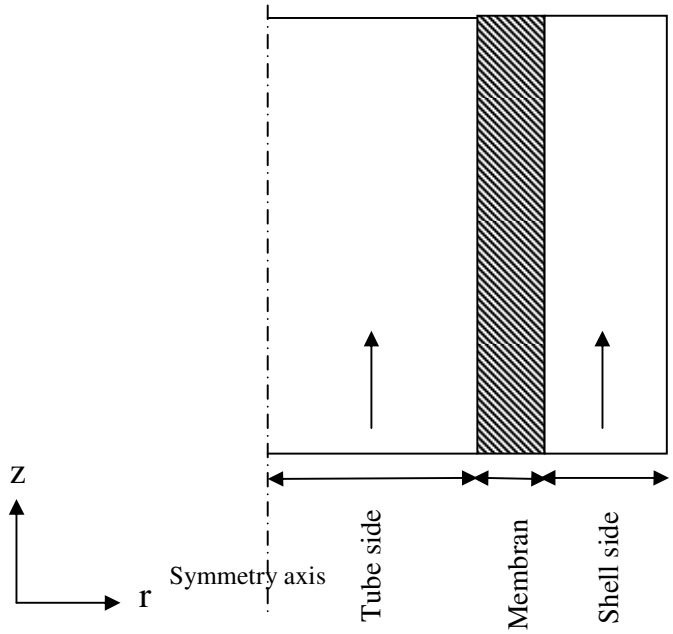

Figure A-2. Geometry of membrane

The reactor geometry was 2D cylindrical and the flow enters the computational domain at a known velocity, composition and temperature.

  - **Boundary condition and coupling variable**

At the inlet (z=0),

C_i0=C0, T1=T2=T0

At the outlet,

It was assumed that the convective part of the mass and heat transport vector was dominating.

At axial symmetry,

r=0

At the tube wall (membrane side),

The mass flux was defined by mass transfer,

$n \cdot N_i = 0$ (Except oxygen species)

N_i is the mass flux vector for species i, n is the normal vector to the boundary

For oxygen species; $-n \cdot N_{O_{21}} = \frac{\pi L C_i D_a}{2Sln(\frac{r_1}{r_2})} ln\,(\frac{P_1}{P_2})$

However, oxygen may permeate through the membrane. Coupling variables were used to calculate the oxygen flux across the membrane. The oxygen partial pressures on the feed and the permeate side were calculated at the respective membrane surfaces and mapped onto the surface where the flux was calculated. The flux was mapped back to the other surface to account for both the hydrogen sink and the source in the respective compartments.

A heat transfer was defined in non-isothermal mode; heat flux was removed from wall,

$$-n \cdot q = U \times (T_1 - T_2)$$

At the shell wall,

A mass transfer was defined as $n \cdot N_{O_{23}} = 0$

A heat transfer was defined in non-isothermal mode; heat flux was removed from wall,

$$-n \cdot q = U \times (T_2 - T_{ex})$$

APPENDIX B

Thermodynamic and transport property of gas

In this Appendix, the thermodynamic and transport properties of pure gases and gaseous mixtures will be summarized. These gases include CH_4, C_2H_4, C_2H_6, CO_2, CO, H_2, H_2O, N_2 and O_2

B.1 Permeability

The Kozeny-Carman equation was used to estimate permeability evolution versus porosity, grain size and tortuosity, was given by:

$$k_{absolute} = \frac{1}{2}\frac{\emptyset^3}{S^2\tau^2} \qquad \text{(B.1)}$$

Where ε was porosity, S was average pore radius (m) and τ was tortuosity

B.2 Viscosity and Thermal Conductivity of Pure Gases

The empirical equation used to determine the viscosity (η_i) and thermal conductivity (λ_i) for the pure gas i, was given by:

$$\begin{Bmatrix}\eta_i \\ \lambda_i\end{Bmatrix} = A_i \ln T + \frac{B_i}{T} + \frac{C_i}{T^2} + D_i \qquad \text{(B.2)}$$

Where the series of A, B, C and D were the corresponding coefficients for the gas species i. These parameters were summarized by (Bonnie *et al.* (1993)) given in Table B.1 for viscosity coefficient and Table B.2 for thermal conductivity coefficient.

Table B.1 Coefficients of correlations for gas viscosity

i	A	B	C	D	T(K)
CH_4	0.574	-98.544	2001.220	1.754	300-1000
	0.651	23.937	-22020.183	1.124	1000-5000
O_2	0.619	-44.609	-1346.071	1.960	300-1000
	0.638	-1.234	-22885.810	1.806	1000-5000
C_2H_4	0.552	-162.609	6473.404	1.946	300-1000
	0.654	51.157	-54731.184	1.093	1000-5000
C_2H_6	0.556	-152.657	5605.081	1.824	300-1000
	0.654	51.042	-51534.435	1.001	1000-5000
CO	0.604	-43.633	-884.419	1.897	300-1000
	0.651	28.517	-16690.236	1.522	1000-5000
CO_2	0.543	-188.239	8872.657	2.450	300-1000
	0.653	51.739	-62834.882	1.523	1000-5000
H_2	0.689	4.873	-595.651	0.556	300-1000
	0.705	36.288	-7225.555	0.419	1000-5000
H_2O	0.784	-382.604	49040.158	0.852	300-1000
	0.507	-689.669	87454.750	3.029	1000-5000

Table B.2 Coefficients of correlations for thermal conductivity

i	A	B	C	D	T(K)
CH_4	1.18	-174.22	0.00	-0.55	300-1000
	0.49	-915.98	87265.13	4.85	1000-5000
O_2	0.82	-34.37	2278.51	1.01	300-1000
	0.81	119.82	-47335.93	0.95	1000-5000
C_2H_4	0.78	-478.58	32147.86	2.18	300-1000
	0.48	-917.73	115280.60	4.58	1000-5000
C_2H_6	0.87	-456.34	31766.62	1.64	300-1000
	0.47	-969.11	0.11	4.83	1000-5000
CO	0.83	59.14	-9863.94	0.71	300-1000
	0.65	-151.01	-16723.86	2.17	1000-5000
CO_2	0.54	-499.28	37397.50	3.29	300-1000
	0.66	-127.42	-81580.33	2.18	1000-5000
H_2	0.94	190.13	-19701.96	1.75	300-1000
H_2	0.74	-549.42	256763.76	3.56	1000-5000
H_2O	1.55	66.11	5596.99	-3.93	300-1000

B.3 Viscosity and Thermal Conductivity of Multi-component Gaseous Mixtures

Evaluation of both the thermal conductivity and viscosity transport properties of low-pressure multi-component gas mixtures requires application of the kinetic theory of gases. Various methods exist to estimate these properties and most were complex functions of gas composition. Although Todd and Young (2002) claimed that the method of Reichenberg was the most suitable method for this purpose, Reichenberg's expression was much more complicated than typical methods such as Wilke's expression. Therefore, the method of Wilke (Reid *et al.* (1987)) was recommended to determine gas mixture viscosity. This expression was written as

$$\eta_g = \sum_{i=1}^{n} \frac{x_i \eta_i}{\sum_{j=1}^{n} x_j \phi_{ij}} \quad \text{(B.3)}$$

$$\phi_{ij} = \frac{[1+(\eta_i/\eta_j)^{\frac{1}{2}}(M_i/M_j)^{1/4}]^2}{[8(1+M_i/M_j)]^{1/2}} \quad \text{(B.4)}$$

$$\lambda_g = \sum_{i=1}^{n} \frac{x_i \lambda_i}{\sum_{j=1}^{n} \lambda_i A_{ij}} \quad \text{(B.5)}$$

Where A_{ij} is given by the Mason and Saxena modification,

$$A_{ij} = \frac{[1+(\lambda_{tri}/\lambda_{trj})^{1/2}(M_i/M_j)^{1/4}]^2}{[8(1+M_i/M_j)]^{1/2}} \quad \text{(B.6)}$$

$$\frac{\lambda_{tri}}{\lambda_{trj}} = \frac{\eta_i M_j}{\eta_j M_i} \quad \text{(B.7)}$$

B.4 Diffusion Coefficient

The diffusion coefficient plays an important role to determine the rate of gas diffusion inside catalyst bed. Because gases diffuse through the porous catalyst bed, the overall diffusion coefficient including binary, Knudsen and effective diffusion coefficients were described as follows.

B.4.1 Binary diffusion coefficient

The Chapman-Enskog theory was applied to determine the binary diffusion coefficient (D_{ij}) as written by (Reid *et al.* (1987) and Yakabe *et al.* (2000))

$$D_{ij} = 0.001858 \frac{[T^3(M_i+M_j)/M_iM_j]^{1/2}}{p\sigma_{ij}^2\Omega_D} \quad \text{(B.8)}$$

Where σ_{ij} was the characteristics length and Ω_D was the collision integral. Using the Lennard-Jones 12-6 potential model, Ω_D was given by

$$\Omega_D = \frac{A}{T_N^B} + \frac{C}{exp\ (DT_N)} + \frac{E}{exp\ (FT_N)} + \frac{G}{exp\ (HT_N)} \quad \text{(B.9)}$$

Where the constants A to H were, A = 1.06036, B = 0.15610, C = 0.19300, D = 0.47635, E = 1.03587, F = 1.52996, G = 1.76474, H = 3.89411, and TN was defined by

$$T_N = \frac{\kappa T}{\epsilon_{ij}} \quad \text{(B.10)}$$

Where κ was the Boltzmann constant and ε_{ij} is the characteristic Lennard-Jones energy. σ_{ij} And ϵ_{ij}

$$\sigma_{ij} = (\sigma_i + \sigma_j)/2 \quad \text{(B.11)}$$

$$\varepsilon_{ij} = (\varepsilon_i\varepsilon_j)^{1/2} \quad \text{(B.12)}$$

Where σ_i was a diameter of the molecular collision. The values for σ_i and ε_i were summarized in Table B.3

Table B.3 Values for σ_i and ε_i

i	$\boldsymbol{\sigma}$ $(\dot{\boldsymbol{A}})$	$\frac{\boldsymbol{\varepsilon}}{\boldsymbol{k}}(\boldsymbol{K})$
CH_4	3.768	148.6
O_2	3.467	106.7
C_2H_4	4.163	215.7
C_2H_6	4.443	215.7
CO	3.690	91.7
CO_2	2.641	95.2
H_2	2.827	59.7
H_2O	2.641	809.1

B.4.2 Knudsen diffusion coefficient

The Knudsen diffusion coefficient can be predicted using kinetic theory by relating the pore diameter (Ruxton *et al.* (1961)) For straight and round pores, the diffusion coefficient of the i component becomes,

$$D_{i,k} = \frac{\bar{D}}{3}\sqrt{\frac{8RT}{\pi M}} \qquad \text{(B.13)}$$

B.4.3 Effective diffusion coefficient

In order to account for the catalyst porosity and pore tortuosity, the effective binary diffusion and the effective Knudsen diffusion coefficient were defined as

$$D_{ij}^{eff} = D_{ij}\left(\frac{\varepsilon}{\tau}\right) \qquad \text{(B.14)}$$

$$D_{i,k}^{eff} = D_{i,k}\left(\frac{\varepsilon}{\tau}\right) \qquad \text{(B.15)}$$

Where ε is the porosity and τ is the tortuosity. These parameters were the basic parameter used to characterize porous media.

B.4.4 Porosity

The porosity was the intuitive porous media parameter

$$\varphi = \frac{Volume\ of\ voids}{Volume\ of\ Voids + Volume\ of\ Solids} \qquad \text{(B.16)}$$

Note that this definition includes all free space, some of which may not be continuously connected through the media and therefore was not useful for gas transport. A reduced effective porosity, taking into account the degree of interconnection may therefore be more useful than the actual porosity. Porosity can be measured by several means including mercury porosimetry.

B.4.5 Tortuosity

Tortuosity takes into account the greater distance through which the fluid must travel in order to navigate through the porous media than if it were to pass

B.5 Isobaric Heat Capacity

The empirical equation used to determine the isobaric heat capacity for a pure gas i, C_{pi} (j/kg K), was given by:

$$\frac{C_p}{R} = a_1 + a_2 T + a_3 T^2 + a_4 T^3 + a_5 T^4 \qquad \text{(B.17)}$$

Where the series of ai are the corresponding coefficients for the gas species i, these parameters were summarized by Todd and Young (2002) and given in Table B.4

Table B.4 Series of ai are the corresponding coefficients for the gas species i

i	a1	a2	a3	a4	a5
CH_4	5.1499	-1.3671×10^{-2}	4.9180×10^{-5}	-4.8474×10^{-8}	1.6669×10^{-11}
O_2	3.7825	-2.9967×10^{-3}	9.8473×10^{-6}	-9.6813×10^{-9}	3.2437×10^{-12}
C_2H_4	3.9592	-7.5705×10^{-3}	5.7099×10^{-5}	-6.9159×10^{-8}	2.6988×10^{-11}
C_2H_6	4.2914	-5.5015×10^{-3}	5.9944×10^{-5}	-7.0847×10^{-8}	2.6869×10^{-11}
CO	3.5795	-6.1035×10^{-4}	1.0168×10^{-6}	9.0701×10^{-10}	-9.0442×10^{-13}
CO_2	2.3568	8.9846×10^{-3}	-7.1236×10^{-6}	2.4592×10^{-9}	-1.4370×10^{-13}
H_2	2.3443	7.9805×10^{-3}	-1.9478×10^{-5}	2.0157×10^{-8}	-7.3761×10^{-12}
H_2O	4.1986	-2.0364×10^{-3}	6.5204×10^{-6}	-5.4880×10^{-9}	1.7720×10^{-12}

The molar heat capacity of an ideal gaseous mixture of n component gases was given by

$$C_p = \sum_{i=1}^{n} x_i C_{pi} \qquad \text{(B.18)}$$

Where x and C were the mole fraction and molar heat capacity of i component.

B.5 Enthalpy of Reaction

The enthalpy change of any reactions for any temperature (ΔHr×n,T) was calculated by

$$\Delta H^0_{rxn,T} = \Delta H^0_{rxn,T_{ref}} + C_p \Delta T \qquad \text{(B.19)}$$

Where $\Delta H^0_{rxn,T_{ref}}$, denotes the enthalpy change of reaction at reference temperature (typically, 25 ^oC or 298 K, T_{ref} and given in Table B.5) which was determined by

$$\Delta H^0_{rxn,T_{ref}} = \left(\sum n_{pr}\, \Delta H^0_{product}\right) - \left(\sum n_{re} \Delta\, H^0_{reactant}\right) \qquad \text{(B.20)}$$

C_p was defined

$$C_p = \left(\sum n_{pr}\, C_{p,product}\right) - \left(\sum n_{re} C_{p,reactant}\right) \qquad \text{(B.21)}$$

Where n_{pr} and n_{re} are stoichiometric number of moles for products and reactants, respectively, $\Delta H^0_{product}$ and $\Delta H^0_{reactant}$ the enthalpy of formations for products and reactants, respectively, $C_{p,product}$ and $C_{p,reactant}$ the heat capacities for products and reactants, respectivel

Table B.5 Heat of formation of species i

Compound i	ΔH_i^0 **(kJ/mol)**
CH_4	-74.87
O_2	0
C_2H_4	52.47
C_2H_6	-83.85
CO	-110.525
CO_2	-393.509
H_2	0
H_2O	-241.83

APPENDIX C

LIST OF PUBLICATION

Salamah Manundawee , Suttichai Assabumrungrat, Navadol Laosiripojana and Wisitsree Wiyaratn "Two-dimensional mathematical modeling of oxidative coupling of methane in a fixed bed reactor: Comparison between different catalysts", Pure and Applied Chemistry International Conference 2011, Bangkok, Thailand, January, 2011, (oral presentation)

VITA

Miss Salamah Manundawee was born in February 5 th, 1987 in Satun, Thailand. She finished high school from Phimanpittayasan School, Satun in 2004. After that, she studied at Prince of Songkla University, Songkla, Thailand for 4 years and received Bachelor's Degree from the department of Chemical Engineering in March 2009. Then, she required to study in the Master's Degree at the department of chemical engineering, Chulalongkorn University in 2009.

In January 2011, she participated in Pure and Applied Chemistry International Conference (PACCON2011), Bangkok, Thailand for oral presentation and published for "Two-dimensional mathematical modeling of oxidative coupling of methane in a fixed bed reactor: Comparison between different catalysts".